

10191 16101
NACA TN 3830

0066752



TECH LIBRARY KAFB, NM

NATIONAL ADVISORY COMMITTEE FOR AERONAUTICS

TECHNICAL NOTE 3830

GROWTH OF DISTURBANCES IN A FLAME-GENERATED SHEAR REGION

By Perry L. Blackshear, Jr.

Lewis Flight Propulsion Laboratory
Cleveland, Ohio

AFMDC Technical Library
AFL 2811



Washington



November 1956

AFMDC
TECHNICAL LIBRARY



0066752

TABLE OF CONTENTS

	Page
<u>SUMMARY</u>	1
<u>INTRODUCTION</u>	2
<u>DEPENDENCE OF TURBULENT FLAME SPEED ON DISTURBANCES ORIGINATING</u>	
<u>IN SHEAR REGIONS</u>	2
<u>EFFECT OF COMBUSTOR OSCILLATIONS IN INCREASING RATE OF</u>	
<u>FLAME PROPAGATION</u>	4
<u>SYMBOLS</u>	5
<u>THEORY: STABILITY OF FLOW FOR A FLAME IN A DUCT</u>	8
<u>INTRODUCTION</u>	8
The Steady-State Flow Field of a Flame Anchored in a Duct	8
The Stability Problem	9
Intpreting the Results of the Stability Analysis	13
<u>STABILITY ANALYSIS</u>	13
Steady-State Solution	13
First-Order Disturbance Problem	15
Boundary Conditions	17
Solution of the Boundary Value Problem	20
<u>RESULTS</u>	24
Construction of Stability Map	26
Phase Velocity	26
Disturbance Growth	28
Disturbance Velocity Distribution in y-Direction	31
Relation of Theoretical Results to Measurable Quantities	34
Flame slope	34
Phase velocity	34
Flame-front displacement	34
Flame propagation	36
Effect of Flameholder	38
Steady-state velocity distribution	39
Comparison of the stability of a  profile and a  profile	41
<u>SUMMARY OF THEORETICAL RESULTS</u>	43
<u>EXPERIMENTAL EXAMINATION OF DISTURBANCE GROWTH IN A V-FLAME</u>	44
<u>INTRODUCTION</u>	44
<u>APPARATUS</u>	45
Burner Test Section	45
Auxiliary Equipment	46
Sound producing system	46
Flow metering	46
Hot-wire equipment	46

	Page
Pressure measurements	46
Photomultiplier probe	46
Shadowgraph system	47
Stroboscope	47
Properties of System	47
Velocity profiles upstream of flameholder	47
Velocity profile in wake, no flame	47
Turbulence intensity and spectra	48
Calibration of Disturbance Amplitude Against Speaker Input	49
S_T/S_L Determined by Photomultiplier Probe	50
RESULTS	52
Examination of the Method	53
Comparison of Flame Speed with Flame Appearance	55
Distribution of Local S_T/S_L Values with Respect to	
Various Frequencies	57
Disturbance-Displacement Growth	58
Disturbance Phase Velocities	58
Effect of Test-Section Depth	59
Effect of Amplitude	59
Effect of Flameholder Size	59
Effect of Velocity	60
Symmetric Disturbances	61
DISCUSSION	62
1. In what respects do the experimental results and the inter-	
pretations of the stability analysis agree?	62
2. Would the same distribution of displacement and S_T/S_L	
with distance from the flameholder obtain if no growth	
occurred in the flame zone?	63
3. Do eddies shed?	63
4. Does the turbulent-flame propagation velocity depend upon	
upstream turbulence?	63
5. How does S_T/S_L obtained from area measurements compare	
with S_T/S_L taken from photomultiplier data?	65
6. How can flame speeds be predicted on the basis of these	
results?	65
7. Can the results concerning frequency be applied to	
multiple flameholders?	67
8. Can the excitation at the flameholder permit increased	
combustion rates without destroying the burner walls?	68
9. What would be the sacrifice in stability and pressure	
drop for such an excitation?	69
10. Can anything be done about predicting the behavior of	
axially symmetric flames in cylindrical ducts?	70

	Page
<u>SUMMARY OF RESULTS</u>	72
THEORY	72
EXPERIMENT	73
 <u>CONCLUDING REMARKS</u>	 73
 <u>APPENDIX - AXIALLY SYMMETRIC DISTURBANCES IN AXIALLY SYMMETRIC</u>	
<u>FLOW WITH DENSITY JUMPS</u>	75
DISTURBANCE EQUATION	75
BOUNDARY CONDITIONS	76
BOUNDARY VALUE PROBLEM	79
 <u>REFERENCES</u>	 82
 <u>FIGURES</u>	 86
 <u>LIST OF FIGURES</u>	 144
 <u>AUTHOR INDEX</u>	 148

TECHNICAL NOTE 3830

GROWTH OF DISTURBANCES IN A FLAME-GENERATED SHEAR REGION¹

By Perry L. Blackshear, Jr.

SUMMARY

The growth of transverse velocity disturbances in the shear region caused by a flame in a duct is examined theoretically and experimentally.

The theoretical analysis consists of a stability analysis of a flow field arising from a flame in a duct. The flow is found to be neutrally stable to symmetric disturbances and unstable to antisymmetric ones.

In following the history of a disturbance of given frequency from the flameholder downstream, it is found that a most-amplified frequency exists, which is equal to flow velocity divided by duct width. Disturbances at frequencies greater or less than this are amplified less than this one.

The amount that an incoming disturbance is amplified depends on the flame slope. For the most-amplified frequency, the ratio of terminal to initial transverse disturbance velocity is equal to $(1.1)^{1/\text{slope}}$ where the slope is roughly turbulent flame speed divided by flow velocity. This ratio of terminal to initial transverse disturbance velocity is dependent on inlet velocity and flame speed only in the stated manner and is essentially independent of density ratio.

The critical wavelength separating disturbances that grow from those that do not grow varies as a constant times flame width, where the constant is $2\frac{1}{2}$ for flames that are narrow compared with duct width and becomes infinite as the flame reaches the wall. The flow is unstable to disturbances having wavelengths greater than critical. Thus, short-wavelength (i.e., high-frequency) disturbances achieve their terminal amplifications near the flameholder, while long-wavelength disturbances achieve theirs farther downstream. The most-amplified disturbance achieves its terminal amplification when the flame fills 0.60 of the duct.

¹Originally submitted as a doctoral thesis at Case Institute of Technology under professor Harold G. Elrod.

The results are related to measurable quantities in the form of.

- (1) Flame-front displacement
- (2) Phase velocity
- (3) To a first approximation, the effect of disturbance frequency on flame propagation velocity

The experimental part of the program consisted of imposing disturbances of various frequencies upon a flame stabilized in a duct and measuring the effects through shadow photography and photomultiplier probe surveys. The efforts to verify elements of the theory are encouraging but not conclusive. Reasonable agreement is achieved in the comparison of flame-front displacement and phase velocity. In the measurements of the effect of frequency of disturbance on flame speed, there appeared to be a most-effective frequency, just twice the most-amplified frequency given by theory.

There is no direct evidence of transition due to those disturbances. The flow was turbulent in all cases owing to transition in the flameholder boundary layer, either on the flameholder or near the point of separation. There was evidence, however, that the base turbulent flame, wrinkled by the long-wavelength disturbances, was altered (made more turbulent) when the disturbances were present. In other words, the large-amplitude, long-wavelength disturbances cause a sort of transition in the already turbulent flow, amplifying the smaller scale disturbances present.

INTRODUCTION

This work investigates the stability of the flow field arising from an anchored flame in a duct, a subject which is of interest for two reasons:

- (1) Experimental investigations have shown that the turbulent flame speeds attained in a flame anchored in a duct depend more strongly on the turbulence originating in the shear regions generated by the flameholder and flame than on the turbulence in the incident gas stream.
- (2) Some transverse modes of burner resonance encountered have been accompanied by an increase in the rate of flame propagation.

DEPENDENCE OF TURBULENT FLAME SPEED ON DISTURBANCES

ORIGINATING IN SHEAR REGIONS

The problem of describing the flow field that arises when a flame is anchored in a duct was first posed and solved by Scurlock (ref. 1). One result of this work was the relation between the fraction of mixture burned and the local flame width. Scurlock used this result to measure

turbulent flame speeds in an experiment originally designed to give the effect of inlet turbulence on flame speeds. He found that turbulence associated with two regions of shear flow masked, to a great extent, the effect of imposed stream turbulence. These two regions consist of the near wake of the flameholder and the shear region associated with the fully developed flame in a duct. The latter shear region is caused by the pressure gradient acting on gases of different densities. Scurlock calculated the velocity profile in this region.

3877
CY-1 back
In flow past cylinders without flames, eddies are encountered. Scurlock found that the flame seated on a cylindrical flameholder prevented eddies from shedding from the flameholder over the range of Reynolds numbers investigated (up to approximately 15,000). Haddock (ref. 2) and Zukowski (ref. 3) in investigating the mechanism of flame seating on cylindrical rods found that the boundary layer separating from either side of the rod underwent transition from laminar to turbulent flow. The transition point was found to approach the point of separation at a Reynolds number of about 10^4 . The work of references 2 and 3 shows that transition in the flameholder boundary layer is one mechanism for producing turbulence in the shear region near the flameholder.

The role played by the second shear region cited by Scurlock as a source of turbulence has not been directly investigated. After obtaining experimental results similar to those of Scurlock, several investigators (e.g., refs. 4 and 5) have arrived at the conclusion that turbulence is generated in this region. The types of argument leading to these conclusions are briefly indicated in the following discussion.

Theories of turbulent flame propagation have been postulated for two types of turbulence:

- (1) Turbulence with a scale small compared to a laminar flame-front thickness
- (2) Turbulence with a scale large compared with laminar flame-front thickness (refs. 6 to 8)

Experiments conducted in the absence of shear regions gave good agreement between values predicted by the large-scale turbulence theory and experimental values of flame speed (refs. 9 to 12). Experiments conducted in the presence of shear regions (refs. 5, 8, and 13) gave flame speeds higher than those predicted by theory.

There is a current controversy concerning the interpretation of this difference (refs. 5, 8, and 13 to 16). There is general agreement that, when a shear region exists and the shear region in question is of the type associated with an anchored flame in a duct, the higher flame speed is due in part to turbulence amplified by or originating in this shear region.

Rayleigh (ref. 17) observed that some jets and diffusion flames are sensitive to certain imposed transverse disturbances. He performed an inviscid stability analysis on a \wedge velocity profile and found the profile unstable to antisymmetric disturbances, but neutrally stable to symmetric wavy disturbances. This result agreed with his observations on sensitive flames and jets. Some of the limitations of Rayleigh's work are considered in the section THEORY: STABILITY OF FLOW FOR A FLAME IN A DUCT. The analytical method used by Rayleigh is applied in the present examination of the instability of flame-zone flow to imposed disturbances.

EFFECT OF COMBUSTOR OSCILLATIONS IN INCREASING RATE OF FLAME PROPAGATION

A great variety of combustion-chamber resonances have been observed in jet-engine combustors (refs. 18 to 21). These resonances most often involve some mode of acoustic oscillation in the combustion chamber. Reference 18 discusses modes that involve longitudinal gas and flame motion and reports a falloff in combustor performance when these oscillations occur.

Reference 19 discusses a type of resonance identified as a transverse mode of oscillation in the combustion chamber. Accompanying this type of oscillation was an apparent increase in combustion efficiency (ref. 19) and in the rate of flame spreading (ref. 20). There is a possibility that this type of oscillation with an acoustic wavelength controlled by duct dimensions could excite a wavy disturbance that would subsequently be amplified by the flame-generated shear region.

Unfortunately, these transverse modes (called screech) also cause the destruction of the burner walls when the screech becomes severe enough (ref. 20). In reference 21, pictures are shown of the flame near the flameholder when a combustor was resonating in a transverse mode. A strong interaction was apparent in the form of flame wrinkles forming at the flameholder and growing in amplitude as they moved downstream. It seems apparent that at least one of the ways the transverse oscillation increases the rate of flame spreading is by wrinkling, hence extending, the interface between the burned and unburned gases.


If the oscillation that disturbs the flame at the flameholder is supplied locally (by some suitable exciting mechanism) at the flameholder without relying on the sometimes destructive combustor resonance to do the exciting, some of the benefits of screech can be realized without its penalties. The gains in flame speed should be greatest for those frequencies of excitation that are amplified by the flame. It is hoped that

by examining the sensitivity of a flame in a duct to imposed disturbances an excitation frequency may be found that gives the optimum increase in flame speed.

This report is divided into three parts, theory, experiment, and discussion. A separate introduction is given for the first two parts describing the intent. The discussion weighs the results of the other parts and contains some extrapolations.

SYMBOLS

The principal symbols are defined in the following list; special symbols are defined where used.

$(A_D/A_U)_A$	ratio of turbulent undisturbed flame surface area to disturbed flame surface area measured from flame photographs
$(A_D/A_U)_P$	ratio of turbulent undisturbed flame surface area to disturbed flame surface area measured by photomultiplier
$a, A, B,$ C, D	constants of integration
b	width of shear region in Rayleigh's problem
b'	half-width of plateau in velocity profile 
c	complex phase velocity, ft/sec
c_i	imaginary part of complex phase velocity
c_r	real part of complex phase velocity
F	fraction burned
f	frequency, cps
g	gain; $v' = v'_0 g \frac{1}{K}$
g'	gain; $v' = v'_0 g' \frac{1}{K'}$
h	flame-front displacement from mean, ft
h_1	duct half-width, ft

h_2	flame half-width, ft
i	imaginary number, $\sqrt{-1}$
K_1	constant, $\frac{dh_2}{dx}$ for an assumed flame-spreading mechanism
K_2	constant, $\frac{dF}{d \frac{x}{h_1}}$
L_x	Eulerian scale of turbulence, ft
l_f	length of flame measured from wake, ft
l_w	length of flameholder wake, ft
$\frac{n}{m}$	$\frac{r_2^2 + r_1^2}{r_2^2 - r_1^2}$
P	mean pressure, lb/sq ft
p	pressure, lb/sq ft
p'	perturbation pressure, lb/sq ft
Re	Reynolds number
S_L	laminar flame speed, ft/sec
S_T	turbulent flame speed, ft/sec
t	time, sec
U	flow velocity in x-direction, ft/sec
U_0	flow velocity in x-direction at plane of flameholder, ft/sec
U_1	flow velocity in x-direction in cold gas, ft/sec
U^*	flow velocity in x-direction at apex of hot-gas velocity profile, ft/sec
u'	disturbance velocity in x-direction, ft/sec


- 3877
- v' disturbance velocity in y-direction, ft/sec
 - x coordinate in direction of duct axis (direction of mean flow), ft
 - y coordinate at right angle to direction of mean flow, ft
 - α wave number of disturbance, ft⁻¹
 - α_0 wave number of disturbance based on initial velocity and frequency, $f2\pi/U_0$
 - α_s wave number for neutral stability based on inviscid analysis, ft⁻¹
 - β hot-gas velocity gradient, $(U^* - U_1)/h_2$, sec⁻¹
 - γ_1 $e^{-\alpha h_1}$
 - γ_2 $e^{-\alpha h_2}$
 - μ $\frac{1 + \gamma_2^2}{1 - \gamma_2^2}$
 - λ wavelength, ft
 - λ_s $\frac{2\pi}{\alpha_s}$, ft
 - ρ density, lb sec²/ft⁴
 - ρ' perturbation density, lb sec²/ft⁴
 - ρ_1 density of cold gas, lb sec²/ft⁴
 - ρ_2 density of hot gas, lb sec²/ft⁴
 - $\phi(y)$ y-distribution of disturbance amplitude, ft²/sec

THEORY: STABILITY OF FLOW FOR A FLAME IN A DUCT

INTRODUCTION

The Steady-State Flow Field of a Flame Anchored in a Duct

The problem of describing the flow field that exists when a flame is anchored in a duct was first posed and solved by Scurlock in 1948 (ref. 1). Subsequently, Tsien (ref. 22) and others (ref. 23) have elaborated on the problem. The following table summarizes Scurlock's and Tsien's assumptions and results as they pertain to the present work.

Assumptions		
Scurlock	Common	Tsien
1. Fluid is incompressible.	1. Fluid is steady-state, two-dimensional, inviscid, non-heat-conducting, non-turbulent.	1. Two cases are treated, the compressible and incompressible. In the incompressible case Scurlock's assumption (2) holds; in the compressible case, density is allowed to vary in the direction of flow.
2. Density jumps from ρ_1 to ρ_2 across the flame front, is constant in each region.	2. Velocity, density, and pressure are uniform at combustion inlet.	2. The density ratio is a constant across the flame front at any station.
	3. Static pressure is uniform at any cross section.	3. The velocity profile is composed of four straight-line segments.
	4. The flameholder is of negligible size, spans the combustor.	
	5. The flame front is of negligible thickness.	
	6. The chamber is of constant width.	
Results		
1. Velocity profile as a function of flame width:  (slightly concave to incoming gas.)	1. Fraction burned as a function of flame width	1. Peak hot-gas velocity as a function of flame width
2. Momentum pressure drop as a function of flame width (i.e., of fraction burned)	2. Cold-gas velocity as a function of flame width	2. Limiting inlet velocity beyond which complete combustion cannot occur as a function of density ratio (for compressible case)

A stability analysis is made of a parallel flow having a velocity profile approximating the one found by Scurlock by means of straight-line segments and a density distribution as taken by Scurlock, that is, constant ρ_1/ρ_2 .

The Stability Problem

The study of the origins of turbulent motion has received considerable attention in the past, particularly with respect to turbulence occurring in boundary layers. One of the ways the problem has been treated is to assume the existence of infinitesimal wavy disturbances in the flowing stream and seek the conditions under which these disturbances are amplified (refs. 24 and 25). In the application of this method to the study of the stability of the laminar boundary layer, a major objective has been to determine a minimum Reynolds number below which all disturbances decay and the effect of velocity profile on this minimum Reynolds number.

The relation between the amplification of wavy disturbances and the transition to turbulence is supposedly that one leads to the other under certain circumstances. The desire to maintain laminar flow on airfoils makes an understanding of transition an important practical problem. In 1941, Schubauer and Skramsted (ref. 26) conducted an experiment in which the disturbances introduced into a laminar boundary layer were carefully controlled. They found a relation between the wave numbers of amplified, neutral, and damped disturbances and the Reynolds number that confirmed the predictions of the infinitesimal wavy disturbance theory in almost every important respect.

The practical value of learning about the stability of a flow field created by a flame in a duct would be in furnishing information that would enable combustor designers to encourage the growth of disturbances in this region, because turbulence generally aids flame spreading. The type of information needed is (1) a range of Reynolds numbers over which the flow is unstable and (2) the type of disturbance that possesses the greatest rate of amplification within this range. In the following qualitative discussion it appears that most flames of practical interest are in a Reynolds number range (1) where amplified disturbances always exist and (2) where wavelengths of disturbances that will be amplified may be obtained, neglecting viscosity.

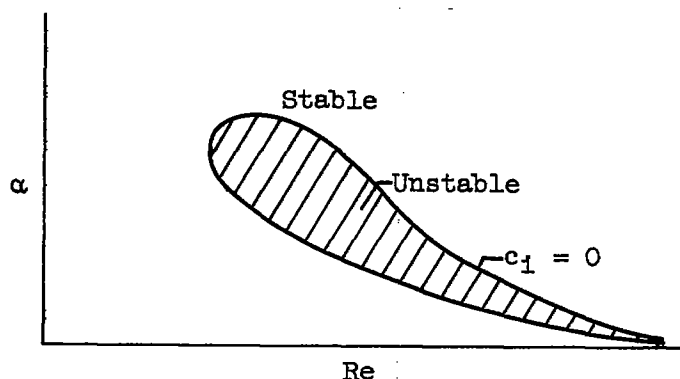
If the disturbance varies as

$$v' = \phi(y)e^{i\alpha(x-ct)}$$

where the wave number α is real, and the phase velocity c is generally complex, then, as shown by Lin (ref. 24), the stability of flows

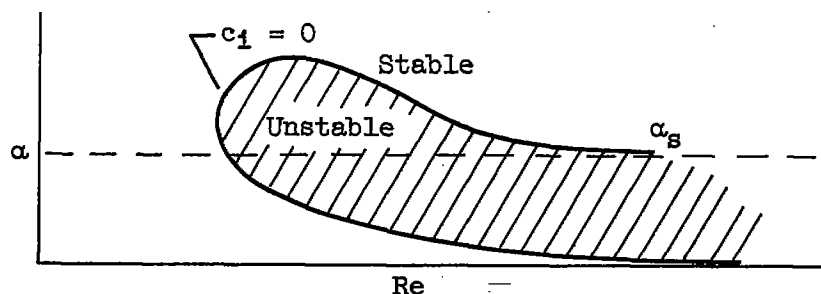
of the boundary-layer type (or of flows with symmetric profiles in a two-dimensional channel) can be illustrated by a graph of values of α for neutral stability (i.e., where the imaginary part of c vanishes) against Reynolds number Re . Two types of profile are discussed.

A profile without a point of inflection would possess the following plot of α against Re for $c_1 = 0$:



This curve is called the neutral envelope for the profile in question. Inside the envelope, disturbances are amplified ($c_i > 0$); outside, disturbances are damped ($c_i < 0$). Proceeding to the right from the minimum Reynolds number attained by the $c_1 = 0$ curve are two branches of the curve $c_1 = 0$. As Re becomes indefinitely great, both asymptotically approach $\alpha = 0$.

For the profile with a point of inflection, a similar relation $\alpha(c, Re)$ is obtained, as shown in the following graph



The significant difference between this plot for a profile with an inflection point and the preceding plot for a profile without an inflection point is that the asymptotic values of the two branches approach different limits for large values of Re . The upper branch approaches $\alpha = \alpha_s$, the wave number for neutral stability obtained by neglecting viscosity; the lower branch approaches $\alpha = 0$ as it does for a profile without an inflection point. The Reynolds number range over which the flow with an inflection point is unstable extends to indefinitely large Reynolds numbers. The flow generated by a flame in a duct has, in effect, an inflection point.

It is desirable either by example or direct calculation to determine the order of magnitude of the Reynolds number range over which the neutral α departs from α_s , that is, where viscosity has a dominating influence. In two examples in the literature, Pretsch (ref. 27) and Lessen (ref. 28) examined a flow with a flex for stability. In both instances the minimum Reynolds number for $c_1 = 0$ was of the order of 10; the maximum Re , where α for $c_1 = 0$ differed from α_s calculated from inviscid theory by more than 2 percent, was of the order of 10^3 . The profile of reference 27 is for a boundary layer with pressure rise; that of reference 28 for the free boundary layer between streams of differing velocities.

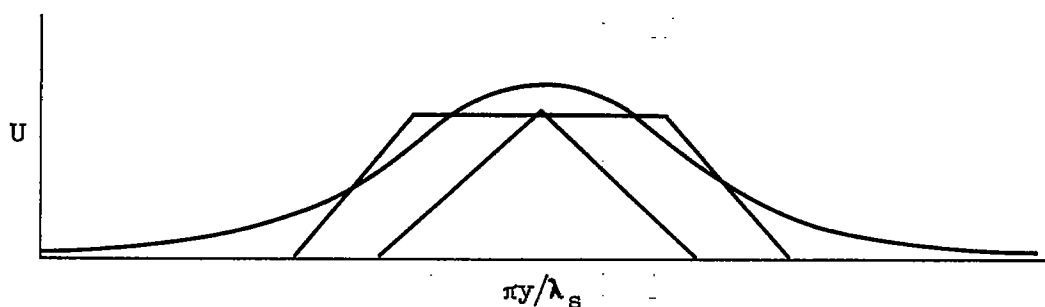
If these values are taken to suggest the order of Reynolds number where the stability of a profile with a flex is sensitive to the effects of viscosity, some idea of flame-zone sizes can be estimated for the range of velocities encountered in jet engines, that is, 50 to 500 feet per second. For example, at 50 feet per second, the flame width where viscous forces would be important would range from $1/3000$ to $1/30$ inch. At 500 feet per second, the range is $1/30,000$ to $1/300$ inch. Most of the flame zones of practical interest are much wider than these dimensions and may be considered well within the range of Reynolds numbers where disturbances are amplified and where viscosity effects are small. Therefore, there is reason to expect the following inviscid stability analysis to give meaningful information on the value of the wave numbers α where amplification can occur.

Lin (ref. 24) and Heisenberg (ref. 29) have criticized the use of broken-line profiles because there is a separate solution for c for each corner of the profile. These objections might be met by the following observations:

(1) The steady-state flow field solved by Scurlock possesses corners (places where the velocity gradient jumps) and can be very closely approximated by straight-line segments without introducing new corners into the profile. The jumps in velocity gradient that occur at the corners result from the assumption that the flame front is of negligible thickness compared to the width of the flame zone.

(2) In the results that follow it is found that the flame zone is unstable to disturbances having wavelengths 2.5 times the flame-zone width and greater. Thus, any rounding of the corners over a distance that is small compared to the flame-zone width should not affect the results; to the long wavelength disturbances that are amplified, the corners will still appear sharp.

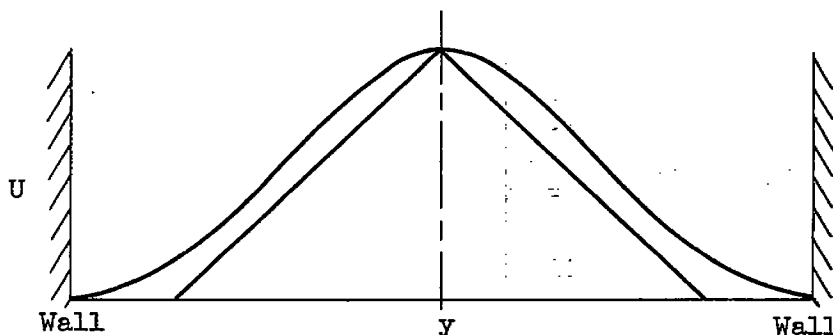
To examine by example the effect of corners in a velocity profile, three profiles of a similar shape are shown in the following sketch. Each of these profiles has been examined for instability and a wavelength for neutral stability has been computed. The scale of the abscissa is chosen so that the value of the neutral wavelength is the same for the three profiles.



The two broken-line profiles are from Rayleigh (ref. 17); the continuous profile from Savic (ref. 30). These solutions correspond to an anti-symmetric disturbance. The flow in each case is inviscid.

A similar comparison can be made between the velocity profile

$U = 1 + \sin\left(\frac{2\pi y}{l} - \frac{\pi}{2}\right)$ treated briefly by Lin (ref. 24) and a corresponding broken-line approximation. Lin's result yields $\alpha_s l = \pi\sqrt{3}$ for the sine profile. Equation (37) in the following analysis was used to obtain the dimensions of a profile having the same $\alpha_s l$. The following two profiles are given for flow between parallel walls, v' vanishing at the walls.



Because the widths of the profiles composed of broken-line segments are so nearly equal to those (having identical neutral wave numbers) whose velocity gradients are continuous, it is believed that the broken-line profile as used here has not involved the introduction of extraneous solutions.

Interpreting the Results of the Stability Analysis

The stability analysis gives an amplification rate αc_i and a phase velocity c_r for disturbances as functions of the wave number α and the fraction of duct occupied by flame h_2/h_1 for any one station along the axis of the duct. From this information a stability map is constructed. The stability map consists of a plot of contours of constant αc_i on an $\alpha h_1 - h_2/h_1$ grid. This is a generalized map and contains no assumption regarding the rate of change of flame width with distance. Lines of constant frequency are shown on the stability map calculated from the phase velocity c_r . From the map and an assumption of the nature of flame-spreading rates, the total amplification of a disturbance of given frequency is calculated.

Some aspects of this information are reduced to measurable quantities that can subsequently be compared with experimental results. These quantities include

- (1) Qualitative dependence of turbulent flame-spreading rate on disturbance frequency
- (2) Relation between critical wave number and flame width
- (3) Qualitative behavior of amplified disturbances as affected by the steady-state condition (velocity, fuel-air ratio)

The section Effect of Flameholder deals with the effect of a flameholder of finite size on the steady-state profile and, hence, on the stability analysis.

STABILITY ANALYSIS

Steady-State Solution

It might be well first to tabulate the equations derived by Tsien (ref. 22) relating U_1 , U_0 , U^* , ρ_1/ρ_2 , h_2/h_1 and fraction burned F . These relations are based on the assumption that the velocity profile can be approximated by straight-line segments.

For the incompressible case:

Apex velocity:

$$\frac{U^*}{U_0} = \sqrt{1 + \frac{\rho_1}{\rho_2} \left[\left(\frac{U_1}{U_0} \right)^2 - 1 \right]} \quad (1)$$

Hot-gas velocity distribution:

$$\frac{U}{U_0} = \sqrt{1 + \frac{\rho_1}{\rho_2} \left[\left(\frac{U_1}{U_0} \right)^2 - 1 \right]} - \left\{ \sqrt{1 + \frac{\rho_1}{\rho_2} \left[\left(\frac{U_1}{U_0} \right)^2 - 1 \right]} - \frac{U_1}{U_0} \right\} \frac{y}{h_2} \quad (2)$$

Flame width:

$$\frac{h_2}{h_1} = \frac{\frac{U_1}{U_0} - 1}{\left(1 - \frac{1}{2} \frac{\rho_2}{\rho_1} \right) \frac{U_1}{U_0} - \frac{1}{2} \frac{\rho_2}{\rho_1} \sqrt{1 + \frac{\rho_1}{\rho_2} \left[\left(\frac{U_1}{U_0} \right)^2 - 1 \right]}} \quad (3)$$

Fraction burned:

$$F = 1 - \frac{U_1}{U_0} \left(1 - \frac{h_2}{h_1} \right) \quad (4)$$

The hot-gas distribution (eq. (2)) and the relation between h_2/h_1 and U_1/U_0 (eq. (3)) are used in interpreting the results of the stability analysis. In the analysis the hot-gas velocity distribution (eq. (2)) is represented by

$$U = U_1 + (h_2 - y)\beta \quad (y > 0)$$

$$U = U_1 + (h_2 + y)\beta \quad (y < 0)$$

where

$$\beta = (U^* - U_1)/h_2$$

Nothing is said about the distribution of h_2/h_1 with distance x . This must come from further assumptions regarding flame slope, flame

speed, or rate of change of F with x . For the present it is sufficient to say that the rate of change of h_2/h_1 with x is small; that is,

$$\frac{\partial(h_2/h_1)}{\partial x} \lambda \ll \frac{h_2}{h_1}$$

where λ is the wavelength of a disturbance of interest.

The stability of the profile assumed by Tsien, which closely approximates that calculated by Scurlock, is treated as a parallel-flow problem.

First-Order Disturbance Problem

Two excellent summary papers are available on the stability of parallel flows, one by Lin (ref. 24) and one by Pillow (ref. 25). No attempt to review the field is made herein. The method employed here dates back to some of Rayleigh's early work (ref. 17) with very slight modification. The development of the disturbance equation that follows is from Goldstein (ref. 31).

The flow is assumed parallel, inviscid, incompressible, plane, and non-heat-conducting. Gravity is neglected. The equations of motion are

$$\frac{\partial p}{\partial x} = -\rho \left(\frac{\partial u}{\partial t} + u \frac{\partial u}{\partial x} + v \frac{\partial u}{\partial y} \right) \quad (5)$$

$$\frac{\partial p}{\partial y} = -\rho \left(\frac{\partial v}{\partial t} + u \frac{\partial v}{\partial x} + v \frac{\partial v}{\partial y} \right) \quad (6)$$

The fluid is assumed incompressible (but the density is allowed to vary with y), so that

$$\frac{\partial \rho}{\partial t} + u \frac{\partial \rho}{\partial x} + v \frac{\partial \rho}{\partial y} = 0 \quad (7)$$

and the equation of continuity is

$$\frac{\partial u}{\partial x} + \frac{\partial v}{\partial y} = 0 \quad (8)$$

Let

$$\left. \begin{aligned} u &= U(y) + u'(x, y, t) \\ v &= v'(x, y, t) \\ p &= P + p'(x, y, t) \\ \rho &= \bar{\rho}(y) + \rho'(x, y, t) \end{aligned} \right\} \quad (9)$$

where primed quantities are of first order of smallness. Assume u' , v' , p' , and ρ' to vary with x and t as $e^{i\alpha(x-ct)}$ where α is real and c , in general, complex.

By substituting equation (9) in equations (5) to (8) and retaining terms of the first order, equations (5) to (8) become

$$\bar{\rho} \left[i\alpha(U - c)u' + \frac{dU}{dy} v' \right] = -i\alpha p' \quad (10)$$

$$\bar{\rho} [i\alpha(U - c)v'] = -\frac{\partial p'}{\partial y} \quad (11)$$

$$i\alpha(U - c)\rho' + v' \frac{d\bar{\rho}}{dy} = 0 \quad (12)$$

$$\frac{\partial v'}{\partial y} + i\alpha u' = 0 \quad (13)$$

Eliminating p' , ρ' , and u' from equations (10) to (13) yields an equation for v'

$$(U - c) \left(\frac{\partial^2 v'}{\partial y^2} - \alpha^2 v' \right) - v' \frac{\partial^2 U}{\partial y^2} + \frac{1}{\bar{\rho}} \frac{d\bar{\rho}}{dy} \left[(U - c) \frac{\partial v'}{\partial y} - v' \frac{\partial U}{\partial y} \right] = 0 \quad (14)$$

It is apparent that, though equations (7) and (12) are useful in defining the type of incompressible flow field assumed, they are not required to obtain the disturbance equation (14) unless it becomes necessary to specify ρ' .

Defining

$$v' = -i\alpha\phi(y)e^{i\alpha(x-ct)}$$

3877

equation (14) becomes

$$(U - c) \left(\frac{\partial^2 \phi}{\partial y^2} - \alpha^2 \phi \right) - \phi \frac{d^2 U}{dy^2} + \frac{1}{\rho} \frac{d\rho}{dy} \left[(U - c) \frac{\partial \phi}{\partial y} - \phi \frac{dU}{dy} \right] = 0 \quad (15)$$

In regions where $\bar{\rho}$ and dU/dy are constant, equation (15) reduces to

$$\frac{\partial^2 \phi}{\partial y^2} - \alpha^2 \phi = 0 \quad (16)$$

with the solution

$$\phi = A_1 e^{\alpha y} + A_2 e^{-\alpha y} \quad (17)$$

The disturbance velocities given by definition and equation (13) are

$$\left. \begin{aligned} u' &= (A_1 \alpha e^{\alpha y} - A_2 \alpha e^{-\alpha y}) e^{i\alpha(x-ct)} \\ v' &= -i\alpha(A_1 e^{\alpha y} + A_2 e^{-\alpha y}) e^{i\alpha(x-ct)} \end{aligned} \right\} \quad (18)$$

where the real part is taken in the end.

Boundary Conditions

The geometry of the flow field is shown in figure 1. The quantity β is given by $\beta = (U^* - U_1)/h_2$.

Equation (16) and the solutions (eqs. (18)) apply to each of the regions 1 to 4 considered separately. The establishment of the boundary-value problem consists in assigning suitable boundary conditions at the walls and at the boundaries of regions 1 to 4. These boundary conditions are:

- (1) v' vanishes at $y = \pm h_1$
- (2) v' is continuous at interfaces
- (3) p' is continuous at interfaces (or equivalently, the complete equation (14) integrated across each interface is satisfied)

Let the equation of the interface at $y = h_1$ be

$$y = h_1 + h(x, t) \quad (19)$$

(In the following derivation the subscripts i and j represent conditions evaluated in a region i or j .) Then, to the first order of approximation, at the interface,

$$v' = \frac{\partial h}{\partial t} + U \frac{\partial h}{\partial x} \quad (20)$$

where U is the mean velocity at the interface. In order for the pressure to be continuous at the interface, it is necessary that

$$\frac{dp_i}{dx_1} = \frac{dp_j}{dx_1}$$

where x_1 is along the interface, or equivalently in the x, y -system

$$\frac{\partial p_i}{\partial x} + \frac{\partial p_i}{\partial y} \frac{\partial h}{\partial x} = \frac{\partial p_j}{\partial x} + \frac{\partial p_j}{\partial y} \frac{\partial h}{\partial x} \quad (21)$$

where at the interface

$$\frac{\partial y}{\partial x} = \frac{\partial h}{\partial x}$$

From the equation of motion,

$$\frac{\partial p}{\partial x} = -\rho \left(\frac{\partial u}{\partial t} + u \frac{\partial u}{\partial x} + v \frac{\partial u}{\partial y} \right)$$

$$\frac{\partial p}{\partial y} = -\rho \left(\frac{\partial v}{\partial t} + u \frac{\partial v}{\partial x} + v \frac{\partial v}{\partial y} \right)$$

where

$$u = U + u'$$

$$v = v'$$

$$p = P + p'$$

By retaining terms of 0 and first-order approximations,

$$\left. \begin{aligned} \frac{\partial p}{\partial x} &= \frac{\partial p'}{\partial x} = -\rho \left(\frac{\partial u'}{\partial t} + U \frac{\partial u'}{\partial x} + v' \frac{\partial U}{\partial y} \right) \\ \frac{\partial p}{\partial y} &= \frac{\partial p'}{\partial y} = -\rho \left(\frac{\partial v'}{\partial t} + U \frac{\partial v}{\partial x} \right) \end{aligned} \right\} \quad (22)$$

or $\partial p/\partial x$ and $\partial p/\partial y$ are first-order terms. But, from equation (20), it is clear that $\partial h/\partial x$ is of the first order so that the products $(\partial p/\partial y)(\partial h/\partial x)$ are of the second order, and equation (21) becomes

$$\frac{\partial p_i}{\partial x} = \frac{\partial p_j}{\partial x} \quad (23)$$

or

$$\rho_i \left(\frac{\partial u_i}{\partial t} + U_i \frac{\partial u_i}{\partial x} + v_i \frac{\partial U_i}{\partial y} \right) = \rho_j \left[\frac{\partial u_j}{\partial t} + U_j \frac{\partial u_j}{\partial x} + v_j' \left(\frac{\partial U_j}{\partial y} \right) \right] \quad (24)$$

at the interface between the regions i and j . Equation (24) results from a necessary condition for the pressure to be continuous at surfaces where \bar{p} or dU/dy undergo jumps.

In order to show that this condition is equivalent to requiring that the integrated equation (14) be satisfied at the interface, equation (14) is written

$$\frac{\partial}{\partial y} \left\{ \bar{p} \left[(U - c) \frac{\partial v'}{\partial y} - v' \frac{\partial U}{\partial y} \right] \right\} - \bar{p}(U - c)\alpha^2 v' = 0 \quad (25)$$

Integrating across the interface, equation (25) becomes

$$\bar{p}_i \left[(U_i - c) \frac{\partial v_i}{\partial y} - v_i' \frac{\partial U_i}{\partial y} \right] = \bar{p}_j \left[(U_j - c) \frac{\partial v_j}{\partial y} - v_j' \frac{\partial U_j}{\partial y} \right]$$

which, with the insertion of the continuity equation, becomes

$$\bar{p}_i \left[(U_i - c) \frac{\partial u_i}{\partial x} + v_i' \frac{\partial U_i}{\partial y} \right] = \bar{p}_j \left[(U_j - c) \frac{\partial u_j}{\partial x} + v_j' \frac{\partial U_j}{\partial y} \right] \quad (26)$$

But u' varies as $e^{i\alpha(x-ct)}$, so that equation (26) can be recognized as another way of writing equation (24).

The boundary conditions can be written

$$v_1' = 0 \quad \text{at} \quad y = h_1 \quad (27a)$$

$$v_1' = v_2' \quad \text{at} \quad y = h_2 \quad (27b)$$

$$\frac{\partial p_1'}{\partial x} = \frac{\partial p_2'}{\partial x} \quad \text{at} \quad y = h_2 \quad (27c)$$

$$v_2' = v_3' \quad \text{at} \quad y = 0 \quad (27d)$$

$$\frac{\partial p_2'}{\partial x} = \frac{\partial p_3'}{\partial x} \quad \text{at} \quad y = 0 \quad (27e)$$

$$v_3' = v_4' \quad \text{at} \quad y = -h_2 \quad (27f)$$

$$\frac{\partial p_3'}{\partial x} = \frac{\partial p_4'}{\partial x} \quad \text{at} \quad y = -h_2 \quad (27g)$$

$$v_4' = 0 \quad \text{at} \quad y = -h_1 \quad (27h)$$

where the subscripts 1 to 4 denote flow regions.

Solution of the Boundary Value Problem

The solutions of equation (16) for regions 1 to 4 (fig. 1) are written as follows:

$$\left. \begin{array}{l} \text{Region 1} \quad \phi_1 = A_1 e^{\alpha y} + A_2 e^{-\alpha y} \\ \text{Region 2} \quad \phi_2 = B_1 e^{\alpha y} + B_2 e^{-\alpha y} \\ \text{Region 3} \quad \phi_3 = C_1 e^{\alpha y} + C_2 e^{-\alpha y} \\ \text{Region 4} \quad \phi_4 = D_1 e^{\alpha y} + D_2 e^{-\alpha y} \end{array} \right\} \quad (28)$$

Inserting equations (28) into equations (27) results in eight equations in the eight unknowns A_1, A_2, \dots, D_2 . The requirement that A_1, A_2, \dots, D_2 have nontrivial solutions is

3877

$$\begin{bmatrix}
 1 & r_1^2 & 0 & 0 & 0 & 0 & 0 & 0 \\
 1 & r_2^2 & -1 & -r_2^2 & 0 & 0 & 0 & 0 \\
 \frac{\rho_1}{\rho_2} (u_1 - c) & -\frac{\rho_1}{\rho_2} (u_1 - c) r_2^2 & -\left[(u_1 - c) + \frac{\beta}{\alpha} \right] & \left[(u_1 - c) - \frac{\beta}{\alpha} \right] r_2^2 & 0 & 0 & 0 & 0 \\
 0 & 0 & 1 & 1 & -1 & -1 & -1 & -1 \\
 0 & 0 & (u^* - c) + \frac{\beta}{\alpha} & -\left[(u^* - c) - \frac{\beta}{\alpha} \right] & -\left[(u^* - c) - \frac{\beta}{\alpha} \right] & \left[(u^* - c) + \frac{\beta}{\alpha} \right] & 0 & 0 \\
 0 & 0 & 0 & 0 & r_2^2 & 1 & -r_2^2 & 1 \\
 0 & 0 & 0 & 0 & \left[(u_1 - c) - \frac{\beta}{\alpha} \right] r_2^2 & -\left[(u_1 - c) + \frac{\beta}{\alpha} \right] & -\frac{\rho_1}{\rho_2} (u_1 - c) r_2^2 & \frac{\rho_1}{\rho_2} (u_1 - c) \\
 0 & 0 & 0 & 0 & 0 & 0 & r_2^2 & 1
 \end{bmatrix} = 0 \quad (29)$$

Where $r_1 \equiv e^{-\alpha h_1}$ and $r_2 \equiv e^{-\alpha h_2}$. By assigning $U_1 = 0$ (this merely alters the real part of c) and operating on rows 1, 2, 3, 6, 7, and 8, equation (29) can be reduced to the determinant

$$\begin{bmatrix}
 c - \frac{\beta}{\alpha} + \frac{n}{m} \frac{\rho_1}{\rho_2} c & \left[\frac{n}{m} \frac{\rho_1}{\rho_2} c - \left(c + \frac{\beta}{\alpha} \right) \right] r_2^2 & 0 & 0 \\
 1 & 1 & -1 & -1 \\
 h_2 \beta - c + \frac{\beta}{\alpha} & -\left(h_2 \beta - c - \frac{\beta}{\alpha} \right) & -\left(h_2 \beta - c - \frac{\beta}{\alpha} \right) & h_2 \beta - c + \frac{\beta}{\alpha} \\
 0 & 0 & \left(\frac{n}{m} \frac{\rho_1}{\rho_2} c - c - \frac{\beta}{\alpha} \right) r_2^2 & \frac{n}{m} \frac{\rho_1}{\rho_2} c + c - \frac{\beta}{\alpha}
 \end{bmatrix} = 0 \quad (30)$$

where

$$\frac{n}{m} \equiv \frac{r_2^2 + r_1^2}{r_2^2 - r_1^2}$$

On expanding and simplifying, equation (30) becomes

$$\left[c - \frac{\beta}{\alpha} \left(\frac{n}{m} \frac{\rho_1}{\rho_2} + \mu \right)^{-1} \right] \left[c^2 \left(\frac{n}{m} \frac{\rho_1}{\rho_2} \mu + 1 \right) - c \left(h_2 \beta - \frac{n}{m} \frac{\rho_1}{\rho_2} \frac{\beta}{\alpha} + h \beta \frac{n}{m} \frac{\rho_1}{\rho_2} \mu \right) + \frac{h \beta^2}{\alpha} \mu - \frac{\beta^2}{\alpha^2} \right] = 0 \quad (31)$$

where

$$\mu \equiv \frac{1 + r_2^2}{1 - r_2^2}$$

One root can be seen to be wholly real

$$c = \frac{\beta}{\alpha} \left(\frac{n}{m} \frac{\rho_1}{\rho_2} + \mu \right)^{-1} \quad (32)$$

This can be identified as the root belonging to a symmetric disturbance by assigning $v_2^i = v_3^i = 0$ at $y = 0$ in equation (27). In this case equation (30) reduces to

$$\begin{bmatrix} c - \frac{\beta}{\alpha} + \frac{n}{m} \frac{\rho_1}{\rho_2} c & \frac{n}{m} \frac{\rho_1}{\rho_2} c - \left(c + \frac{\beta}{\alpha} \right) r_2^2 \\ 1 & 1 \end{bmatrix} = 0 \quad (33)$$

which yields as before

$$c = \frac{\beta}{\alpha} \left(\frac{n}{m} \frac{\rho_1}{\rho_2} + \mu \right)^{-1}$$

The remaining two roots,

$$c = \frac{\beta}{\alpha} \left\{ \frac{h_2 \alpha + \frac{n}{m} \frac{\rho_1}{\rho_2} (\mu \alpha h_2 - 1) \pm \sqrt{\left[h_2 \alpha + \frac{n}{m} \frac{\rho_1}{\rho_2} (\mu \alpha h_2 - 1) \right]^2 - 4 \left(\frac{n}{m} \frac{\rho_1}{\rho_2} \mu + 1 \right) (\alpha h_2 \mu - 1)}}{2 \left(\frac{n}{m} \frac{\rho_1}{\rho_2} \mu + 1 \right)} \right\} \quad (34)$$

can similarly be identified as roots belonging to an antisymmetric disturbance. One way of doing this is to set v_2^i at $y = h_2$ equal to v_3^i at $y = -h_2$ or (from eq. (28))

$$B_1 + B_2 r_2^2 - C_1 r_2^2 - C_2 = 0 \quad (35)$$

Using equation (35) in place of equations (27f), (27g), and (27h), the determinantal equation becomes

$$\begin{bmatrix} 1 & r_2^2 & 0 & 0 & 0 & 0 \\ 1 & r_2^2 & -1 & -r_2^2 & 0 & 0 \\ \frac{\rho_1}{\rho_2}(-c) & \frac{\rho_1}{\rho_2} c r_2^2 & \left(c - \frac{\beta}{\alpha}\right) r_2^2 & -\left(c + \frac{\beta}{\alpha}\right) r_2^2 & 0 & 0 \\ 0 & 0 & 1 & 1 & -1 & -1 \\ 0 & 0 & -c + \frac{\beta}{\alpha} & c + \frac{\beta}{\alpha} & c + \frac{\beta}{\alpha} & -c + \frac{\beta}{\alpha} \\ 0 & 0 & 1 & r_2^2 & -r_2^2 & -1 \end{bmatrix} = 0 \quad (36)$$

with roots of equation (34) for c as before. That the root for the symmetric disturbance $c = \frac{\beta}{\alpha} \left(\frac{n}{m} \frac{\rho_1}{\rho_2} + \mu \right)^{-1}$ is wholly real implies neutral stability. For the symmetric disturbance, then, the inviscid analysis does not yield information on wave numbers where amplification occurs, but merely suggests that the profile is relatively stable to symmetric disturbances and neutrally stable in the limit of infinite Reynolds number.

The roots corresponding to the antisymmetric disturbances (eq. (34)) are complex when

$$4 \left(\frac{n}{m} \frac{\rho_1}{\rho_2} \mu + 1 \right) (\alpha h_2 \mu - 1) > \left[h_2 \alpha + \frac{n}{m} \frac{\rho_1}{\rho_2} (\mu \alpha h_2 - 1) \right]^2 \quad (37)$$

The complex root having the positive imaginary part corresponds to an amplified disturbance. The denominator of the right side of equation

(34), $2\left(\frac{n}{m} \frac{\rho_1}{\rho_2} \mu + 1\right)$, when written in full,

$$2\left(\frac{\rho_1}{\rho_2} \frac{e^{-2\alpha h_2} + e^{-2\alpha h_1}}{e^{-2\alpha h_2} - e^{-2\alpha h_1}} \frac{1 + e^{-2\alpha h_2}}{1 - e^{-2\alpha h_1}} + 1\right)$$

is positive for $h_2 < h_1$, that is, for the flame zone contained within the duct. Therefore, the amplified root of equation (34) is

$$c = \frac{\beta}{\alpha} \left\{ \frac{h_2\alpha + \frac{n}{m} \frac{\rho_1}{\rho_2} (\mu\alpha h_2 - 1) + \sqrt{\left[h_2\alpha + \frac{n}{m} \frac{\rho_1}{\rho_2} (\mu\alpha h_2 - 1)\right]^2 - 4\left(\frac{n}{m} \frac{\rho_1}{\rho_2} \mu + 1\right)(\alpha h_2 \mu - 1)}}{2\left(\frac{n}{m} \frac{\rho_1}{\rho_2} \mu + 1\right)} \right\} \quad (38)$$

Because this is an inviscid analysis, the damped root of equation (34) can have no meaning (ref. 24) and is subsequently ignored.

RESULTS

The disturbance amplitude grows with time as $e^{\alpha c_1 t}$, where αc_1 from equation (38) is

$$\alpha c_1 = \frac{\Delta U}{2h_2} \sqrt{\frac{\left[h_2\alpha + \frac{n}{m} \frac{\rho_1}{\rho_2} (\mu\alpha h_2 - 1)\right]^2}{\frac{n}{m} \frac{\rho_1}{\rho_2} \mu + 1} - 4 \frac{\alpha h_2 \mu - 1}{\frac{n}{m} \frac{\rho_1}{\rho_2} \mu + 1}} \quad (39)$$

Since

$$\beta = \frac{U^* - U_1}{h_2} = \frac{\Delta U}{h}$$

The quantity under the radical in equation (39) is independent of local $\frac{U^* - U_1}{h_2}$ values. This quantity is plotted in figure 2 as a function $2\alpha h_2$ for the following conditions:

$$\frac{\rho_1}{\rho_2} = 1 \quad \lim_{h_1 \rightarrow \infty} \frac{h_2}{h_1} = 0$$

$$\frac{\rho_1}{\rho_2} = 5, 7 \quad \frac{h_2}{h_1} = 0.25, 0.50, 0.75$$

The first set of conditions corresponds to Rayleigh's solution for the stability of an unconfined jet. The latter set of conditions represents density ratios that are expected in a flame in a duct for three flame widths.

The values of the parameter $\alpha c_1(2h_2/\Delta U)$ in figure 2 go from 0 at $2\alpha h_2 = 0$ through a maximum, then to 0 again at a finite value of $2\alpha h_2$. For a given value of $2h_2/\Delta U$, this parameter behaves as the amplification rate αc_1 .

It is clear from figure 2 that, for constant density, the flow is more unstable the smaller h_2/h_1 becomes. For constant h_2/h_1 , the flow is more unstable the smaller ρ_1/ρ_2 becomes.

The influence of density ratio and wall proximity on the stability of the subject profile is in keeping with experimental observations of another type of profile with a flex, namely, the wake of a cylindrical rod. The stabilizing effect of density ratio is illustrated in reference 1, wherein it is noted that a flame anchored in the wake of the rod inhibits vortex shedding. The stabilizing effect of wall proximity is illustrated in reference 32 wherein it is noted that wall proximity increases the minimum Reynolds number for the occurrence of shed vortices.

The stabilizing influence of the walls is further illustrated in figure 3. Figures 3(a) and (b) show the values of $2\alpha h_2$ for neutral stability and maximum instability plotted against h_2/h_1 . Figure 3(c) shows the amplification parameter $\alpha c_1(2h_2/\Delta U)$ for maximum amplification rate plotted against h_2/h_1 . Both the amplification rate and the range of the parameter $2\alpha h_2$ diminish as the flame fills the duct.

Construction of Stability Map

In considering the effect of disturbance amplification in the flame zone, local-growth-rate contours as a function of wave number and flame-width ratio h_2/h_1 present nearly all the important information. Such a plot is called the stability map of a flame in a duct. The map is constructed from the data of figures 2 and 3 and from the steady-state relation of U^*/U_0 and U_1/U_0 as functions of h_2/h_1 (eqs. (1) and (3))

in the following manner: Given: $\frac{U_1}{U_0} \left(\frac{h_2}{h_1} \right)$, $\frac{U^*}{U_0} \left(\frac{h_2}{h_1} \right)$, and

$\alpha c_1 \frac{2h_2}{\Delta U} \left(2\alpha h_2, \frac{h_2}{h_1} \right)$ for a given $\frac{\rho_1}{\rho_2}$. The quantity desired is

$\alpha c_1 \frac{2h_1}{U_0} \left(2\alpha h_1, \frac{h_2}{h_1} \right)$. This quantity is obtained through suitable cross

plots of figures 2 and 3 and equations (1) and (3) by setting $2\alpha h_1 = 2\alpha h_2 / (h_2/h_1)$:

$$\alpha c_1 \frac{2h_1}{U_0} = \alpha c_1 \frac{2h_2}{U^* - U_1} \times \frac{\frac{U^*}{U_0} - \frac{U_1}{U_0}}{h_2/h_1} \quad (40)$$

The resulting stability map is shown in figure 4. Contours of constant dimensionless amplification rates $\alpha c_1 \frac{2h_1}{U_0}$ are shown as functions of the dimensionless wave number $2\alpha h_1$ and dimensionless flame width h_2/h_1 for $\rho_1/\rho_2 = 7$ (fig. 4(a)) and $\rho_1/\rho_2 = 5$ (fig. 4(b)). These contours are in a region bounded by $2\alpha h_1 = \infty, 0$; $h_2/h_1 = 0$; and the line of $2\alpha h_1$ for neutral stability, that is, the critical $2\alpha h_1$ as a function of h_2/h_1 .

Phase Velocity

A disturbance that distorts the flow and therefore distorts the flame front has a wavelength $\lambda = 2\pi/\alpha$. Such a disturbance if introduced at the flameholder travels along the flame front at the phase velocity c_r . This can be seen from the variation of the disturbance with x distance and time; that is,

$$v' \sim e^{i\alpha(x-ct)} = e^{\alpha c_1 t} e^{i\alpha(x-c_r t)}$$

In order to follow the amplification rate of a given disturbance, it is necessary to follow a disturbance of constant frequency.

The relation between frequency and wavelength is

$$f = \frac{c_r}{\lambda} = \frac{\alpha c_r}{2\pi} \quad (41)$$

The quantity $\frac{c_r - U_1}{U^* - U_1}$ from equation (38) is given by

$$\frac{c_r - U_1}{U^* - U_1} = \frac{1}{\alpha h_2} \frac{h_2 \alpha + \frac{n}{m} \frac{\rho_1}{\rho_2} (\mu \alpha h_2 - 1)}{2 \left(\frac{n}{m} \frac{\rho_1}{\rho_2} \mu + 1 \right)} \quad (42)$$

for

$$\left[h_2 \alpha + \frac{n}{m} \frac{\rho_1}{\rho_2} (\mu \alpha h_2 - 1) \right]^2 - 4 \left(\frac{n}{m} \frac{\rho_1}{\rho_2} \mu + 1 \right) (\alpha h_2 \mu - 1) < 0$$

and by

$$\frac{c_r - U_1}{U^* - U_1} = \frac{1}{\alpha h_2} \frac{h_2 \alpha + \frac{n}{m} \frac{\rho_1}{\rho_2} (\mu \alpha h_2 - 1) + \sqrt{\left[h_2 \alpha + \frac{n}{m} \frac{\rho_1}{\rho_2} (\mu \alpha h_2 - 1) \right]^2 - 4 \left(\frac{n}{m} \frac{\rho_1}{\rho_2} \mu + 1 \right) (\alpha h_2 \mu - 1)}}{2 \left(\frac{n}{m} \frac{\rho_1}{\rho_2} \mu + 1 \right)} \quad (43)$$

for

$$h_2 \alpha + \frac{n}{m} \frac{\rho_1}{\rho_2} (\mu \alpha h_2 - 1) - 4 \frac{n}{m} \frac{\rho_1}{\rho_2} \mu + 1 (\alpha h_2 \mu - 1) \geq 0$$

A plot of this quantity against αh_2 is given for $\rho_1/\rho_2 = 7$ at $h_2/h_1 = 0.25, 0.50$, and 0.75 in figure 5(a). Also shown in figure 5(a) for comparison is $(c_r - U_1)/(U^* - U_1)$ for $\rho_1/\rho_2 = 5$, $h_2/h_1 = 0.25$ and $\rho_1/\rho_2 = 1$, $h_2/h_1 = 0$.

Note that

$$\lim_{\alpha h_2 \rightarrow 0} \frac{c_r - U_1}{U^* - U_1} = 0$$

From the steady-state solutions,

$$\lim_{h_2/h_1 \rightarrow 0} (U^* - U_1) = 0$$

Therefore, at the flameholder $c_r = U_1 = U_0$. Then it is convenient to relate the local wave number to the wave number at the flameholder by

$$\alpha = \alpha_0 \frac{U_0}{c_r} \quad (44)$$

where α_0 is the wave number at the flameholder. It is related to the frequency of the disturbance f and U_0 by $\alpha_0 = f2\pi/U_0$. By means of equations (42), (43), (44), (1), and (3), values of $\alpha\left(\alpha_0, \frac{h_2}{h_1}\right)$ were calculated and they are shown in figure 4 as lines of constant frequency. These lines enable one to follow the local amplification rate of a disturbance of given frequency from the flameholder to some station downstream and are so employed in a later section.

An additional calculation for the phase velocity was made for later comparison with experimental data. In figure 5(b) is shown a plot of c_r/U_1 against h_2/h_1 for $\rho_1/\rho_2 = 7$ and $2\alpha_0 h_1 = 8, 12, 16$. These data enable one to compare directly measured values of phase velocity with those predicted from the stability analysis.

Disturbance Growth

Figure 6 presents a qualitative picture of the nature of the disturbances propagating at phase velocity.

The streamline distributions are given for a neutral disturbance in a reference plane moving at the phase velocity c_r ; in this frame of reference, the streamlines are no longer a function of time. There is motion relative to the "cat's eyes" of the disturbance centers. In the hot flame core, the gas moves faster than c_r ; in the colder gas outside the flame, the gas moves more slowly than c_r .

To picture what happens to an amplified disturbance, imagine the y-amplitude of the wrinkles in figure 6 to be growing from right to left. In addition the flame width is increasing gradually; c is also increasing gradually, and, therefore, the x- and y-spacing of the "cat's eyes" is increasing in the direction of flow until a neutral situation is reached.

At each x-station the disturbance has a local growth rate α_1 that acts over a short time Δt . Then (since x is related to time by $dx = c_r dt$) at any time t after the disturbance originated at the flameholder, the amplitude is

$$v' = v'_0 e^{\int_0^t \alpha_1 dt} \quad (45)$$

where v'_0 is the amplitude of the disturbance at the flameholder on the centerline of the profile.²

Up to this point, the independent variables have been the dimensionless wave number $2\alpha h_1$ and flame width h_2/h_1 . In order to evaluate equation (45), it is necessary to use the relation

$$\frac{dx}{dt} = c_r \quad (46)$$

and some assumption concerning the variation of h_2/h_1 with x . Two simple assumptions are used that bracket the variation of h_2/h_1 with x found by experiment and facilitate the integration of equation (45). These assumptions are (1) that the flame is linear:

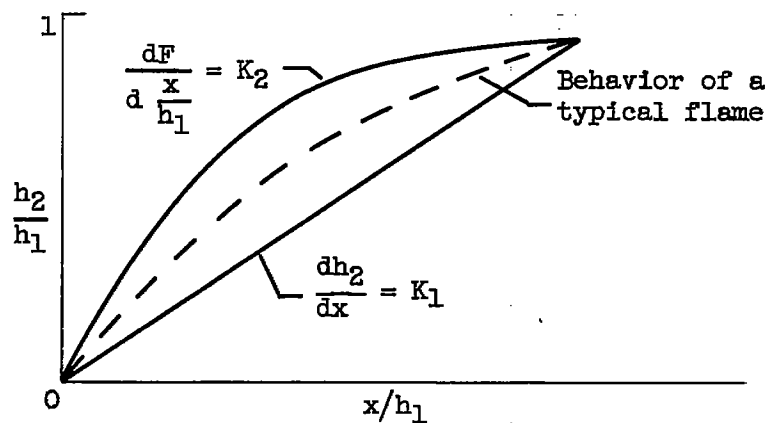
$$\frac{d \frac{h_2}{h_1}}{d \frac{x}{h_1}} = K_1 \quad (47)$$

and (2) that the change in fraction burned with distance is linear:

$$\frac{dF}{d \frac{x}{h_1}} = K_2 \quad (48)$$

²The linking of the parallel flow solutions by conserving v' along the centerline is the simplest but not necessarily the best of several available choices.

A qualitative comparison of the way these assumptions describe a flame surface is given in the following sketch:



Inserting equations (46) and (47) in equation (45) results in

$$v^* = v_0^* \left(e^{\frac{1}{2} \int_0^{h_2/h_1} \alpha c_i \frac{2h_1}{U_0} \frac{U_0}{c_r} d \frac{h_2}{h_1}} \right)^{1/K_1} \quad (49)$$

The term in parentheses is called the gain g . It is independent of the value of the propagation rate K_1 .

A similar derivation can be made for the alternate form of heat release, that is, for

$$\frac{dF}{d \frac{x}{h_1}} = K_2$$

which yields

$$v^* = v_0^* \left(e^{\frac{1}{2} \int_0^F \alpha c_i \frac{2h_1}{U_0} \frac{U_0}{c_r} dF} \right)^{1/K_2} \quad (50)$$

where the term in parentheses g^* is independent of the value of K_2 .

The values of g and g' can be obtained by graphical integration. They give relative values of amplification of a disturbance of given frequency when integrated along a constant-frequency line in figure 4.

In figure 7 are given the results of such an integration carried from $h_2/h_1 = 0$ to $h_2/h_1 = 1$ for a range of $2\alpha_0 h_1$ and for the following conditions: In figure 7(a) for $\rho_1/\rho_2 = 5, 7$, g is given as a function of $2\alpha_0 h_1$. In figure 7(b) for $\rho_1/\rho_2 = 7$, g' is given as a function of $2\alpha_0 h_1$. It is apparent from figure 7 that, for the conditions examined, there is a most-amplified frequency corresponding to a value of $2\alpha_0 h_1 \approx 6$. Recall $f = 2\alpha_0 h_1 U_0 / 2\pi 2h_1$ or the most-amplified frequency is approximately $f \approx U_0 / 2h_1$. This frequency does not depend upon a rate of flame spreading. It was obtained by assuming that a mode of flame spreading is specified. Approximately the same frequency obtains for the two modes of flame spreading specified.

In figure 7(a) not only is the most-amplified frequency at $\rho_1/\rho_2 = 5$ very near that for $\rho_1/\rho_2 = 7$, but the numerical values of the gains are very nearly the same as well. This latter occurrence is due to two opposing influences: For a given $U^* - U_1$, the profile having the lower value of ρ_1/ρ_2 has a higher amplification rate, and a disturbance of given frequency is amplified over a wider range of h_2/h_1 . On the other hand, at any value of h_2/h_1 , $U^* - U_1$ is smaller for the smaller ρ_1/ρ_2 . These opposing influences yield the results shown in figure 7(a).

The growth of the disturbances for fractional values of h_2/h_1 (or F) was calculated by taking the integral in equation (49) or (50) to fractional values of h_2/h_1 (or F). The results are shown in figures 8(a) and (b) respectively, in which the gains g and g' are plotted against h_2/h_1 or F for values of $2\alpha_0 h_1$ from 2 to 18. It can be seen that, for some values of $h_2/h_1 < 5$, there are frequencies higher than those corresponding to $2\alpha_0 h_1 \approx 6$ that locally exhibit a maximum gain. The fact that for values of $h_2/h_1 < 0.5$ there is a local amplification that depends on frequency is used later in comparing analysis with experiment. It can be seen that as h_2/h_1 decreases, the frequency that is most amplified increases.

Disturbance Velocity Distribution in y-Direction

The way the disturbance velocity v' varies along the axis of the duct is shown in figure 8. In reducing the results of this analysis to

measurable quantities, there is need for a qualitative picture of the way the disturbance velocity v' varies across the duct. Such a picture can most easily be obtained by considering a neutrally stable disturbance.

From equations (18) and (28),

$$\frac{v'_{2,y}}{v'_0} = \frac{1}{r_y} \frac{\frac{B_1}{B_2} + r_y^2}{\frac{B_1}{B_2} + 1} \quad 0 \leq y \leq h_2 \quad (51)$$

where

$v'_{2,y}$ disturbance velocity at y in region 2

v'_0 disturbance velocity at centerline

$$r_y \equiv e^{-\alpha y}$$

In the region $h_2 \leq y \leq h_1$, $v'_{1,y}/v'_{2,h_2}$ can be obtained from equations (18), (27), and (28) in the form

$$\frac{v'_{1,y}}{v'_{2,h_2}} = \frac{-r_1^2 + r_y^2}{-r_1^2 + r_2^2} \frac{r_2}{r_y} \quad (52)$$

The ratio B_1/B_2 can be obtained from the equation represented by the first row in the determinantal equation (30)

$$\left(c - \frac{\beta}{\alpha} + \frac{n}{m} \frac{\rho_1}{\rho_2} c \right) B_1 + \left(-c - \frac{\beta}{\alpha} + \frac{n}{m} \frac{\rho_1}{\rho_2} c \right) r_2^2 B_2 = 0$$

or

$$\frac{B_1}{B_2} = -r_2^2 \frac{\left[\left(\frac{n}{m} \frac{\rho_1}{\rho_2} - 1 \right) - \frac{\beta}{\alpha c} \right]}{\left[\left(\frac{n}{m} \frac{\rho_1}{\rho_2} + 1 \right) - \frac{\beta}{\alpha c} \right]} \quad (53)$$

Recall that $\beta/\alpha c$ in equation (30) is the same as $\frac{1}{\alpha h_2} \frac{U^* - U_1}{C - U_1}$, which for real values of c is given in equations (42) and (43).

A series of calculations was made to obtain the representative behavior of v_{h_2}'/v_0' across the duct, and the results are shown in figure 9 for $\rho_1/\rho_2 = 7$. The critical h_2/h_1 is taken as the value of h_2/h_1 where for a given frequency the imaginary part of c becomes 0. Figure 9(a) shows the value of v_{h_2}'/v_0' at the critical h_2/h_1 plotted against initial wave number $2\alpha_0 h_1$. It can be seen from this figure that for $2\alpha_0 h_1 > 8$ (i.e., for $(h_2/h_1)_{\text{critical}} < 0.46$) the value of $v_{h_2}'/v_0' \approx 0.2$. The ratio falls off as $2\alpha_0 h_1 < 8$ (i.e., for $(h_2/h_1)_{\text{critical}} > 0.46$) as the flame approaches the wall.

In figure 9(b) the value of the ratio v_{h_2}'/v_0' is given for a fixed frequency corresponding to $2\alpha_0 h_1 = 12$ following a disturbance along the duct from the flameholder ($h_2/h_1 = 0$) to the station where the flame touches the wall h_2/h_1 . The dotted portion is interpolated between $h_2/h_1 = 0$ where $v_{h_2}' = v_0'$ and $h_2/h_1 = (h_2/h_1)_{\text{critical}}$ where the calculation starts. It is obvious from this curve that, if one measures v_{h_2}' instead of v_0' , the apparent growth rate is not as rapid for $h_2/h_1 < (h_2/h_1)_{\text{critical}}$ as for v_0' simply because of the velocity distribution. Also, for $h_2/h_1 > (h_2/h_1)_{\text{critical}}$ there is an apparent decay in v_{h_2}' owing to this distribution, despite the fact that the value of v_0' is neutrally stable. This latter point is employed in comparing the analytical with the experimental results.

The significance of figure 9 is summarized as follows:

- (1) Although the inviscid treatment eliminates consideration of damping, it is clear that, at the flame front, the velocity amplitude diminishes at $h_2/h_1 > (h_2/h_1)_{\text{critical}}$ because of the velocity distribution.
- (2) In some instances, even though the flow is unstable and the disturbance velocity amplitude is increasing along the center of the flame, the disturbance velocity amplitude at the flame front may not necessarily be increasing.

(3) The disturbance that is most-amplified at the center of the profile (i.e., $2\alpha_0 h_1 = 6$) is not necessarily the most-amplified at the flame front, owing to the velocity distribution; the frequency of the latter is somewhat greater than the frequency of the former.

Relation of Theoretical Results to Measurable Quantities

In the experimental phase, current instrumentation techniques impose limitations on what can be measured. For example, the velocity v'_0 cannot be measured directly by hot-wire techniques because the flame temperature is too high ($\approx 4000^\circ \text{R}$). The purpose of this section is to collect certain results of the foregoing analysis that lend themselves to direct measurement.

Flame slope. - In equations (49) and (50) the growth of a disturbance v'/v'_0 is found to be proportional to a calculable quantity, gain,

raised to a power $1/K$. The quantity K is alternately $K_1 = \frac{d \frac{h_2}{h_1}}{d \frac{x}{h_1}}$ or

$K_2 = \frac{dF}{d \frac{x}{h_1}}$ depending on the mode of flame propagation assumed.

For both modes, K is smaller the more gradual the rate of flame spreading. To a first approximation, then, the amplification of a disturbance increases as the ratio of propagation velocity to flow velocity decreases. This trend can be checked experimentally.

Phase velocity. - One quantity that can be measured immediately is the phase velocity c_r . A plot of c_r/U_1 for three frequencies is given in figure 5(b). Thus, for a given flow setting both the absolute magnitudes of c_r/U_1 can be compared and the trend with frequency and with h_2/h_1 variation can be examined.

Flame-front displacement. - The transverse velocity v' acting at the flame surface $y = h_2$ causes a wavy wrinkle to appear in the surface. If a quantity h is defined as the distance from crest to valley of these wrinkles, this quantity equals twice the y amplitude of the streamlines of the flow at the flame front. If a neutral case is considered and the distribution of v' in the flame zone is approximated by

$$v' = v'_c + (v'_0 - v'_c) \left(1 - \frac{y}{y_c}\right)$$

the equations of the streamlines are given by

$$\frac{y}{y_c} \approx 1 - \epsilon \cos \alpha x \pm \sqrt{1 - 2\Psi^* + 2K \cos \alpha x}$$

where

y_c coordinate where $U = c$

$$\epsilon = \frac{v_0 - v_c}{(U^* - c)\alpha y_c}$$

Ψ^* dimensionless stream function, $\frac{1}{(U^* - c)y_c} \int_0^y U dy$

$$K = \frac{v_c}{(U^* - c)\alpha y_c}$$

v_0' amplitude of disturbance velocity at centerline

v_c' amplitude of disturbance velocity at y_c

At $h_2 \leq h_{2,critical}$, $2\Psi^*$ varies between 0.96 and 0.99. Because $2K$ can be taken arbitrarily small, for $2K/(1 - 2\Psi^*) \ll 1$,

$$\frac{y}{y_c} = 1 - \epsilon \cos \alpha x \pm \sqrt{1 - 2\Psi^*} \left[1 + \frac{K \cos \alpha x}{(1 - 2\Psi^*)} \right]$$

or, for $y > y_c$,

$$\begin{aligned} \frac{y}{y_c} &= 1 + \sqrt{1 - 2\Psi^*} + \left(\frac{K}{\sqrt{1 - 2\Psi^*}} - \epsilon \right) \cos \alpha x \\ &\approx 1 + 0.2 + \frac{1}{\alpha y_c} \left[\frac{\frac{v_c'/U_0}{U^* - U_c}}{\frac{U_0}{(0.2)}} - \frac{\frac{v_0'/U_0 - v_c'/U_0}{U^* - U_0}}{\frac{U_0}{(0.2)}} \right] \\ &\approx 1.2 + \frac{v_0'/U_0}{\alpha y_c \frac{U^* - c}{U_0}} \left(\frac{6v_c'}{v_0} - 1 \right) \end{aligned}$$

3877

CY-5 back

But v'_c/v_0 is a weak function of α and h_2/h_1 and is approximately 0.2.

Employing the identity

$$\frac{U^*}{U_0} - \frac{c}{U_0} = \left(\frac{U^*}{U_0} - \frac{U_1}{U_0} \right) \left(1 - \frac{c - U_1}{U^* - U_1} \right)$$

and a value of $(c - U_1)/(U^* - U_1)$ from figure 5(a)

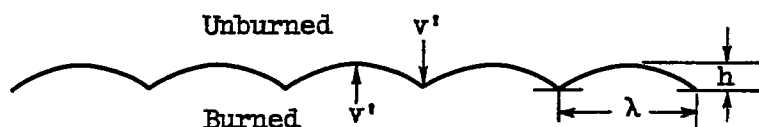
$$\frac{U^*}{U_0} - \frac{c}{U_0} = \left(\frac{U^*}{U_0} - \frac{U_1}{U_0} \right) (0.85)$$

where the quantity $U^*/U_0 - U_1/U_0$ is a function of ρ_1/ρ_2 , h_2/h_1 only. Without going into further detail, then, some predictions can be made from the theory that may be checked by experiment. First, h may be expected to behave qualitatively as shown in figure 10.

The shape of the curve in figure 10 can be used to locate the approximate x position of $(h_2/h_1)_{\text{critical}}$. There is a point of inflection where v'_{h_2/h_1} reaches a maximum and a knee as v'_{h_2/h_1} ceases to grow. The knee position falls between the h_2/h_1 for maximum amplification and $(h_2/h_1)_{\text{critical}}$. Thus, the data that can be sought are the absolute values of h_2/h_1 where the knee occurs for a given frequency, and the relative positions of the knee for different frequencies.

Flame propagation. - As stated in the INTRODUCTION, one of the reasons for pursuing the stability analysis is to find a disturbance frequency that permits the greatest increase in flame spreading with the smallest expenditure of energy. In this paragraph a model of flame propagation is constructed that permits extrapolating the behavior of v' from the stability analysis to a measurable behavior of flame propagation.

The flame front is assumed to be a zone in which the density goes from ρ_1 to ρ_2 in a distance that is short compared to the disturbance wavelength. This front is propagating into the gas of density ρ_1 at a rate $S_{T,U}$, that is, the undisturbed turbulent flame speed. Owing to the normal propagation of the front, an initially wavy surface becomes a cusped surface. Assuming such a surface composed of cylindrical arcs (following sketch)



permits a calculation of the flame-front stretching due to a displacement h . If the undisturbed area $A_U = \lambda$ and the disturbed area A_D are approximately equal to arc length,

$$\frac{A_D}{A_U} \approx \sqrt{1 + \left(\frac{2h}{\lambda}\right)^2} \quad (54)$$

An equilibrium h is reached when

$$\frac{A_D}{A_U} = \sqrt{\frac{1 + \frac{2v'}{S_{T,U}}}{1 + \frac{v'}{S_{T,U}}}} \quad (55)$$

Then A_D/A_U behaves roughly as $\left(1 + \frac{1}{2} \frac{v'}{S_{T,U}}\right)$ for small amplitude. One sees that equation (54) contains a nonlinear term $4h^2/\lambda^2$. The development so far has been a linear one. The linear development would be expected to furnish only a first approximation for amplitudes large enough so that $4h^2/\lambda^2$ is no longer negligible compared to unity.

The sequence of events that leads to a prediction of A_D/A_U is:

- (1) The flame is initially wrinkled by the velocity v' acting at the flame surface.
- (2) As the wrinkles grow, the flame shape shifts from a sine wave to a cusped surface, owing to normal propagation.
- (3) After a certain time an equilibrium is reached between the disturbance velocity v' and the undisturbed propagation velocity $S_{T,U}$.

The ratio of the disturbed surface to the undisturbed surface when equilibrium is reached is, for small disturbances,

$$\frac{A_D}{A_U} = \left(1 + \frac{1}{2} \frac{v'}{S_{T,U}}\right) = \frac{S_{T,D}}{S_{T,U}} \quad (56)$$

Before this equilibrium value of A_D/A_U is reached, the flame surface is given by (again for the neutral case)

$$\frac{y_{h_2}}{y_c} \approx 1.2 + \frac{0.2 v'_0}{\Delta U \alpha y_c} \cos \alpha x$$

But $2h/\lambda$ of equation (54) is given by

$$\begin{aligned} \frac{2h}{\lambda} &\approx \left(\frac{y_{h_2}}{y_c} - 1.2 \right) \frac{y_c 2\alpha}{\pi} \\ &\approx \frac{v'_0}{\Delta U} \frac{0.4}{\pi} \cos \alpha x \end{aligned}$$

Thus, in the transient case as in the equilibrium case (eq. (55)) A_D/A_U behaves as v' . The quantity A_D/A_U when measured locally should behave like g in figure 8, if the effect of distribution is neglected. When the latter effect is taken into account, v' for fixed $2\alpha_0 h_1$ measured at h_2 achieves a maximum value somewhere between h_2/h_1 for maximum amplification and neutral stability.

Thus, at any station, h_2/h_1 , there should be a frequency of disturbance that would cause the greatest increase in flame speed and, at this station, the increase in flame speed should be greater for greater values of $v'/S_{T,U}$.

Figure 11 gives a plot of $2\alpha_0 h_1$ against h_2/h_1 for maximum amplification and for neutral stability. For any value of h_2/h_1 , the frequency giving the greatest $v'/S_{T,U}$ (at the flame surface) has a value of $2\alpha_0 h_1$ that falls between these curves. The lag in time required for the flame to become wrinkled initially will move the curve for maximum A_D/A_U to slightly higher $2\alpha_0 h_1$ values. The curves given should be considered the lower limits of $2\alpha_0 h_1$ for maximum A_D/A_U , and they serve as a basis for comparison with the experimental data.

Effect of Flameholder

When a flame is anchored in a duct, some form of flameholder must be used. The most common form of flameholder studied in recent years is the cylinder with axis normal to the stream. The cross section of the cylinder

has assumed many different shapes. There are properties of the flow in the wake common to all the shapes studied. In this section some of these properties are used to deduce the effect of a flameholder on the flow field far from the flameholder and, hence, on the stability of the flow field far from the flameholder.

Steady-state velocity distribution. - The properties of the flow field in the immediate wake of the flameholder as described in references 1 and 33 are shown in figure 12. There is an attached eddy pair in the wake of the flameholder. The gas in this zone is hot, acquires energy from the downstream hot gas, and delivers energy to the outside cold gas by diffusion.

At some position on the surface of the recirculation zone, sufficient energy is acquired by the cold gas for ignition to occur and a flame to propagate into the cold-gas stream as shown in figure 12. The pressure measured at the walls has an axial distribution shown qualitatively in figure 12 (refs. 1 and 33).

If the static pressure is assumed constant across the duct at any axial station, the effect of the first positive, then vanishing, then negative pressure gradient upon gases of unlike densities permits an estimation of the velocity profile downstream of the flameholder.

In figure 13 are sketched the velocity profiles at stations a, b, and c of figure 12. At station a the pressure gradient in the axial direction has been positive for a small distance and is still positive at a. This fixes the sense of the velocity difference between cold and hot gases on either side of the flame and the sense of the velocity gradient of the hot gas at the flame front. At station b the gas has had a positive pressure gradient history, again fixing the sense of the velocity difference, and at b the pressure gradient vanishes, causing the velocity gradient at the flame front to vanish. At station c the gas has a negative pressure gradient history from b sufficient to cause the sense of velocity difference and gradient at the flame front as shown in figure 13(c). The gas particle at the position of the velocity maximum passed through the flame at station b. If the profile is approximated by straight-line segments with a corner at this velocity maximum as shown in figure 14, some quantitative relation based on the continuity equation and experimental observations can be obtained.

From continuity,

$$\frac{1}{2} b' U^* = S_w l_w \frac{\rho_1}{\rho_2} \quad (57)$$

and

$$b \frac{U^* + U_1}{2} = S_f l_f \frac{\rho_1}{\rho_2} \quad (58)$$

where

ρ_1/ρ_2 density ratio of cold to hot gas

U_1 cold-gas velocity

U^* maximum hot-gas velocity

b, b' defined by fig. 14

l_w axial length of wake to station b (fig. 12)

l_f axial length from station b to station of interest downstream
of b

S_w mean flame speed over l_w

S_f mean flame speed over l_f

Combining equations (47) and (58) gives

$$\frac{1}{2} \frac{b'}{b} = \frac{U^* + U_1}{2U^*} \frac{S_w l_w}{S_f l_f} \quad (59)$$

In order to obtain an order of magnitude of $\frac{1}{2} \frac{b'}{b}$ of interest in the stability analysis, the terms on the right side of equation (59) are given the following values: $(U^* + U_1)/U^* = 1.5$ (from ref. 1 for $F = 0.25$, $\rho_1/\rho_2 = 6$), where F is fraction burned; $\frac{S_w}{S_f} \approx \frac{1}{S_T/S_L} \approx \frac{1}{2.5}$, where S_T/S_L is ratio of turbulent to laminar flame speed; $l_w \approx 4D$ (from ref. 1), where D is flameholder width. Defining l as $l_w + l_f$,

$$\frac{l_w}{l_f} = \frac{1}{\frac{l}{l_w} - 1} = \frac{4}{\frac{l}{D} - 4}$$

equation (59) becomes

$$\frac{1}{2} \frac{b'}{b} = \frac{1.2}{\frac{l}{D} - 4} \quad \left(\frac{l}{D} > 4 \right) \quad (60)$$


At a station $l/D = 8$, from equation (60),

$$\frac{1}{2} \frac{b'}{b} = 0.6$$



Farther downstream, at $l/D = 24$ for example,

$$\frac{1}{2} \frac{b'}{b} = 0.06$$

The foregoing stability analysis is for a profile in which $b' = 0$.

From this section it can be seen that, near the flameholder ($l/D = 8$), the hot-gas velocity distribution differs in shape from the  profile examined neglecting the flameholder. At this station 60 percent of the flame-zone width has a flat distribution. Remote from the flameholder ($l/D = 24$), 6 percent of the hot-gas width has a flat velocity distribution.

In the next section the magnitude and direction of the error incurred in neglecting this flattening is estimated.

Comparison of the stability of a  profile and a  profile. - In figure 2 a comparison is made of amplification rates as a function of $2\alpha h_2$ for several values of ρ_1/ρ_2 and h_2/h_1 . It can be seen that the effect of increasing ρ_1/ρ_2 and h_2/h_1 is stabilizing; that is, the magnitude of the amplification rates and the range of $2\alpha h_2$ over which positive values exist are reduced. The plots of amplification rate against $2\alpha h_2$ are affine. It appears reasonable that, in examining the effect of truncating the profile, an examination at a single value of ρ_1/ρ_2 and h_2/h_1 would yield representative results.

The conditions considered here are the ones formulated by Rayleigh in equations (24) and (25) (p. 387, ref. 17) and correspond to the case where $\rho_1/\rho_2 = 1$ and $h_2/h_1 = 0$ (or $h_1 = \infty$). Calculations were made

in which $\frac{1}{2} \frac{b'}{b}$ was taken as a parameter in such a way that the results

3877

CY-6

yield values of $\alpha c_1 \frac{2b}{\Delta U}$ and $2\alpha b$ at maximum instability and a critical value of $2\alpha b$ where αc_1 vanishes. The results of these calculations are shown in figure 15.

When $b' = 0$, the results correspond to those of figure 2; the flow is unstable to antisymmetric disturbances, neutrally stable to symmetric disturbances.

As $\frac{1}{2} \frac{b'}{b}$ increases, the amplification rate and the critical values of $2\alpha b$ decrease for the antisymmetric disturbances. The flow gradually becomes unstable to symmetric disturbances as $\frac{1}{2} \frac{b'}{b}$ increases. At $\frac{1}{2} \frac{b'}{b} > 2.0$, the flow is as unstable to symmetric as to antisymmetric disturbances and possesses the same critical values of $2\alpha b$. The values of $\frac{1}{2} \frac{b'}{b}$ of interest here are of the order 0.6 to 0.06. The flame half width h_2 is $\frac{1}{2} b' + b$. In the following table the values of the important parameters $\alpha c_1 \frac{2h_2}{\Delta U}$, $(2\alpha h_2)_{\max} c_1$, and $(2\alpha h_2)_{\text{critical}}$ are compared for $\frac{1}{2} \frac{b'}{b} = 0, 0.06, 0.6$ for antisymmetric disturbances:

$\frac{1}{2} \frac{b'}{b}$	0	0.06	0.6
$\left(\alpha c_1 \frac{2h_2}{\Delta U} \right)_{\max}$	0.492	0.508	0.688
$(2\alpha h_2)_{\max} c_1$	2.44	2.49	3.28
$(2\alpha h_2)_{\text{critical}}$	3.69	3.71	4.57

For a given $2h_2/\Delta U$, the amplification rate is increased as the hot-gas velocity is progressively truncated.

The wave-number range over which the flow is unstable is widened. Both of these effects bespeak a greater instability of flow. On the other hand it can be easily demonstrated that, for a given ΔU , h_2/h_1 is greater when the profile is truncated so that the destabilizing effect of the flameholder is partially but not completely attenuated.

The difference between the parameters calculated at $\frac{1}{2} \frac{b'}{b} = 0$ and 0.6 shows that near the flameholder the amplification rates may be of the order of 20 percent higher for some wave numbers than were those previously found. Because the flame zone must start with a finite width dependent upon the flameholder width (say, D), those frequencies having such wave numbers that $2\alpha DK$ exceeds $2\alpha DK_{\text{critical}}$ are suppressed. Here, K is some proportionality factor less than unity.

Certainly, neglect of the effect of a finite-size flameholder facilitates generalizing the results of the stability analysis. The investigations of this section indicate that for flameholders small as compared to duct width, there is a large part of the flame zone in which such neglect appears warranted.

SUMMARY OF THEORETICAL RESULTS

1. The flow field of a flame in a duct is unstable to antisymmetric disturbances having wavelengths of the order of 2.5 times the local flame width and greater. As h_2/h_1 approaches unity, this critical wavelength approaches 0.

2. The amplification rate depends directly upon the magnitude of the velocity difference (apex velocity minus cold-gas velocity) and inversely upon the flame width. For fixed values of these quantities, the maximum amplification rate decreases with increasing values of ρ_1/ρ_2 and h_2/h_1 , going to zero for $h_2/h_1 = 1$.

3. When the history of a disturbance is followed through the course of an entire flame, it is found that a wave number for maximum disturbance growth obtains. This maximum growth is for such a wave number at the flameholder that $2\alpha_0 h_1 = 6$ which corresponds to a frequency $f = U_0/2h_1$. The actual growth is substantially independent of density ratio. This is due to two compensating factors:

- (a) The amplification rate is lower for a higher density and given velocity difference.
- (b) The velocity difference is greater for a higher density ratio.

4. The disturbances achieve their terminal amplification at a value of h_2/h_1 roughly inversely proportional to the frequency of the disturbance. Thus, higher frequencies achieve their amplification near the flameholder; the lower frequencies, remote from the flameholder.

3877

CY-6 back

5. The magnitude of the terminal amplification depends upon the inverse of flame slope or roughly $(S_T/U_0)^{-1}$. The amplification that can be achieved for the maximum of $2\alpha_0 h_1 = 6$, is about $1.1 U_0/S_T$. For example, for $S_T/U_0 = 1/20$, amplification is 8-fold. For $S_T/U_0 = 1/100$, amplification is 14,000-fold.

6. The disturbance propagates with a phase velocity up to 60 percent greater than the cold-gas velocity.

7. The flameholder serves to inhibit the growth of antisymmetric disturbances having higher frequencies but permits symmetric disturbances to be amplified near the flameholder. At 8 diameters downstream of the flameholder, the stability picture is substantially that obtained by neglecting the flameholder.

EXPERIMENTAL EXAMINATION OF DISTURBANCE GROWTH IN A V-FLAME

INTRODUCTION

The experimental research investigated the effect of imposing controlled disturbances on a V-flame anchored in a duct for two reasons:

- (1) To gain quantitative information on the mechanism of the breakdown of the flame-generated shear region that would explain the occurrence of flame-amplified turbulence
- (2) To find a type of excitation that promotes flame propagation without causing shell failure as does combustor resonance

The method of excitation consists in exciting a column of gas in the flameholder support tube. This method offers a control on the amplitude when excitation is accomplished with a speaker, but could be accomplished by means of an edge tone excited by the flowing stream for application in an engine. Only the speaker excitation is used here. The sound issues from a port at the flameholder and disturbs the flame at the flameholder. The two types of ports used operated as follows:

- (1) Sound issued from a port just upstream of one flameholder edge, causing the fluctuating flow about the flameholder to be quasi-antisymmetric.
- (2) Sound issued from the center of the flameholder, causing the fluctuating flow at the flameholder to be symmetric.

The principal disadvantage in this form of excitation is that, for some frequencies, modes of burner cavity resonance are excited. An objective in the experimental work, therefore, is to determine whether an

observed flame front distortion accompanying an imposed disturbance is due to flame-zone instability or to some form of duct resonance.

No effort was made to determine effects of fuel-air ratio or fuel-type variation. The primary variable investigated was the frequency of excitation and its effect on the flames studied. The only attempts at correlating the results are the comparison with the results of the preceding stability analysis.

The chief frustration encountered is the impossibility of obtaining a laminar V-flame at velocities where values of S_T/U_0 are sufficiently low for the preceding theory to be valid. The reason for this difficulty is the instability of the boundary layer, which separates from the flameholder and undergoes transition to turbulent motion quite close to the point of separation. All the results are obtained with the flow already somewhat turbulent.

The primary tool in measuring flame speeds is the photomultiplier probe, first applied in a rigorous way to the study of turbulent flame speeds by Clark and Bittker (ref. 34). An independent confirmation of the method is obtained by comparing combustion efficiency measured by the photomultiplier probe and by momentum pressure drop.

APPARATUS

Burner Test Section

A photograph of the burner (fig. 16) shows the important components. Air and propane were filtered, metered, and mixed before entering the two-stage calming section. In this section the mixture passed through six banks of 200-mesh screen and then through a 3/8-inch-radius nozzle plate into the 1/2- by 2-inch (or alternately 1- by 2-in.) rectangular glass-walled test section (fig. 17). The top and bottom walls of this test section were 1/2- by 1/2-inch (alternately 1/2- by 1-in.) brass stock. The side walls were 1/4-inch Vycor plates, resting on brackets and held against the 1/2-inch top and bottom pieces by clamps.

The exhaust system consisted of a 6-inch-diameter pipe connected to a hood and a blower to force the gases outside. A 4- to 6-inch spacing was maintained between the test section and the exhaust duct, and between the exhaust duct and the hood; no indication of resonance due to the exhauster was encountered.

The flameholder consisted of a flat hollow paddle terminated on one end by a 60° gutter and on the other end by a 3/8-inch tube leading to a piston-type loud speaker. The three flameholders used in this program are shown in figure 18. The flameholders used to supply the disturbances

were resonators that had resonant frequencies every 190 to 200 cycles when coupled to the speaker. The flameholders ranged from 36 to 38 inches in length. The flameholder designed to produce antisymmetric disturbances allowed the sound to issue from a slot just upstream of one edge of the flameholder. The one designed to give symmetric disturbances allowed the sound to issue from the center.

The flameholders pictured were approximately 0.25 to 0.30 inch thick. In one test a 0.50-inch gutter was tacked onto the 0.306-inch antisymmetric flameholder to examine the effect of flameholder size.

In no case was the distribution of v' downstream of the flameholder measured. It is not known how much the experimental distribution differs from the measured theoretical distribution. The essential features in both experimental and theoretical disturbances are that antisymmetric disturbances cause the flow to flap back and forth at the centerline of the duct, while symmetric disturbances cause it to dilate about the centerline.

Auxiliary Equipment

Sound producing system. - The speaker was supplied a sinusoidal signal from a signal generator through a power amplifier. The speaker and flameholder could be positioned as desired.

Flow metering. - Air and propane were metered through rotameters.

Hot-wire equipment. - An NACA constant-temperature, frequency-compensated, hot-wire anemometer was used (ref. 35). Spectra and u' were measured at various locations in the duct. Measurements of u' were made primarily with a vacuum-tube voltmeter. Two spot checks were made against a root-mean-square computer, and the correction factor was found to be approximately unity. Spectra were measured with a wave analyzer.

Pressure measurements. - Velocity surveys were made with a 0.018-inch hypodermic tubing, and alternately a 0.030-inch stainless tubing, for impact tubes. Measurements were read on a water micromanometer. Velocity measurements were made at the plane of exhaust with room pressure as static.

Photomultiplier probe. - The photomultiplier tube was installed in a probe as shown in figure 19. Light reached the photomultiplier tube after passing through two vertical slots, which were 1/4- and 1/16-inch wide and 2 feet apart, and through filters if desired. Photomultipliers were supplied by a ripple-free regulated d-c source.

Voltmeters with a-c and d-c current were used where indicated.

Shadowgraph system. - The optical arrangement used in taking shadowgraph pictures is shown in figure 20. The light source could be used continuously or as a 4-microsecond flash. The camera was focused 1.5 feet in front of the test section. The shutter and flash were manually synchronized.

Stroboscope. - A stroboscope consisting of a slotted aluminum disk and a synchronous motor was used to view the disturbed flame in the preliminary phases of the investigation. The stroboscope can be seen in the lower left corner of figure 16.

Properties of System

Velocity profiles upstream of flameholder. - Figure 21 gives the velocity profiles measured 3 and 12 inches from the nozzle; in each case the flameholder is positioned so that the measurement is taken upstream of the gutter. Measurements were also taken at the plane of the nozzle, and no variation greater than 1/2 foot per second from 55 feet per second was found. These measurements are for a nominal flow setting of 50 feet per second.

Flame photographs were taken and flame-speed measurements were made at nominal velocities of 50 and 100 feet per second in 1/2- and 1-inch-wide test sections; the profiles of figure 21 therefore represent the highest percentage boundary layer of those encountered.

Velocity profile in wake, no flame. - Figure 22 gives the velocity profiles in the wake of a 0.306-inch-wide, 60° gutter at a nominal velocity of 46 feet per second. This set of profiles shows a comparison of the spreading of a wake with and without an antisymmetric disturbance at 200 cycles per second. The only amplitude measurement available for this disturbance is a root-mean-square u' of 5 feet per second, measured 1/8 inch above the lip of the flameholder.

The effect of other frequencies on wake spreading was examined by placing total-pressure tubes 3 inches downstream of the flameholder at the center of the wake and varying the frequencies. The results are interpreted in the following manner: Read the velocity while disturbances are being introduced. Find the distance from the wake at which this velocity is attained without the sound (say x). An index of the lengths required to accomplish equal degrees of mixing without and with the disturbance is then the ratio $x/3$. A plot of this ratio against frequency is given in figure 23.

Because the apparent diffusion rate decreased at frequencies greater than 1000 cycles per second, it was thought this might imply a decrease in form drag for frequencies greater than 1000 cycles per second. Static

measurements were made at the base of the gutter. No change in base pressure was observed for the higher frequency disturbances. Those lower frequencies which increased mixing also decreased base pressure, that is, increased form drag. This probably means that the velocity is increased in the wake for frequencies less than 1000 cycles per second. There seems little hope, however, of reducing flameholder drag by imposing high-frequency disturbances of this kind.

Turbulence intensity and spectra. - The turbulence component u' in the direction of flow was measured with 0.0002- by 0.08-inch tungsten wires, using the NACA constant-temperature anemometer amplifier. The wire was oriented parallel to the flameholder lips. No flame was present for these measurements. The results are presented in the following table:

Nominal velocity, U , ft/sec	Distance from nozzle lip, x , in.	Distance from top wall, y , in.	Vertical distance from station, in.	Turbulence component, u' , ft/sec	Scale of turbulence, L_x , in.
50 100	0 0	$1/2$ $1/2$ } Measured from centerline	$1/4$ $1/4$	0.306 .420	
50 50 50 50 50 100	6 6 6 6 6 6	$1/8$ $1/8$ $1/4$ $1/4$ $1/2$ $3/4$ } Measured from flameholder lip	$1/4$ $1/8$ $1/4$ $1/8$ $1/4$ $1/4$	1.38 1.68 .818 .978 1.021 3.35	0.2 .15 .15 .17
		$1/8$	$1/4$	2.44	

The spectra measured at several stations were compared with spectra found representative for isotropic turbulence (refs. 35 and 36). A typical plot is shown in figure 24. The scale L_x is estimated as the one whose spectrum most nearly corresponds to the measured spectrum (refs. 35 and 36). This scale³ where determined is given in the preceding table.

The apparent transition from laminar to turbulent flow in the boundary layer on the flameholder surface occurred if the flameholder was about 1 inch or more from the test-section nozzle; the disturbance velocity in the boundary was roughly that in the nozzle itself. With the

³This is the scale that would be used for calculating a turbulent burning velocity from existing theory (ref. 8). Herein, it is of interest because of the scale of disturbance the flame amplifies; $L_x \sim 1$.

flameholder within 1 inch of the nozzle, eddies were found to shed at 420 cycles per second when no flame was present. With the flameholder at 1 inch or more from the nozzle, transition occurred upstream of the flameholder lip and no clearly defined eddy-shedding frequency was found in the wake.

With a flame anchored on the flameholder, no eddy shedding was observed without external excitation. The flame appeared turbulent for both flameholder positions greater or less than 1 inch from nozzle. It appears, therefore, that the transition to turbulence in the separated boundary affects the turbulent flame appearance in about the same manner as transition in the attached boundary layer does. The lean blowout fuel-air ratio was adversely affected when the transition was moved from the attached to the free boundary layer.

In an effort to obtain a laminar flame zone, some exploratory work was done to move the transition point farther downstream of the point of separation from the flameholder. Small unheated cylindrical rods (as in ref. 3) placed about 1 inch from the nozzle entrance were used as flameholders. It was possible to move the transition point about 1 inch downstream of the flameholder (at 50 ft/sec). Lean blowout, however, was moved to a fuel-air ratio rich enough to cause excessive heating in the glass walls, which impaired the use of the shadowgraph system. In the transient period immediately after ignition while the walls were still cool, it was possible to observe a clear picture of the flame. In order to study the flame at length, this course was abandoned, and it was decided to accept the turbulent transition at or upstream of the lip of the flameholder.

Calibration of Disturbance Amplitude Against Speaker Input

Owing to the interaction between the standing wave tube supplying the sound to the flameholder and the standing waves in the test section, it was necessary to calibrate the sound input with the flameholder at the position and velocity to be used in the burning tests. For most runs the flameholder was placed midway between acoustically open ends in the test section in order to suppress velocity disturbances at the flameholder due to all even modes of vibration of the test section.

The inputs were set in the following manner: The flameholder position and flow velocity to be used in a burning run were set. The hot wire was placed $1/8$ inch above the flameholder lip, $1/8$ inch upstream of flameholder lip so as to be centered over the port from which the sound issued. Resonant frequencies were excited in the flameholder support tube. The input to the speaker required to give the desired u' at the wire was recorded for each frequency. The wire was removed, fuel introduced and ignited, and the burning run was made. The distribution of

3877

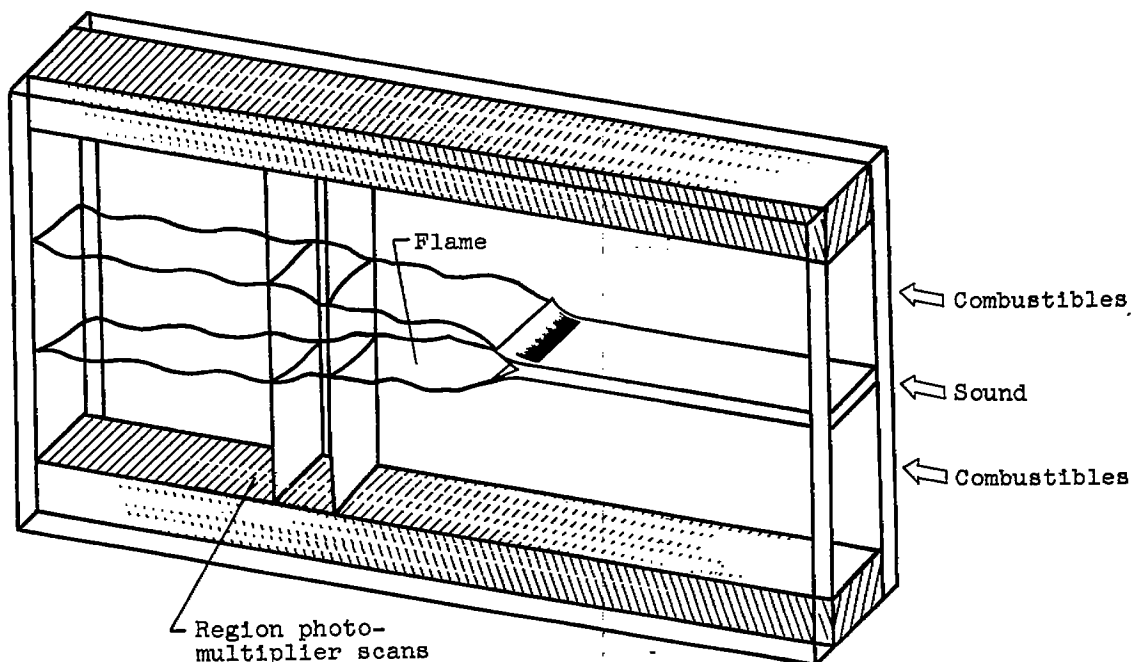
CY-7

v' resulting from this sort of excitation was not explored. The change in the nature of interaction between test sections and the standing wave tube with and without combustion was not explored but was presumed to be small, since only about 30 percent of the combustible mixture was burned in the test section.

S_T/S_L Determined by Photomultiplier Probe

The author (ref. 37) and Kaskan (ref. 38) have used photomultiplier tubes to sense transient area changes in a laminar flame distorted by sound. Clark and Bittker (ref. 33) used photomultiplier tubes to study bunsen flames that were alternately laminar and turbulent by comparing the average intensity of light emitted from the flame. They found that turbulent and laminar flames having identical mixture ratios and feed rates produced identical quantities of light. Therefore, it appears that, if used with caution, the photomultiplier tube can become an average-heat-release-rate meter.

In the following discussion, the local heat release rate is characterized by the ratio of turbulent to laminar flame speed S_T/S_L . This ratio S_T/S_L is defined as the heat released per unit time divided by the heat that a pair of laminar flames aligned with the axis of the duct would release per unit length per unit time. The relation is illustrated by considering the way the quantities are measured.



In the test section shown in the preceding sketch, flame fronts are anchored on the top and bottom of the flameholder and appear to span from wall to wall. The photomultiplier scans a narrow region of the test section. The voltages read from the photomultiplier tube output are recorded at the same fuel-air ratio for a turbulent flame and again for a laminar flame. The flame-front half angle is measured in each case and each voltage multiplied by the cosine of the half angle. The ratio of the resulting product for the turbulent flame to that for the laminar flame is defined as S_T/S_L . In the region of interest the cosine of the half angle was approximately 1 for the turbulent flames so that, in effect, the unit length of the flame fronts becomes the unit length of the combustor.

In obtaining the laminar flame, the same fuel and air rotameter settings were used as for the turbulent flame but a large fraction of the mixture was bled off upstream of the flameholder. Three banks of 200-mesh screen were installed just upstream of the flameholder and the resulting flame appeared laminar. Near the flameholder the flame did not span from wall to wall, so that the voltage recorded for this region was quite low. Far downstream from the flameholder the flame front became twisted so that it represented a flame depth greater than the wall-to-wall depth. In between these two regions was a region in which the flame appeared to touch the walls and have negligible twist. The voltage recorded by the photomultiplier probe as it scanned this region was nearly constant. The extreme voltages recorded in this region envelop a band within which the true voltage corresponding to a pair of laminar flames was thought to lie.

In order to pinpoint an exact value for the laminar voltage as well as to check the method (the zone of uncertainty is quite small), an auxiliary determination of S_T/S_L was made. Readings were made of photomultiplier-probe voltages at seven equally spaced stations along the combustor from flameholder to exhaust nozzle, and an average voltage was calculated. Simultaneously, measurements of the momentum pressure drop across the flame zone were made. With the help of Scurlock's results (ref. 1), the fraction of combustible burned F was determined from the measured momentum pressure drop. Then, from

$$F = \frac{\text{Length} \times 2 \times S_T \times \text{depth}}{U_0 \times \text{depth} \times \text{height}}$$

(where the length, depth, and height are the dimensions of the combustor) an average S_T was calculated. Using this S_T , the measured average voltage, and the value for laminar flame speed S_L taken from Dugger (ref. 39), voltage corresponding to a laminar flame was obtained from

$$\frac{V_L}{S_L} = \frac{V_T}{S_T}$$

where V_L and V_T are the photomultiplier voltages for laminar and turbulent flames. This voltage lies within the zone of uncertainty found by direct viewing of the laminar flame. These results are reported more fully in the section Examination of the Method.

It is obvious that citing Clark and Bittker (ref. 34) does not imply that any photomultiplier calibration was obtained from their work. Reference 34 established that (for a given combustor at a given composition and flow rate) a photomultiplier voltage is proportional to the heat released within sight of the photomultiplier tube and is independent of the existence or lack of turbulence. The agreement of the two methods for determining S_T/S_L seems to justify this use of the photomultiplier probe.

It was hoped initially to follow the amplitude of a flame wrinkle by measuring the a-c component of the photomultiplier signal. The reasoning was that the flame would be wrinkled sufficiently for its local instantaneous slope to serve as a detectible index of flame-wrinkle amplitude. This slope, of course, would show up as an increased voltage at the photomultiplier because the length of the flame cutting across the field of view would be increased.

The data taken showed an amplitude more dependent on the distance from the duct exhaust than on the distance from the flameholder. It was discovered that the sound waves introduced as the source of excitation at the flameholder reflected from the exhaust of the combustor. The a-c component read by the probe, therefore, was largely influenced by the time-varying displacement of local flame zones due to plane waves of sound. Figure 25 shows a comparison of the filtered a-c signal for two frequencies as a function of distance from the flameholder. One set is obtained from the photomultiplier probe with burning, the other set from a hot-wire anemometer without burning.

The use of the photomultiplier probe was restricted to surveying for the effect of disturbances on local S_T/S_L values on a time-average basis only.

RESULTS

The analytical part of this paper suggests certain behavior that can be examined experimentally. Accordingly, tests are included that furnish the necessary data for a comparison with the results of the analysis. One

of the primary variables studied is the effect of the frequency of excitation on disturbance growth. The frequency range of interest happened to include some of the resonant frequencies of the combustor gas volume as well as the spontaneous eddy-shedding frequency of the flameholder in cold flow. Part of the tests studied the effect of combustor resonance or spontaneous eddy shedding on the results.

Certain precautionary measures were taken in choosing geometry and operating conditions. To guard against burner resonance, the combustor was kept short so that only about 30 percent of the combustible was consumed. It was found that, when this value was exceeded, spontaneous burner resonance sometimes occurred. To guard against spontaneous eddy shedding, the conditions were kept within the Reynolds number reported in reference 1 to be free of spontaneous eddy shedding when a flame is anchored on the flameholder. Although these measures guarded against the occurrence of spontaneous oscillations due to the above two causes, they could not prevent the system from favoring certain frequencies within the range of interest. These influences, then, received special attention.

Markstein has shown (ref. 14) that instabilities of a laminar flame front cause the front to assume a cellular structure under certain conditions. The occurrence of such cells clearly could confuse an interpretation of the results. Consequently, the data were taken solely at conditions where the cells do not spontaneously arise.

Examination of the Method

Runs were made at three fuel-air ratios at 50 feet per second and a range of disturbance frequencies. The flameholder position was 6 inches from the open end of the duct and 6 inches from the tunnel entrance. The 0.306-inch-wide gutter with antisymmetric disturbances was used. The change in impact pressure with and without combustion was measured by a single impact tube upstream of the flameholder. Since the difference is of the order of inches of water and the rate of mass flow is constant, it is assumed that the difference is entirely due to a change in static pressure. By use of Scurlock's results (ref. 1) and the measured pressure drop, the fraction burned was calculated. Concurrently, the light intensity at seven stations along the flame was measured and averaged.

Figure 26 shows a comparison of the fraction burned with the average voltage (which is proportional to the average intensity) made by plotting both against the frequency of disturbance for the three fuel-air ratios examined. The following table demonstrates the amount of scatter in the ratio of fraction burned to mean voltage.

Fuel-air ratio	Frequency, f, cps					Average F/V _T
	0	380	470	760	1500	
	F/V _T					
0.0444	0.137	0.131	0.134	0.137	0.131	0.134
.0515	.1017	.1070	.1065	.1063	.1035	.1056
.0580	.0818	.0817	.0863	.0858	.0852	.085

From the relation

$$\frac{F}{V_T} = \frac{2S_T \times \text{length} \times \text{depth}}{U_0 \times \text{height} \times \text{depth} \times V_T}$$

(where length, height, and depth are dimensions of the combustor) an average value of S_T/V_T is calculated. Using the average values in the preceding table for F/V_T at each fuel-air ratio, the following values of S_T/V_T were obtained

Fuel-air ratio	S_T/V_T , (ft/sec)/volt
0.0444	1.115
.0515	.88
.0580	.709

For these fuel-air ratios and the employed inlet temperature and pressure, a laminar flame speed was obtained from Dugger (ref. 39). Then, from

$$V_L = \frac{S_L}{S_T/V_T}$$

the voltage that would correspond to a laminar flame was calculated.

In the following table are tabulated Dugger's flame speed values S_L , the value of V_L calculated from the preceding relation, and the zone of V_L measured directly by viewing a pair of laminar flames in the test section.

Fuel-air ratio	S_L (ref. 39)	$V_L = \frac{S_L}{S_T/V_T}$	V_L by direct measurement
0.0444	0.74	0.663	0.658 to 0.682
.0515	1.10	1.25	1.15 to 1.39
.0580	1.32	1.862	-----

The V_L taken from values of $\frac{S_L}{S_T/V_T}$ that resulted from momentum-pressure-drop measurements falls within the limits of V_L by direct measurement in the table and is used as the calibration of the photomultiplier probe. Local values of S_T/S_L reported subsequently are defined by the ratio of voltage read at that station to this V_L for the applicable fuel-air ratio.

Comparison of Flame Speed with Flame Appearance

Shadowgraphs were taken at the same conditions used in the preceding comparison between average voltage and Δp . Some of these shadowgraphs, along with the distribution of S_T/S_L for each case, are presented in figure 27.

In most of these photographs the gross disturbance caused by the input sound can be identified. If a line is drawn along the turbulent flame front faired through all but these gross wrinkles, its length divided by the length of a line faired along the undisturbed surface should be equal to

$$\left(\frac{A_D}{A_U}\right)_A \equiv \frac{\text{Area of flame disturbed at frequency } f}{\text{Area of undisturbed flame surface}}$$

A similar ratio is available from the average voltages obtained by the photomultiplier survey in figure 26 defined by

$$\left(\frac{A_D}{A_U}\right)_P = \frac{(V_T)_{\text{disturbed}}}{(V_T)_{\text{undisturbed}}}$$

The following table shows a comparison of the $(A_D/A_U)_A$ obtained by the former method and $(A_D/A_U)_P$ obtained from the photomultiplier readings.

Frequency, x, cps	Fuel-air ratio			
	0.0444		0.0515	
	$\left(\frac{A_D}{A_U}\right)_P$	$\left(\frac{A_D}{A_U}\right)_A$	$\left(\frac{A_D}{A_U}\right)_P$	$\left(\frac{A_D}{A_U}\right)_A$
0	1	1	1	1
380	.18	1.15	1.09	1.11
570	1.304	1.185	1.19	1.12
770	1.23	1.23	1.10	1.18
1500	1.10	1.085	1.09	1.07

In general the correlation is good. It may be significant that at 570 cps the $(A_D/A_U)_P$ is about 10 percent greater than $(A_D/A_U)_A$. At this frequency, it is relatively easy to measure the area; that is, experimental scatter should not be as great as 10 percent. The evidence suggests the generation of additional turbulence in the flame, over and above the growth of the low-frequency-imposed disturbance. It is regrettable that a laminar stabilized flame could not be obtained in this equipment, because this frequency could conceivably cause a transition point from laminar to turbulent flow.

For each plot (fig. 27(a) to (e)) u' is a constant, so that u'/S_L decreases with increasing fuel-air ratio f/a . S_T/S_L decreases, for the most part, with increasing fuel-air ratio and, therefore, with decreasing u'/S_L .

At a given x position, the ratio $(A_D/A_U)_P$ defined by $\frac{(S_T/S_L)_{\text{disturbed}}}{(S_T/S_L)_{\text{undisturbed}}}$ descends with ascending fuel-air ratio. This is in keeping with the interpretation in the STABILITY ANALYSIS. The following table gives the values of A_D/A_U at 570 cps for the three fuel-air ratios.

x, in.	Fuel-air ratio					
	0.0444		0.0515		0.0580	
	$\frac{A_D}{A_U}$	$\frac{u_{570}^*}{S_{T0}}$	$\frac{A_D}{A_U}$	$\frac{u_{570}^*}{S_{T0}}$	$\frac{A_D}{A_U}$	$\frac{u_{570}^*}{S_{T0}}$
1	1.522	2.025	1.129	1.220	1.076	1.055
2	1.183	1.437	1.205	1.107	1.122	.962
3	1.166	1.376	1.175	1.08	1.119	.937
4	1.177	1.358	1.151	1.058	1.147	.913
5	1.197	1.352	1.129	1.038	1.116	.873

Distribution of Local S_T/S_L Values with Respect
to Various Frequencies

Figure 28(a) shows a plot of S_T/S_L against distance from the flameholder. Figure 28(b) is a cross plot of S_T/S_L against frequency at several stations. Great care was taken in keeping fuel-air ratio, velocity, and plate voltage to the photocell constant throughout the run. The 0.306-inch flameholder, modified to prevent leakage about the edges, was used. The disturbance velocity measured as described earlier gave a $u' = 2.16$ feet per second for all frequencies.

In order to compare these data with theory, the following computations were made:

(1) From the preceding calibration the fraction burned is calculated as a function of combustor length for the upper envelope of the S_T/S_L curves for the disturbed flames.

(2) An idealized h_2/h_1 against length was obtained from this fraction burned using Scurlock's results (ref. 1).

(3) Increments of length over which a given frequency has a maximum S_T/S_L were read from figure 28(a).

(4) These increments were plotted against h_2/h_1 and compared with the theoretical plot taken from figure 11. Recall that

$$f = \frac{2\alpha_0 h_1 U_0}{2\pi 2h_1}$$

Results of steps (1) and (2) are shown in figure 29, and steps (3) and (4) in figure 30.

Similar data were taken at the lower amplitude, $u' = 1.44$ feet per second, and gave similar results.

Disturbance-Displacement Growth

In this section the actual disturbance-displacement growth is compared with that of qualitative theory (fig. 10).

In an effort to produce low-disturbance amplitudes, the glass walls of the test section were reduced to 6 inches in length and the flameholder moved to 5/8 inch downstream of the nozzle entrance. At this position the speaker inputs were calibrated with the hot wire as previously discussed, and shadowgraphs were taken for several low amplitudes. As mentioned under "Turbulence intensity and spectra", the flameholder boundary layer underwent transition in the separated layer. The photographs of figure 31(a) show that, at these low intensities, the apparent width of the flame was not appreciably altered. The mean flame width measured from a direct photograph was used to determine h_2/h_1 .

The displacement h was measured as the distance from surrounding crests to a given trough in the flame surface. Measurements were made on both sides of the flame for each photograph. No attempt was made to separate the component of h because of superposition of a random velocity disturbance upon the imposed disturbance. The data for two amplitudes and two frequencies obtained in this manner are shown in figures 31(b), (c), and (d). The dashed curve is the qualitative curve from figure 10.

The knee should occur between $(h_2/h_1)_{\max}$ and $(h_2/h_1)_{\text{critical}}$ as discussed in the section Relation of Theoretical Results to Measurable Quantities. The vertical dashed lines in figure 31 are drawn through these two values. It can be seen that, and with the general shape of the qualitative dashed curve known, if a line were faired through the data points, it would exhibit a knee in the region bounded by $(h_2/h_1)_{\max}$ and $(h_2/h_1)_{\text{critical}}$. A comparison of figures 31(c) and (d) shows that the knee moves to increased values of h_2/h_1 as frequency is reduced. Both the value of h_2/h_1 where the knee occurs and the variation of this value with frequency agree with the results of the analysis.

Disturbance Phase Velocities

From the photographs of figure 31(a), values of c_r/U_1 were determined, again using the mean flame width to furnish h_2/h_1 . The quantity

U_1/U_0 was then determined from Tsien's results (eq. (3)). Wavelengths were measured from trough to trough, and the mean position of a pair of troughs located the applicable value of h_2/h_1 . The results for two frequencies are shown in figure 32.

The dashed lines are the values of c_r/U_1 obtained from figure 5(b), which is based on the results and interpretation of the stability analysis. The scatter of the experimental data is quite bad, but the magnitude and trends of the data remote from the flameholder are quite good. Values of c_r/U_1 less than unity are obtained for values of $h_2/h_1 < 1.5$, which implies flow reversal within this region.

Effect of Test-Section Depth

A single run was made to determine the effect of the test-section depth on the results. Figure 33 shows the data obtained with the 1-inch-deep combustor at a velocity of 50 feet per second and a fuel-air ratio of 0.0493. The turbulence at the center of the duct was half that of the 1/2-inch duct. Combustor depth seems to have some influence on the turbulent flame speed, but not on the effect of imposed disturbances.

The undisturbed flame speed in the 1-inch duct arrived at almost twice laminar flame speed in a longer time than with the 1/2-inch duct. The effect of imposed disturbance on amplification as a function of frequency remains the same, however. This can be seen from a comparison of figure 33 with figure 28(a). The range over which a given frequency dominates, taken from this run, is also plotted in figure 30.

Effect of Amplitude

The effect of amplitude on single frequencies is shown in figure 34, where flame speeds for two levels of excitation (580 and 960 cps) are compared. For the lower frequency, the increase $\Delta(S_{TD}/S_{TU})$ varies directly as u' at the two conditions. For the higher frequency, the curves cross. Thus, for lower excitation the effect is felt farther along the flame than for higher excitation.

This behavior is not data scatter and was checked repeatedly. The same sort of thing occurs at 1500 cps, although not so markedly. The reason for this anomalous behavior is not immediately apparent.

Effect of Flameholder Size

Figure 35 compares S_T/S_L and flame appearance for two flameholder sizes at a velocity of 50 feet per second and a fuel-air ratio of 0.044.

Figure 35(a) shows data for a 1/2-inch flameholder and a variety of excitation frequencies. The 580-cps excitation is again the dominant one, but not so markedly as before. Figure 35(b) shows the set of corresponding shadowgraphs. Figures 35(c), (d), and (e) compare values of S_T/S_L for 0.500-inch and 0.306-inch flameholders and give a shadowgraph picture for each case. The effect of flameholder size can be summarized as follows:

(1) In each case, flame speed is noticeably decreased with the larger flameholder.

(2) The impact of the 580-cps frequency is not nearly so great in the 1/2-inch flameholder as in the 0.306-inch flameholder.

The decrease in flame speed with increase in flameholder size might be explained by the theory that (1) the wake region is longer and (2) the growth of the higher frequencies is therefore somewhat inhibited by this long, relatively stable wake.

Effect of Velocity

Momentum-pressure-drop and flame-speed readings were taken over a range of frequencies, using a 0.306-inch flameholder, a velocity of 100 feet per second, and fuel-air ratio of 0.0493.

The results are shown in figure 36(a). The metering systems drifted slightly at this setting, making it difficult to hold fuel flow steady and causing some scatter in the calibration S_L .

The most sensitive frequency at 100 feet per second was 1700 cps, which is about three times the frequency observed at 50 feet per second. Clearly the effect is not allied with a spontaneous eddy-shedding frequency. The fraction burned is not so great as at 50 feet per second. Also, the flame speed increased sharply up to the end of the duct. These two factors would tend to emphasize the higher frequencies within the limited duct length, and would seem to be directly related to the instability of the flame zone. The single data point at 1700 cps is included in figure 30.

This run was directed toward finding a frequency other than 580 for maximum effect, mainly to prevent duct resonance. A different frequency for maximum effect was obtained. Shadowgraph photographs of these flames are shown in figure 36(b). Again, the disturbance is antisymmetric.

The possible effect of duct resonance on these results must be considered. The modes of resonance likely to occur in a combustor are the

3877 "organ-pipe" or longitudinal modes, the transverse modes, and a single mode coupling the combustion chamber with the volume upstream of the nozzle. In the configuration studied, the longitudinal modes have frequencies, roughly, of 250 or 500 cps plus multiples of 500. The transverse modes have a minimum frequency of 3000 cps, so they are not considered here. The last type of oscillation gives a frequency of the order of 45 to 90 cps and is below the range of interest.

A longitudinal mode could affect the results in two distinct ways: (1) If the flameholder were placed in a standing wave system at a pressure node, the time-varying velocity past the flameholder would cause large initial disturbances that would be symmetric with respect to the duct axis. (2) If the flameholder were placed at a pressure loop, there would be a coupling between the combustor and flameholder resonance that would be initially compensated for by the input calibration already discussed. If the nature of duct resonance shifts the resonant frequencies so that this compensation is no longer adequate, the input u' is no longer constant for all the frequencies.

Because the photographs of figure 36(b) show the disturbances to be antisymmetric, the first manner of coupling is rejected. To explore the second manner of coupling, the input u' for the frequencies on either side of the most sensitive ones (i.e., 1500 to 1700 cps; see fig. 36(a)) were increased by a factor of 3. In no case was it possible to increase the fraction burned as much as the 1500- to 1700-cps disturbances did. It is concluded that the results shown in figure 36(a) are due to the sensitivity of the flame zone to the imposed disturbance and are not due to duct resonance.

Symmetric Disturbances

A symmetric disturbance was used for tests with a 0.315-inch flameholder, velocity of 50 feet per second, and fuel-air ratio of 0.044. No separate calibration of input sound was attempted, the inputs of the antisymmetric-disturbance tests being used.

The results are shown in figure 37(a) and corresponding photographs in figure 37(b). Comparisons with flame speeds obtained with antisymmetric disturbances are given. There was a leak of approximately 1/16 inch past one edge, which provided an additional flame surface and increased the apparent mean flame speed near the flameholder but did not disturb the results at some distance from the flameholder. In general, symmetric and antisymmetric disturbances gave roughly comparable shifts in flame speed near the flameholder. At a distance from the flameholder, antisymmetric disturbances increased the flame speed more than did symmetric disturbances. These results are in accordance with figure 10.

DISCUSSION

This section is devoted to a discussion of the questions raised by the analytical and experimental phases of the investigation.

1. In what respects do the experimental results and the interpretations of the stability analysis agree? - The areas of agreement are summarized in the following table:

Interpretation of stability analysis	Investigation of sensitivity of a flame in a duct to transverse velocity disturbance
1. The flow is stable to symmetric disturbances, unstable to antisymmetric disturbances. A qualification is made near a flameholder where the two types of disturbances are equally unstable.	1. The flame seems about equally unstable to symmetric and antisymmetric disturbances near flameholder, is more unstable to antisymmetric disturbances far from flameholder.
2. In moving along the flame at phase velocity, a disturbance of given frequency grows until the flame width becomes about 0.4 of the wavelength, then an apparent decay of the disturbance begins.	2. A disturbance of given frequency first grows, then decays. The critical flame width where decay starts is slightly smaller than that predicted.
3. There is a most-amplified frequency having a wave number $2\alpha_0 h_1 = 6 \rightarrow 8$.	3. There is a most-amplified frequency which, for the lengths investigated, corresponds to $2\alpha_0 h_1 \approx 12$.
4. The phase velocity ranges from a velocity equal to the cold-gas velocity at the flameholder up to 1.5 times the cold-gas velocity far from flameholder.	4. The phase velocity behaves much as predicted except near the flameholder, where it is lower than the cold-gas velocity.
5. The amplification depends on v'/S_{T_0} for a given dh_2/dx .	5. The amplification depends on v'/S_{T_0} for a given dh_2/dx .

The details of the system that would define more exactly the shortcomings of the stability analysis as well as the adequacies await the development of a transient-velocity measuring technique that can be used in a flame zone. In at least one instance there was evidence that a form of transition took place (see Comparison of Flame Speed with Flame Appearance). The stability analysis cannot indicate when this takes place.

2. Would the same distribution of displacement and S_T/S_L with distance from the flameholder obtain if no growth occurred in the flame zone? - This seems unlikely. For example, if the input disturbance distribution simulates a source at the corner of the flameholder, only near the flameholder would there be a marked transverse velocity component. The highest frequencies would show the greatest increases in flame speed.

3. Do eddies shed? - They certainly seem to. In figure 38 photographs of a lean flame, both the shadowgraphs and the direct photographs taken through the stroboscope, are compared with a smoke-trace photograph of eddies shedding from a rod at a Reynolds number of 73 (ref. 32). The appearance of flame clearly indicates that eddy shedding is present.

As the fuel-air ratio is increased, the range over which these eddies appear near the flameholder narrows. Figure 39 shows a plot of frequencies at which eddies appeared against fuel flow from lean to rich blow-out. These data were obtained by exciting the flame at frequencies at which the constant-speed stroboscope would permit observation, that is, approximately every 100 cps.

Eddies are characterized by lobes of flame of about equal size on either side of the flameholder. These are contrasted to mere sinuosity of the flame. At 700 cps the lobes appeared symmetric, indicating duct resonance at this frequency. At 800 cps the lobes were antisymmetric and were observed throughout the fuel-air ratio range. At the lean fuel-air ratios, most of the disturbances produced eddy shedding.

4. Does the turbulent-flame propagation velocity depend upon upstream turbulence? - It should. Bolz and Burlage (ref. 11) and Mickelsen and Ernstein (ref. 12) have shown turbulent flame speeds to be in fair agreement with Scurlock's theory (ref. 8), omitting flame-generated turbulence effects. These data were obtained in turbulent "soap-bubble" flames. Thus, in addition to the effect of the instabilities mentioned here, the incident turbulence should have an effect.

The most important point, however, is that the instability merely acts as an amplifier for a relatively narrow range of frequencies, the output within limits of the linearized theory being proportional to the input. Part of the input is, of course, the turbulent motion. The other, and in some cases the most important part, is the role played by the sound in the duct which, upon hitting the flameholder, produces a transverse velocity that may be subsequently amplified. In that this sound is related to the incident turbulence, the turbulence has an effect.

Some data on an effect of incident turbulence were obtained while exploring the properties of the system. Figure 40 shows a plot of S_T/S_L against distance from the flameholder x for two flameholder positions and two fuel-air ratios. The table in the section "Turbulence intensity and spectra" shows that the turbulence intensity increases from inlet nozzle to exhaust and from the wall to the interior of the test section. Taking as representative the value of u' measured 3/16 inch above the flameholder lip, the values of the turbulence parameter u'/S_L vary over a factor of 2 for the two flameholder positions. It is apparent that, everywhere except near the flameholder, there is little effect of the initial u'/S_L values measured. The data are insufficient for pinpointing the cause of this lack of effect. Two surmises appear warranted:

(1) The flame was noisier at the 9-inch position than at the 6-inch position because of flame-duct interaction. u' was measured in the absence of a flame.

(2) The turbulence found upstream of the flameholder was due to transition in the boundary layer. The u' in the boundary layer was growing for both positions measured. It is thought that the growth of this u' is accelerated when the boundary layer separates from the flameholder and quite rapidly achieves a value that would be relatively insensitive to u' prior to separation.

Additional data on the effect of upstream turbulence were obtained by putting three banks of 200-mesh screen just upstream of the flameholder. Shadowgraphs of the flame in this case with and without a 560 cps disturbance are shown in figure 41. Also plotted in this figure is S_T/S_L measured with and without screens against distance x . In the absence of imposed disturbances, S_T/S_L is lower with the screens than without. Although the conditions were set for 50 feet per second, leaks were found between the mixing section and the flameholder for this run so that the velocity was not known. The reduction in S_T/S_L is thought primarily due to the reduction in u' by the presence of the screens.

It is of interest to compare the flame-speed data obtained in this investigation with data taken in a similar apparatus. Figure 42 shows a comparison of S_T/S_L obtained by photomultiplier tube with S_T/S_L obtained by Scurlock (ref. 8) by measuring a mean flame width. Because S_L was taken as a property of the mixture, the values of S_T/S_L near the flameholder are low. The values of S_T/S_L obtained with the relatively high turbulence appear higher than those obtained by Scurlock. The possible displacement of the absolute magnitudes of S_T/S_L due to the different methods used would not warrant interpreting these data to give a quantitative dependence on turbulence intensity.

5. How does S_T/S_L obtained from area measurements compare with S_T/S_L taken from photomultiplier data? - The shadowgraphs indicate considerable wrinkling of the flame surface. In addition, it appears that density gradients exist within the outer envelope of flame surface, implying heat release there.

Since no single continuous flame surface is apparent, measuring flame area from these pictures seems impossible. For the sake of comparison, however, some relative surface extension should be of interest to those who would formulate a theory of turbulent flame propagation. Such measurements were made in the following manner: The negatives of a group of photographs were used to project an image of the flame on a screen. The image of a 6-inch test section measured $2\frac{1}{2}$ feet in length. A map measure was used to find the length of the outer envelope of the group of flame images, ignoring the obvious density gradients within the outer envelope. Lengths were measured on the top and bottom surface of each flame, averaged, and divided by projected length. The resulting quotient is defined as $(S_T/S_L)_A$.

In the following table, the ratios so obtained are compared with the average S_T/S_L obtained from a photomultiplier survey $(S_T/S_L)_P$.

Fuel-air ratio	U_0 , ft/sec	Flame-holder size, in.	Photo-graph from fig. -	Excitation frequency, f, cps	$(\frac{S_T}{S_L})_A$	$(\frac{S_T}{S_L})_P$	$\frac{(\frac{S_T}{S_L})_P}{(\frac{S_T}{S_L})_A}$
0.0444	50	0.306	28(a)	0	1.436	2	1.392
.0444	50	.306	28(e)	560	1.77	2.54	1.430
.0515	50	.306	28(a)	0	1.40	1.82	1.30
.0444	50	.5	28(a)	0	1.36	1.735	1.28
.0493	100	.306	37(b)	0	1.65	2.460	1.490

In general, the trends indicated by the $(S_T/S_L)_P$ are followed by the $(S_T/S_L)_A$. In view of the obvious internal structure and three-dimensional nature of the wrinkles, no argument for or against the wrinkled flame as an adequate turbulent flame model can be introduced.

6. How can flame speeds be predicted on the basis of these results? - The most promising method of predicting flame speeds would be based on an incident and amplified spectra, as recommended by Markstein (ref. 14). For example: If the incident v' spectrum corresponds to an L_x of 0.15 inch and each frequency is amplified as the theory states, the spectra at $h_2/h_1 = 0.5$ and 0.25, for $1/K_1 \approx 20$, would correspond to

the ones shown in figure 43. Between the two spectra would be a continuously shifting spectrum. What is needed, then, is a model of flame propagation that would allow for a continuously shifting spectrum of turbulence. This model should have the advantage of allowing for the appearance of discrete frequencies that dominate the balance of the spectrum.

An interesting point comes up in regard to spectra. It is seen experimentally as well as theoretically that very little effect is derived from exciting the flame at a frequency less than $\frac{2}{3} \frac{U}{2h_1}$ or greater than $4U/2h_1$ (see figs. 26, 36, and 7). It would appear, therefore, that for the present conditions (i.e., velocity of 50 ft/sec, 2-in. duct) the energy in the spectrum of turbulence below 200 cps will not increase flame spreading.

A plot of the percentage of energy in the turbulence at all frequencies below f against fL_x/U from Dryden (ref. 40) is shown in figure 44. For an assumed scale $L_x = \frac{1}{6} 2h_1$, the frequency below the frequency $\frac{2}{3} \frac{U}{2h_1}$ represents about 35 percent of the total turbulence energy. This amount of energy is contained in disturbances whose frequency is too low to be amplified to any usable extent by the flame zone. Similarly from figure 44, the energy in the spectrum below the frequency $f = \frac{4U}{2h_1}$ (or $f \frac{L_x}{U} \approx 0.66$) is 85 percent of the total turbulence energy. Thus, about 15 percent of the turbulence energy is at frequencies too high to be appreciably amplified by the flame zone.

The scale of isotropic turbulence that would put the largest percentage of energy in the frequency range $\frac{2}{3} \frac{U}{2h_1} < f < \frac{4U}{2h_1}$ can be found from the extremum of the quantity (ref. 38)

$$\tan^{-1} \left(2\pi \frac{4U}{2h_1} \frac{L_x}{U} \right) - \tan^{-1} \left(2\pi \frac{2}{3} \frac{U}{2h_1} \frac{L_x}{U} \right)$$

or

$$L_x = \frac{1}{10} 2h_1$$

In this case the amount of energy within the frequency range is 55 percent of the total as compared to 50 percent for $L_x = \frac{1}{6} 2h_1$; 40 percent for $L_x = \frac{1}{3} 2h_1$; and 45 percent for $L_x = \frac{1}{20} 2h_1$.

7. Can the results concerning frequency be applied to multiple flameholders? - If n flameholders are arranged so that the flow field can be divided into n identical segments, Scurlock's results hold for each segment. The results in the theoretical sections of this report for the stability of the flow field apply to each segment and rely on the condition that v' vanishes at the boundary of each segment. Although one of several modes of instability may satisfy this condition, it is obvious that the foregoing results do not give any information about the other modes.

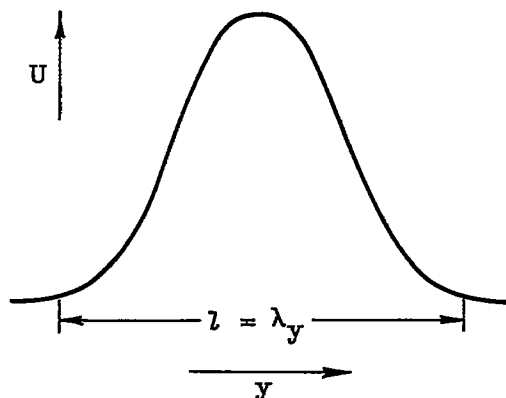
To illustrate the occurrence of multiple modes, consider a profile examined by Lin (ref. 24, pp. 219-220) where

$$U = A + B \sin \frac{2\pi}{\lambda_y} y$$

Lin shows that the wave numbers for neutral stability of the different modes available are dependent upon the number of inflection points in the flow and can be given by

$$(\alpha l)^2 = \left(\frac{2\pi l}{\lambda_y} \right)^2 - (n\pi)^2$$

The choice of $l = \lambda_y$ yields the following profile which is similar to the one studied earlier in this report for a single flameholder

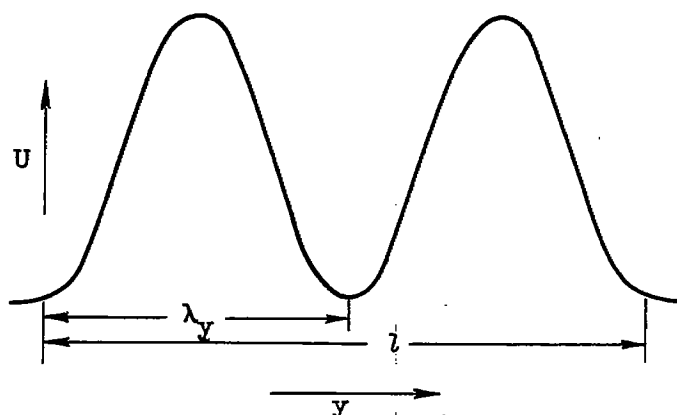


For this case neutral stability occurs at $\alpha \lambda_y = \alpha l = \pi\sqrt{3}$, 0.

3877

CY-9 back

If two flameholders are present, the profile (following sketch) may be approximated by setting $l = 2\lambda_y$.



For this case the wave numbers for neutral stability of the four modes obtained are

$$\alpha\lambda_y = \alpha \frac{l}{2} = \pi \frac{\sqrt{15}}{2}, \pi\sqrt{3}, \pi \frac{\sqrt{7}}{2}, 0$$

Two new modes appear in addition to the two for the single profile.

Similarly, for three flameholders,

$$\alpha\lambda_y = \alpha \frac{l}{3} = \pi \frac{\sqrt{35}}{3}, \pi \frac{\sqrt{32}}{3}, \pi\sqrt{3}, \pi \frac{\sqrt{20}}{3}, \pi \frac{\sqrt{\pi}}{3}, 0$$

that is, there appear four roots in addition to the two for $l = \lambda_y$.

In short, the single mode investigated in this report is applicable to the case of multiple flameholders, but only as one of several modes that combine to give the entire instability.





8. Can the excitation at the flameholder permit increased combustion rates without destroying the burner walls? - Yes. In these tests the sound level at the exhaust plane was only 93 decibels with the flame excited. When the flame is excited by the destructive duct resonance, the sound level is of the order of 200 decibels (ref. 19).

In order to apply this type of excitation to an engine, the control exerted herein (a speaker system) would not be needed. Instead, the disturbance can be introduced by suitably placed whistles, mounted on the

flameholder and driven by the flowing stream. The whistle ideally should have a number of strong overtones and a fundamental equal to the most sensitive frequency $U_0/2h$. The overtones would serve to increase the heat-release rate near the flameholder, while the fundamental would increase the heat-release rate far from the flameholder.

9. What would be the sacrifice in stability and pressure drop for such an excitation? - Both these penalties require further investigation, but from work that has been done the price does not seem high. For example: When the flameholder was placed $5/8$ inch from the nozzle entrance and a 6-inch-long test section was installed, lean blow-out at 50 feet per second occurred at a fuel-air ratio of 0.042. At a fuel-air ratio of 0.0453, the disturbance amplitudes required to cause blowout were found for several frequencies. The results are shown in figure 45. Minimum disturbance velocity was required at 780 cps. At this condition the flameholder without flame had an eddy-shedding frequency of 420 cps. The Strouhal number is thus 0.206, agreeing well with the results of Roshko (ref. 36). The cold-duct resonance fundamental was 1000 cps. The reason for this result is not known. The main point here, however, is to show the effect of disturbances to be used for promoting flame propagation upon flameholder stability. It was found that, at a fuel-air ratio of 0.047, it was impossible to induce blowout with speaker inputs as much as 10 times those used in the earlier tests. It seems safe to say that the imposed disturbances will narrow the stability range slightly but not prohibitively and the amount of narrowing will depend upon the frequencies imposed.

An interesting observation was made in the study of lean blowout. As the lean blowout fuel-air ratio was approached, the flame emitted a low-frequency noise at 87 cps. The average heat release rate dropped abruptly. A survey taken with the photomultiplier probe showed the flame to be intermittently extinguished for all positions greater than $7/8$ inch downstream of the flameholder. Typical wave forms observed at several stations downstream of the flameholder are shown in the following table.

Distance downstream of flameholder, in.	Wave form of photomultiplier signal
$\frac{7}{8}$	
$1\frac{1}{8}$	
2	
4	

Random photographs taken at this condition show intervals during which no flame was present in part of the combustor. These photographs appear in figure 46.




It is curious that the flame surface facing upstream at the break in the flame is strong and well-defined both in the photomultiplier and the shadowgraph observations. The flame surface facing downstream is conversely ill-defined in both methods of observation. Near the point of rupture the photomultiplier signal is approximately symmetric. No explanation for this is apparent. The most significant feature of these data is that this form of resonance accompanied by intermittent blowoff downstream of the sheltered zone was the only form of excitation that reduced the heat-release rate in the combustor. On this basis it is tempting to generalize that all oscillations that do not cause flame parture must increase the heat release rate in the combustor.



For the frequency of maximum amplification (560 cps), an increase of as much as 30 percent in heat release or about 0.2 percent of the kinetic energy of the flowing stream KE_{stream} was obtained in the 6-inch-long combustor for an energy flux

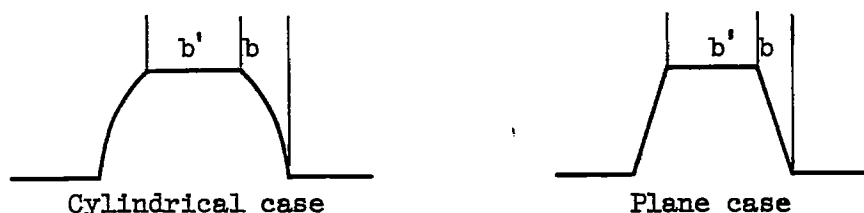
$$\frac{E_{sound}}{KE_{stream}} \approx \frac{6}{2500}$$

In this case the noise level at the exhaust was 93 decibels.

Another way of increasing the heat release rate that is indirectly suggested by the present paper is to locally accelerate the flow or alter the profile to a more unstable one by use of a convergent-divergent combustion chamber. One way these can be combined with the introduction of a v' at the desired frequency is to construct a combustor with a wavy wall. Using this method of excitation would require a new experimental determination of the desired wavelength and amplitude of the wall's waves, but would eliminate any effect on flame anchoring.

10. Can anything be done about predicting the behavior of axially symmetric flames in cylindrical ducts? - A little can be done. First, the steady-state problem, solved by Scurlock, of the cylindrical flame in a cylindrical duct yielded a  profile as opposed to the  profile for plane flow. If the arc part of the curved profile is assumed parabolic, the cylindrically symmetric disturbance equation can be solved by elementary functions for the case of symmetric disturbances. This, however, accomplishes nothing, because the profile is neutrally stable to symmetric disturbances. This is the same result obtained for the  profile in the plane case. For the case of antisymmetric disturbances, the problem is more complicated and no simple solution is apparent.

If the profile is affected by a flameholder in such a way that it may more nearly be approximated by a  profile composed of three straight-line segments and two parabolic arcs, a range of instability for symmetric disturbances is obtained. This profile can be compared with the corresponding profile in plane flow . Such an analysis is given in the appendix. A few calculations are given to permit comparison with the data of figure 15, for conditions that h_1 approaches infinity and ρ is constant throughout. The results are compared in the following table:



$\frac{1}{2} \frac{b'}{b}$	$2\alpha b$	
	Plane case	Cylindrical case
0.1	2.26	2.08
.2	2.55	2.42
1.0	2.55	2.54

In these cases the critical wave numbers agree quite closely. At a first guess it would seem that the results for the case of plane flow would be a fair approximation for the case of cylindrical flow.

In order to obtain a rough experimental check on this supposition, a $\frac{1}{2}$ -inch-I.D. glass tube and its accommodating nozzle were installed in place of the rectangular test section. The $\frac{1}{2}$ - by 0.306-inch antisymmetric flameholder was retained. At 50 feet per second and a fuel-air ratio of 0.047, resonance-free operation was obtained at a combustor length of $4\frac{1}{2}$ inches or less. With the flameholder set to give this length, the disturbance inputs were calibrated as before to give a disturbance velocity of 1.8 feet per second. Then the burning run was made with the settings indicated by calibration. The flame speeds were measured by the photomultiplier probe plus a measurement of an average local flame diameter. The results are shown in the following table:

Frequency, f, cps	S_T/S_L		
	1 In. from flameholder	2 In. from flameholder	4 In. from flameholder
0	2.27	3.31	3.58
200	----	3.56	3.77
385	2.59	3.56	3.95
580	2.68	3.56	3.95
770	2.82	3.65	4.25
980	2.89	3.70	3.80
1170	2.89	3.70	3.73
1360	2.96	3.65	3.73
1740	3.09	3.65	3.99

The flame speed in this case is almost twice as high as in the plane burner. Part of this increase is undoubtedly due to the disturbances introduced by the corners of the flameholder. The fraction burned in this case is 20 percent at the position 4 inches from the flameholder, corresponding to $h_2/h_1 = 0.7$. Therefore, the frequencies in 4 inches of this duct may be compared with those obtained in 6 inches or more of the rectangular duct. The values of $2\alpha_0 h_1$ giving the greatest increase in flame speed at the termini of the respective ducts are

Frequency, f, cps	$2h_1$, in.	U_0 , ft/sec	Geometry	$2\alpha_0 h_1$ for max. S_T/S_L
570	2	50	Plane	11.95
770	1.5	50	Cylindrical	12.10

Of course, these data were obtained in a single test, performed to satisfy curiosity. The agreement does make it seem likely that a carry-over of about 1:1 would be feasible in going from the plane case to the cylindrically symmetric case.

SUMMARY OF RESULTS

THEORY

The flow field of a flame in a duct is unstable to transverse disturbances having wavelengths 2.5 times the local flame width.

The amount a given frequency disturbance will grow varies directly as the frequency and inversely as the rate of flame spreading dh/dx and is independent of velocity and density ratio across the flame front.

The frequency where maximum velocity-disturbance growth obtains is $f = \frac{2.8}{\pi} \frac{U_0}{2h_1}$, where U_0 is approach velocity and $2h_1$ is duct width.

This maximum growth occurs by the time the flame fills 64 percent of the duct and implies an amplification $v'/v_0 = (1.108)^{1/K_1}$ where $K_1 = dh/dx$. Frequencies higher or lower than this are amplified less. Higher frequencies achieve their terminal amplification at smaller values of h_2/h_1 . For example, a frequency of $\frac{1.5}{\pi} \frac{U_0}{2h_1}$ has an amplification of $v'/v_0 = (1.07)^{1/K_1}$, where $K_1 = dh_2/dx$ by the time the flame fills 28 percent of the duct.

By using a crude model of flame propagation, it is possible to predict the qualitative effect that amplified disturbances of discrete frequencies will have upon turbulent flame speed.

EXPERIMENT

The effects of disturbances imposed at the flameholder are in substantial agreement with those predicted by theory. In addition, the results show:

1. Eddies shed from the flameholder with flame when suitably excited.
2. The turbulent- to laminar-flame-speed ratio varies inversely as flameholder size, directly as ratio of flow velocity to flame speed or ratio of disturbance velocity to flame speed.
3. Potentially, the most useful theory of turbulent flame propagation would be based on an incident and locally shifting spectrum of turbulence.
4. Gains in local heat release rates can be obtained by using acoustic disturbances at a flameholder without damage to walls or excessive energy expenditure.

CONCLUDING REMARKS

The form of instability that is discussed in this paper is of interest in formulating a theory of turbulent flame propagation along with

plane combustion wave instability, and the boundary layer instability, mentioned earlier. At present it is not known whether the latter two forms of instability can be encouraged to influence turbulent flame propagation more than they do spontaneously. The little evidence that is available makes it appear that they cannot. The type of instability that is discussed in the present paper is of additional significance for the reason that its effect on the ratio of turbulent to laminar flame speed can be increased in some important applications. Several methods of increasing this ratio are as follows:

1. Increase the disturbance velocity at the frequency the flame zone can amplify.
2. Increase the amplification rate by locally raising the mean velocity in the combustor.
3. Increase the amplification rate by locally varying the velocity profile.

A method of employing all three of these improving factors would be to build a combustor having a wavy wall.

Although the second and third methods listed will clearly cause an increase in pressure drop, the first method substantially increased the heat release rate at a cost of a very small fraction of the kinetic energy in the approach stream flow and a slight reduction in the operating range of the flameholder.

Lewis Flight Propulsion Laboratory
National Advisory Committee for Aeronautics
Cleveland, Ohio, July 23, 1956

APPENDIX - AXIALLY SYMMETRIC DISTURBANCES INAXIALLY SYMMETRIC FLOW WITH DENSITY JUMPS

This appendix examines the stability of the flow field arising from a flame in a duct for the case of axial symmetry. The results are used in the body of the text to compare wave numbers for neutral stability of comparable plane and axially symmetric flow fields. The symbols are defined where used.

DISTURBANCE EQUATION

Pillow (ref. 25) defines the quantity ψ as

$$\psi = \phi(r) e^{i\alpha(z-ct)} \quad (A1)$$

The velocity in the z-direction is

$$u = U + u'$$

In the r-direction,

$$v = v'$$

where

$$v' = -\frac{\partial \psi}{\partial z}, \quad u' = \frac{1}{r} \frac{\partial(r\psi)}{\partial r} \quad (A2)$$

and the continuity equation is satisfied identically. Pillow shows that the disturbance equation then becomes

$$\left[(U - c) - \frac{1}{i\alpha R} (M - \alpha^2) \right] (M - \alpha^2) \phi - \phi \left(U'' - \frac{1}{r} U' \right) = 0 \quad (A3)$$

where

$$M = \frac{d^2}{dr^2} + \frac{1}{r} \frac{d}{dr} - \frac{1}{r^2} \quad (A4)$$

and R is Reynolds number.

If the study is restricted to cases where $R \rightarrow \infty$, and $U'' = \frac{1}{r} U'$ (i.e., parabolic profiles or flat profiles), then equation (A3) becomes

$$(M - \alpha^2)\phi = 0$$

3877

CY-10 back

or

$$\frac{d^2\phi}{dr^2} + \frac{1}{r} \frac{d\phi}{dr} - \frac{1}{r^2} + \alpha^2 = 0 \quad (A5)$$

with solutions

$$\phi = a_1 I_1(\alpha r) + a_2 K_1(\alpha r) \quad (A6)$$

where I_1 and K_1 are modified Bessel functions of the first and second kind. Therefore,

$$\begin{aligned} v' &= \frac{\partial \psi}{\partial z} = -i\alpha \phi(r) e^{i\alpha(z-ct)} \\ &= -i\alpha e^{i\alpha(z-ct)} [a_1 I_1(\alpha r) + a_2 K_1(\alpha r)] \end{aligned} \quad (A7)$$

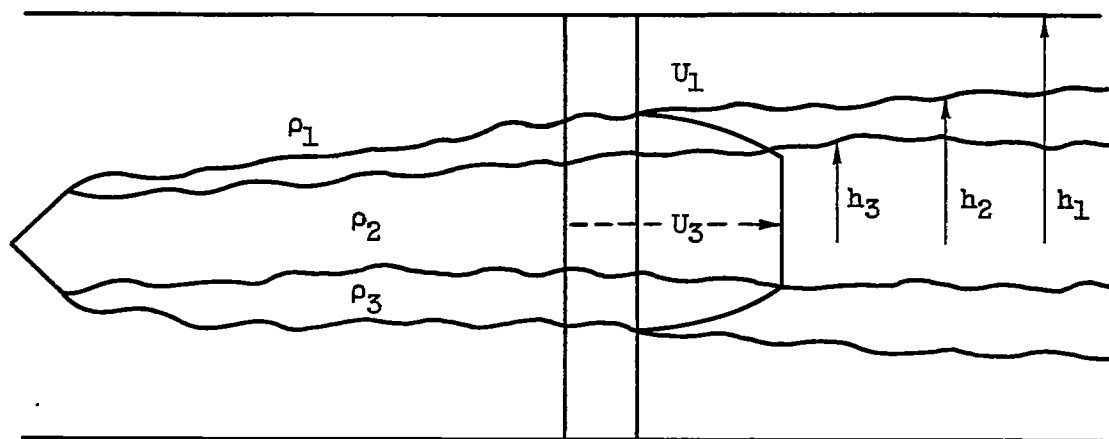
and

$$\begin{aligned} u' &= \frac{1}{r} \frac{\partial(r\psi)}{\partial r} \\ &= \frac{\partial \psi}{\partial r} + \frac{1}{r} \psi \\ &= \phi' + \frac{1}{r} \phi e^{i\alpha(z-ct)} \\ &= e^{i\alpha(z-ct)} \left\{ a_1 \left[\alpha I_1(\alpha r) + \frac{1}{r} I_1(\alpha r) \right] + a_2 \left[\alpha K_1(\alpha r) + \frac{1}{r} K_1(\alpha r) \right] \right\} \end{aligned} \quad (A8)$$

where the prime denotes differentiation with respect to the argument.

BOUNDARY CONDITIONS

Consider the following profile and density distribution



Let solutions to equation (A5) be denoted by ϕ_1, ϕ_2, ϕ_3 for regions 1, 2, and 3 with densities ρ_1, ρ_2 , and ρ_3 , respectively.

As in the plane case, the requirements are

$$\left. \begin{aligned} \phi_1 &= 0 \quad \text{at } h_1 \\ \phi_1 &= \phi_2 \quad \text{at } h_2 \\ \phi_2 &= \phi_3 \quad \text{at } h_3 \\ \phi_3 &= 0 \quad \text{at } r = 0 \end{aligned} \right\} \quad (\text{A9})$$

and because of symmetry

$$\left. \begin{aligned} \left(\frac{\partial \phi}{\partial x} \right)_1 &= \left(\frac{\partial \phi}{\partial z} \right)_2 \quad \text{at } h_2 \\ \left(\frac{\partial \phi}{\partial z} \right)_2 &= \left(\frac{\partial \phi}{\partial z} \right)_3 \quad \text{at } h_3 \end{aligned} \right\} \quad (\text{A10})$$

Since, at $r = h_1$,

$$\phi_1 = a_1 I_1(\alpha h_1) + a_2 K_1(\alpha h_1) = 0$$

then

$$a_1 = -a_1 \frac{I_1(\alpha h_1)}{K_1(\alpha h_1)} \quad (A11)$$

At $r = h_2$, $\phi_1 = \phi_2$ or with equation (A11)

$$\left. \begin{aligned} \phi_1 &= \alpha_1 \left[I_1(\alpha h_2) - \frac{I_1(\alpha h_1)}{K_1(\alpha h_1)} K_1(\alpha h_2) \right] \\ &= \phi_2 = b_1 I_1(\alpha h_2) + b_2 K_1(\alpha h_2) \end{aligned} \right\} \quad (A12)$$

At $r = h_3$, $\phi_2 = \phi_3$ or

$$\left. \begin{aligned} \phi_2 &= b_1 I_1(\alpha h_3) + b_2 K_1(\alpha h_3) \\ &= \phi_3 = c_1 I_1(\alpha h_3) + c_2 K_1(\alpha h_3) \end{aligned} \right\} \quad (A13)$$

Since $K_1(\alpha r) \rightarrow \infty$ as $\alpha r \rightarrow 0$, $I_1(\alpha r) \rightarrow 0$ as $\alpha r \rightarrow 0$, and at $r = 0$, $\phi_3 = 0$,

$$c_2 = 0 \quad (A14)$$

Since

$$\frac{\partial p}{\partial z} = -\rho \left(\frac{\partial u'}{\partial t} + U \frac{\partial u'}{\partial z} + v' \frac{dU}{dr} \right)$$

the pressure conditions yield at h_2 (from eqs. (A7) and (A8))

$$-\rho_1 \left[(-\alpha c + i\alpha U_1) \left(\alpha \phi_1' + \frac{1}{h_2} \phi_1 \right) \right] = -\rho_2 \left[(-i\alpha c + \alpha U_1) \left(\alpha \phi_2' + \frac{1}{h_2} \phi_2 \right) - i\alpha \phi_2 \frac{dU}{dr} \right] \quad (A15)$$

and at h_3

$$+\rho_3 \left\{ [-i(\alpha c) + i(\alpha U_3)] \left(\phi_3' + \frac{1}{h_3} \phi_3 \right) \right\} = +\rho_2 \left\{ [-i(\alpha c) + i(\alpha U_3)] \left(\phi_2' + \frac{1}{h_3} \phi_2 \right) - i(\alpha) \phi_2 \frac{dU}{dr} \right\} \quad (A16)$$

BOUNDARY VALUE PROBLEM

Employing the following notation,

$$\begin{aligned}
 \alpha_1 &= I_1(\alpha h_2) - \frac{I_1(\alpha h_1)}{K_1(\alpha h_1)} K_1(\alpha h_2) \\
 \alpha_2 &= \frac{\rho_1}{\rho_2} \left\{ \alpha I_1'(\alpha h_2) + \frac{1}{h_2} I_1(\alpha h_2) - \frac{I_1(\alpha h_1)}{K_1(\alpha h_1)} \left[\alpha K_1'(\alpha h_2) + \frac{1}{h_2} K_1(\alpha h_2) \right] \right\} \\
 \beta_1 &= I_1(\alpha h_2) \\
 \beta_2 &= K_1(\alpha h_2) \\
 \beta_3 &= I_1(\alpha h_3) \\
 \beta_4 &= K_1(\alpha h_3) \\
 \beta_5 &= \alpha I_1'(\alpha h_2) + \frac{1}{h_2} I_1(\alpha h_2) \\
 \beta_6 &= I_1(\alpha h_2) \left(\frac{dU}{dr} \right)_{h_2} \\
 \beta_7 &= \alpha K_1'(\alpha h_2) + \frac{1}{h_2} K_1(\alpha h_2) \\
 \beta_8 &= K_1(\alpha h_2) \left(\frac{dU}{dr} \right)_{h_2} \\
 \beta_9 &= \frac{\rho_2}{\rho_3} (\alpha I_1')(\alpha h_3) + \frac{1}{h_3} I_1(\alpha h_3) \\
 \beta_{10} &= \frac{\rho_2}{\rho_3} (\alpha K_1')(\alpha h_3) + \frac{1}{h_3} K_1(\alpha h_3) \\
 \beta_{11} &= \frac{\rho_2}{\rho_3} I_1(\alpha h_3) \left(\frac{dU}{dr} \right)_{h_2} \\
 \beta_{12} &= \frac{\rho_2}{\rho_3} K_1(\alpha h_3) \left(\frac{dU}{dr} \right)_{h_3}
 \end{aligned}
 \tag{A17}$$

and

$$r_1 = I_1(\alpha h_3) = \beta_3$$

$$r_2 = \alpha I_1'(\alpha h_3) + \frac{1}{h_3} I_1(\alpha h_3)$$

setting $U_1 = 0$ (this merely alters the real part of c by U_1) the determinantal equation for a_1 , b_1 , b_2 , and c_1 is

$$\begin{bmatrix} a & b_1 & b_1 & c_1 \\ \alpha_1 & -\beta_1 & -\beta_2 & 0 \\ 0 & \beta_3 & \beta_4 & -r_1 \\ -c\alpha_2 & c\beta_5 + \beta_6 & c\beta_7 + \beta_8 & 0 \\ 0 & (U_3 - c)\beta_9 - \beta_{11} & (U_3 - c)\beta_{10} - \beta_{11} & -(U_3 - c)r_2 \end{bmatrix} = 0 \quad (A18)$$

One immediate result of equation (A18) is to show that if dU/dr vanishes at either h_2 or h_3 in region 2, c is real for all α'_s . This can be seen by setting

$$\beta_6 = \beta_8 = \left(\frac{dU}{dr}\right)_{h_2} = 0$$

and factoring c from the third row of equation (A18), or setting

$$\beta_{11} = \beta_{12} = \left(\frac{dU}{dr}\right)_{h_3} = 0$$

and factoring $U_3 = c$ from the fourth row of equation (A18). Either operation leaves a determinantal equation in which c is wholly real.

If

$$\left. \begin{aligned} \left(\frac{dU}{dr}\right)_{h_2} &= g_2 \\ \left(\frac{dU}{dr}\right)_{h_3} &= g_3 \end{aligned} \right\} \quad (A19)$$

and

$$\left. \begin{aligned} g_2 \beta_1 &= \beta_6 \\ g_2 \beta_2 &= \beta_8 \\ \frac{\rho_2}{\rho_3} g_3 \beta_3 &= \beta_{11} \\ \frac{\rho_2}{\rho_3} g_3 \beta_4 &= \beta_{12} \end{aligned} \right\} \quad (A20)$$

then equation (A18) can be reduced to

$$\left[\begin{array}{cc} -\frac{\alpha_2 - g_2 \alpha_1}{\alpha_1} \beta_1 + c \beta_5 & -\frac{\alpha_2 - g_2 \alpha_1}{\alpha_1} \beta_2 + c \beta_7 \\ -\frac{(U_3 - c)r_2 + \frac{\rho_2}{\rho_3} g_3 r_1}{r_1} \beta_3 + (U_3 - c) \beta_9 & -\frac{(U_3 - c)r_2 + \frac{\rho_2}{\rho_3} g_3 r_1}{r_1} \beta_4 + (U_3 - c) \beta_{10} \end{array} \right] = 0 \quad (A21)$$

This is in the form

$$\begin{vmatrix} mc + n & oc + p \\ qc + s & tc + u \end{vmatrix} = 0$$

or

$$mtc^2 - oqc^2 + c(\mu u + nt - os - qp) + nu - ps = 0$$

and the discriminant of c is

$$\begin{aligned} D \equiv & m^2 u^2 + n^2 t^2 + o^2 s^2 + q^2 p^2 + -2\mu nt - 2osqp - \\ & 2\mu os - 2\mu qp - 2ntos - 2ntqp + 4oqnu + 4mtps \end{aligned} \quad (A22)$$

If $D < 0$, then c is complex and an unstable mode exists. The symbols of equation (A22) are defined

$$\left. \begin{aligned} m &= \beta_5 - \beta_1 \frac{\alpha_2}{\alpha_1} \\ n &= \beta_1 g_2 \\ o &= \beta_7 - \beta_2 \frac{\alpha_2}{\alpha_1} \\ p &= \beta_2 g_2 \\ q &= \beta_3 \frac{r_2}{r_1} - \beta_9 \\ s &= U_3 \beta_9 - \frac{\rho_2}{\rho_3} g_3 \beta_3 - U_3 \frac{r_2}{r_1} \beta_3 \\ t &= \beta_4 \frac{r_2}{r_1} - \beta_{10} \\ u &= U_3 \beta_{10} - \frac{\rho_2}{\rho_3} g_3 \beta_4 - U_3 \frac{r_2}{r_1} \beta_4 \end{aligned} \right\} \quad (A23)$$

REFERENCES

1. Scurlock, A. C.: Flame Stabilization and Propagation in High-Velocity Gas Streams. Meteor Rep. 19, Fuels Res. Lab., M.I.T., May 1948. (Contract NOrd 9661.)
2. Haddock, Gordon W.: Flame-Blowoff Studies of Cylindrical Flameholders in Channeled Flow. Prog. Rep. 3-24, Jet Prop. Lab., C.I.T., May 14, 1951.
3. Zukowski, Edward E., and Marble, Frank E.: The Role of Wake Transition in the Process of Flame Stabilization on Bluff Bodies. Combustion Res. and Rev., Butterworths Sci. Pub., 1955, pp. 167-180.
4. Wohl, Kurt: Comments on Turbulent Flames. AGARD Selected Combustion Problems, Butterworths Sci. Pub. (London), 1954, pp. 268-274.

5. Berl, W. G., Rice, J. L., and Rosen, P.: Flames in Turbulent Streams. Jet Prop., vol. 25, no. 7, July 1955, pp. 341-346.
6. Damköhler, Gerhard: The Effect of Turbulence on the Flame Velocity in Gas Mixtures. NACA TM 1112, 1947.
7. Shelkin, K. I.: On Combustion in a Turbulent Flow. NACA TM 1110, 1947.
8. Scurlock, Arch C., and Grover, John H.: Experimental Studies on Turbulent Flames. AGARD Selected Combustion Problems, Butterworths Sci. Pub. (London), 1954, pp. 215-247.
9. Leason, D. B.: Turbulence and Flame Propagation in Premixed Gases. Fuel, vol. XXX, no. 10, Oct. 1951, pp. 233-238; discussion, pp. 238-239.
10. Mickelsen, William R.: The Propagation of a Free Flame Through a Turbulent Gas Stream. M.S. Thesis, Case Inst. Tech., 1953.
11. Bolz, Ray E., and Burlage, Henry, Jr.: The Influence of Turbulence on Flame Propagation Rates. Jet Prop., vol. 25, no. 6, June 1955, pp. 265-275; con't. p. 283.
12. Mickelsen, William R., and Ernstein, Norman E.: Propagation of a Free Flame in a Turbulent Gas Stream. NACA TN 3456, 1955.
13. Karlovitz, Béla: A Turbulent Flame Theory Derived from Experiments. AGARD Selected Combustion Problems, Butterworths Sci. Pub. (London), 1954, pp. 248-262; discussion, pp. 263-274.
14. Markstein, George H.: Comments on Papers. AGARD Selected Combustion Problems, Butterworths Sci. Pub. (London), 1954, pp. 263-265.
15. Tucker, Maurice: Interaction of a Free Flame Front with a Turbulence Field. NACA TN 3407, 1955.
16. Summerfield, Martin, Reiter, Sydney H., Kebely, Victor, and Mascolo, Richard W.: The Structure and Propagation Mechanism of Turbulent Flames in High Speed Flow. Jet Prop., vol. 25, no. 8, Aug. 1955, pp. 377-384.
17. Rayleigh: The Theory of Sound. Vol. II. Dover Pub., 1945.
18. Fenn, J. B., Forney, H. B., and Garmon, R. C.: Burners for Supersonic Ram-Jets. Ind. and Eng. Chem., vol. 43, no. 7, July 1951, pp. 1663-1671.

3877

CY-11 back

19. Blackshear, Perry L., Rayle, Warren D., and Tower, Leonard K.: Study of Screeching Combustion in a 6-Inch Simulated Afterburner. NACA TN 3567, 1955.
20. Truman, John C., and Newton, Roger T.: Why Do High-Thrust Engines Screech? Aviation Age, vol. 23, no. 5, May 1955, pp. 136-143.
21. Kaskan, W. E., and Noreen, A. E.: High-Frequency Oscillations of a Flame Held by a Bluff Body. Trans. A.S.M.E., vol. 77, no. 6, Aug. 1955, pp. 885-891; discussion, pp. 891-895.
22. Tsien, H. S.: Influence of Flame Front on the Flow Field. Jour. Appl. Mech., vol. 18, no. 2, June 1951, pp. 188-194.
23. Fabri, J., Siestrunk, R., and Fouré, C.: On the Aerodynamic Field of Stabilized Flames. Fourth Symposium (International) on Combustion, The Williams & Wilkins Co. (Baltimore), 1953, pp. 443-450.
24. Lin, C. C.: On the Stability of Two-Dimensional Parallel Flows, pt. I. Quarterly Appl. Math., vol. III, no. 2, July 1945, pp. 117-142; pt. II, vol. III, no. 3, Oct. 1945, pp. 218-234; pt. III, vol. III, no. 4, Jan. 1946, pp. 277-301.
25. Pillow, A. F.: A Review of Hydrodynamic Stability and Its Bearing on Transition to Turbulent Flow in the Boundary Layer. Rep. A.35, Div. Aero., Council Sci. & Ind. Res. (Australia), May 1945.
26. Schubauer, G. B., and Skramstad, H. K.: Laminar-Boundary-Layer Oscillations and Transition on a Flat Plate. NACA Rep. 909, 1948. (Supersedes NACA WR W-8.)
27. Pretsch, J.: The Stability of Two-Dimensional Laminar Flow with Pressure Drop and Pressure Rise. Joint Intelligence Objectives Agency, Wash. (D.C.), July 23, 1946.
28. Lessen, Martin: On Stability of Free Laminar Boundary Layer Between Parallel Streams. NACA Rep. 979, 1950. (Supersedes NACA TN 1929.)
29. Heisenberg, Werner: On Stability and Turbulence of Fluid Flows. NACA TM 1291, 1951.
30. Savic, P.: On Acoustically Effective Vortex Motion in Gaseous Jets. Phil. Mag., ser. 7, vol. 32, Sept. 1941, pp. 245-252.
31. Goldstein, S.: On The Stability of Superposed Streams of Fluids of Different Densities. Proc. Roy. Soc. (London), ser. A, vol. 132, Aug. 1, 1931, pp. 524-548.

32. Goldstein, Sydney, ed.: Modern Developments in Fluid Dynamics. Vols. I and II. Clarendon Press (Oxford), 1938.
33. Mestre, André: Étude des Limites de Stabilité en Relation avec la Résistance des Obstacles à l'Écoulement. Combustion Res. and Rev., Butterworths Sci. Pub., 1955, pp. 72-86.
34. Clark, Thomas P., and Bittker, David A.: A Study of the Radiation from Laminar and Turbulent Open Propane-Air Flames as a Function of Flame Area, Equivalence Ratio, and Fuel Flow Rate. NACA RM E54F29, 1954.
35. Mickelsen, William R., and Laurence, James C.: Measurement and Analysis of Turbulent Flow Containing Periodic Flow Fluctuations. NACA RM E53F19, 1953.
36. Roshko, Anatol: On the Development of Turbulent Wakes from Vortex Streets. NACA Rep. 1191, 1954. (Supersedes NACA TN 2913.)
37. Blackshear, Perry L., Jr.: Driving Standing Waves by Heat Addition. NACA TN 2772, 1952. (See also Fourth Symposium (International) on Combustion, The Williams & Wilkins Co., 1953, pp. 553-566.)
38. Kaskan, W. E.: An Investigation of Vibrating Flames. Fourth Symposium (International) on Combustion, The Williams & Wilkins Co., 1953, pp. 575-591.
39. Dugger, Gordon L.: Effect of Initial Mixture Temperature on Flame Speed of Methane-Air, Propane-Air, and Ethylene-Air Mixtures. NACA Rep. 1061, 1952. (Supersedes NACA TN's 2170 and 2374.)
40. Dryden, Hugh L.: A Review of the Statistical Theory of Turbulence. Quarterly Appl. Math., vol. I, no. 1, Apr. 1943, pp. 7-42.

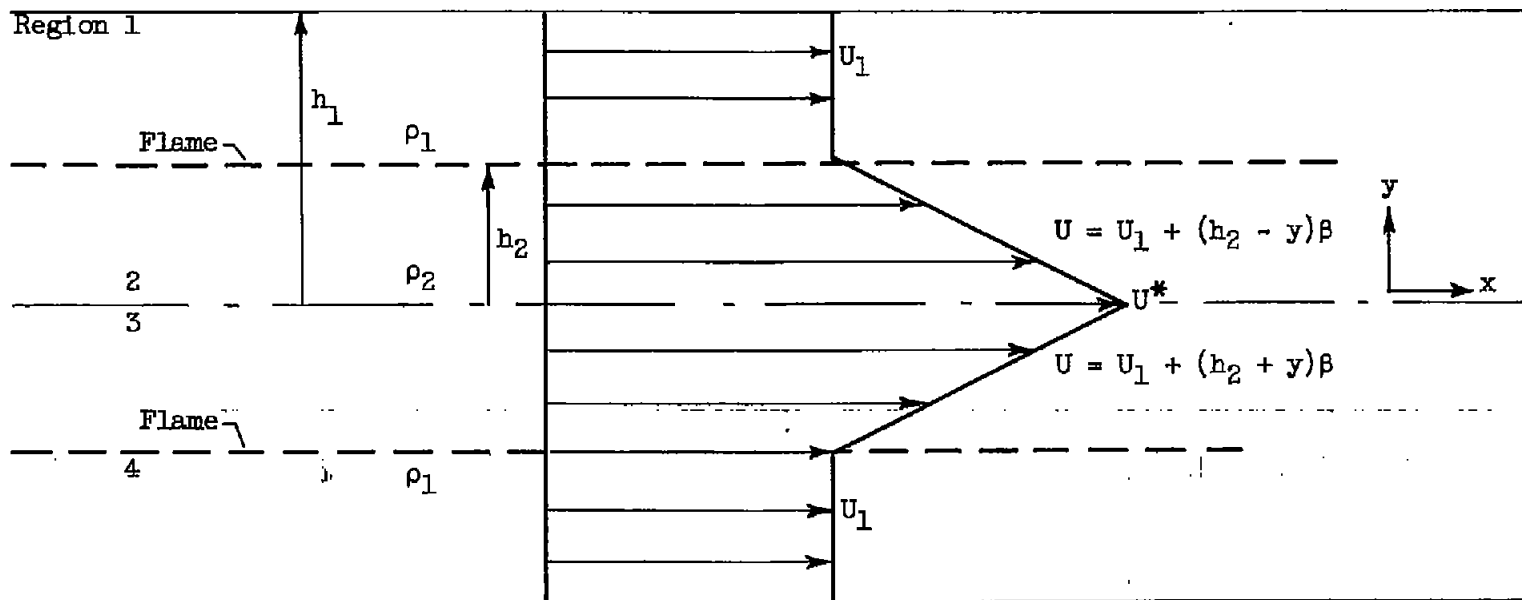


Figure 1. - Geometry of flow field. U , flow velocity in x -direction; ρ , density.

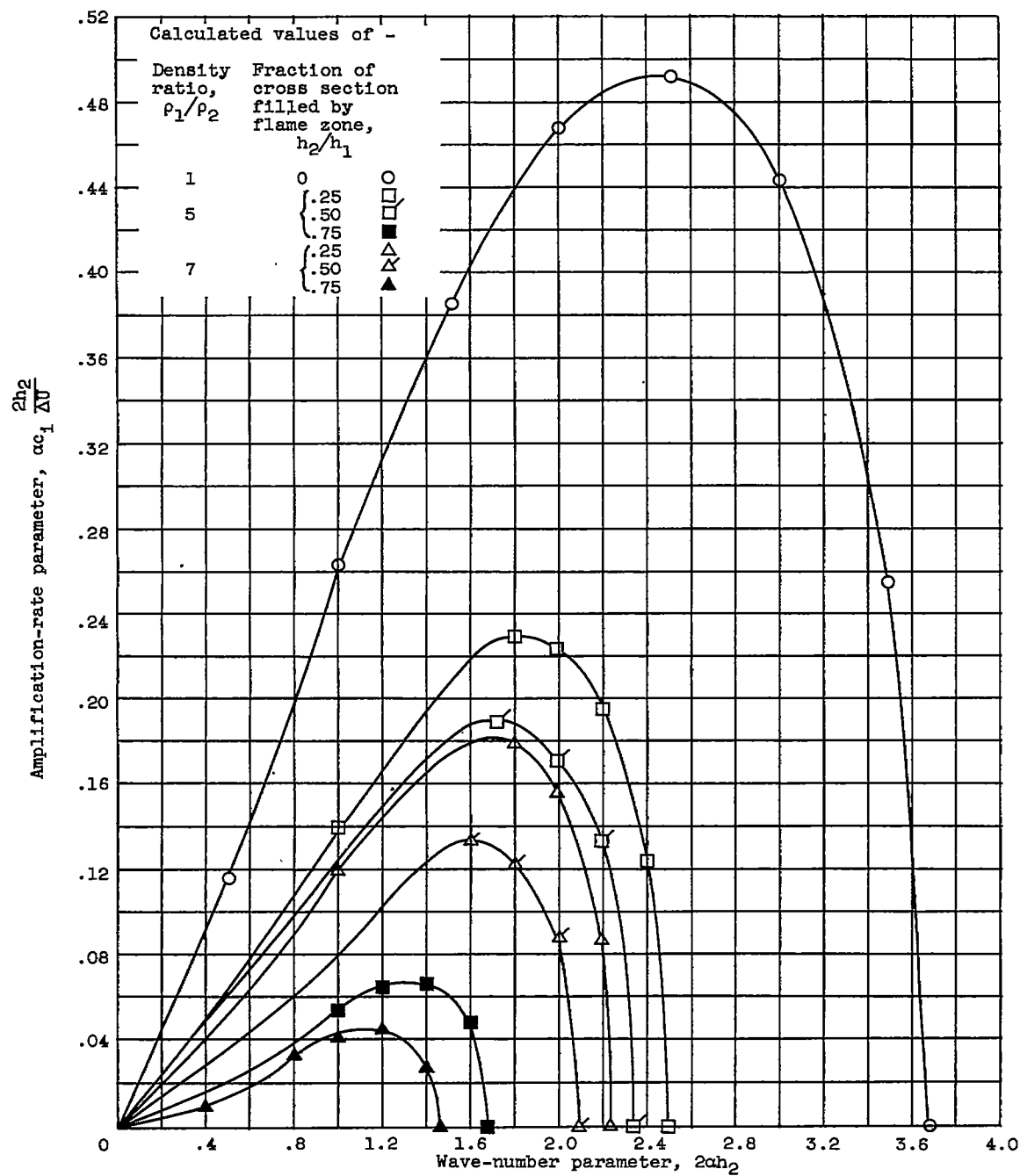


Figure 2. - Amplification-rate parameter $\alpha c_1 \frac{2h_2}{\Delta U}$ for \wedge profile.

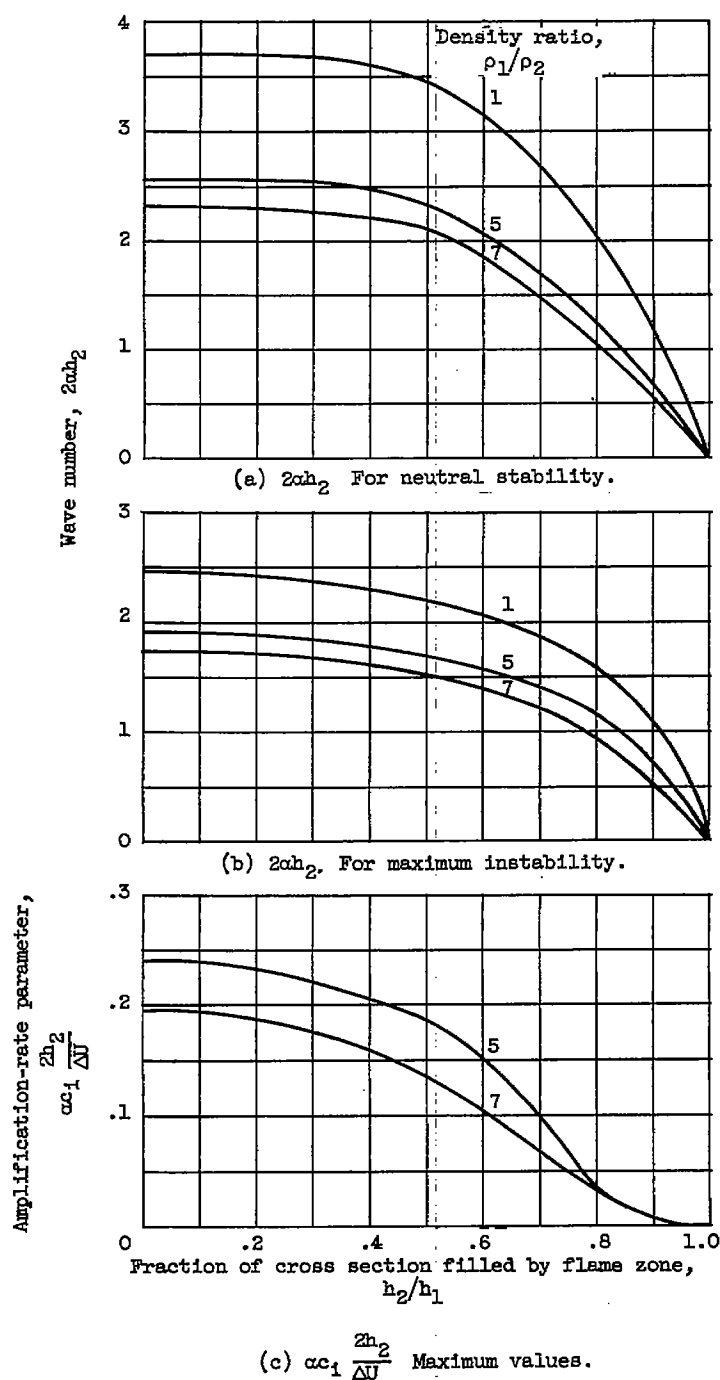


Figure 3. - Wave number $2\alpha h_2$ for neutral stability and maximum instability, and amplification-rate parameter $\alpha c_1 \frac{2h_2}{\Delta U}$ at maximum instability for \wedge profile.

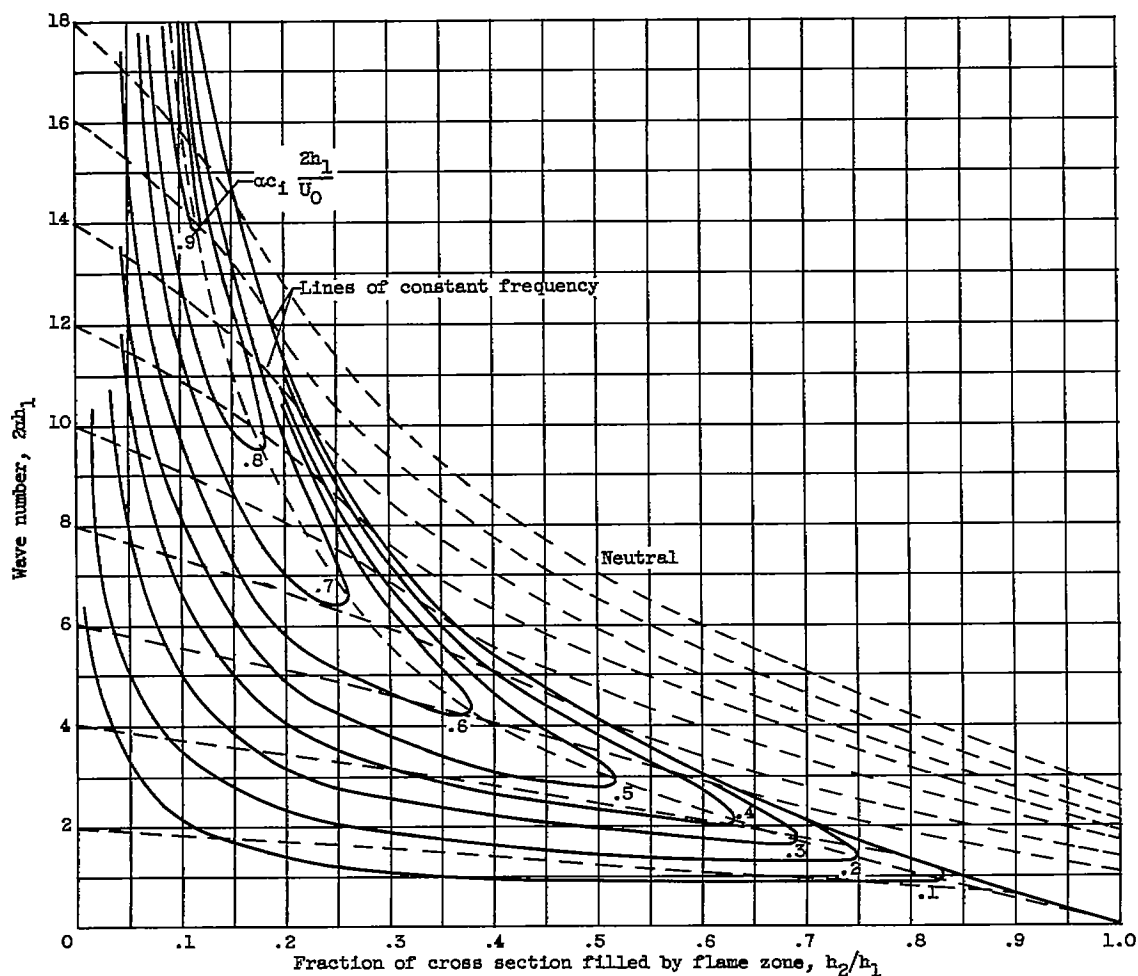
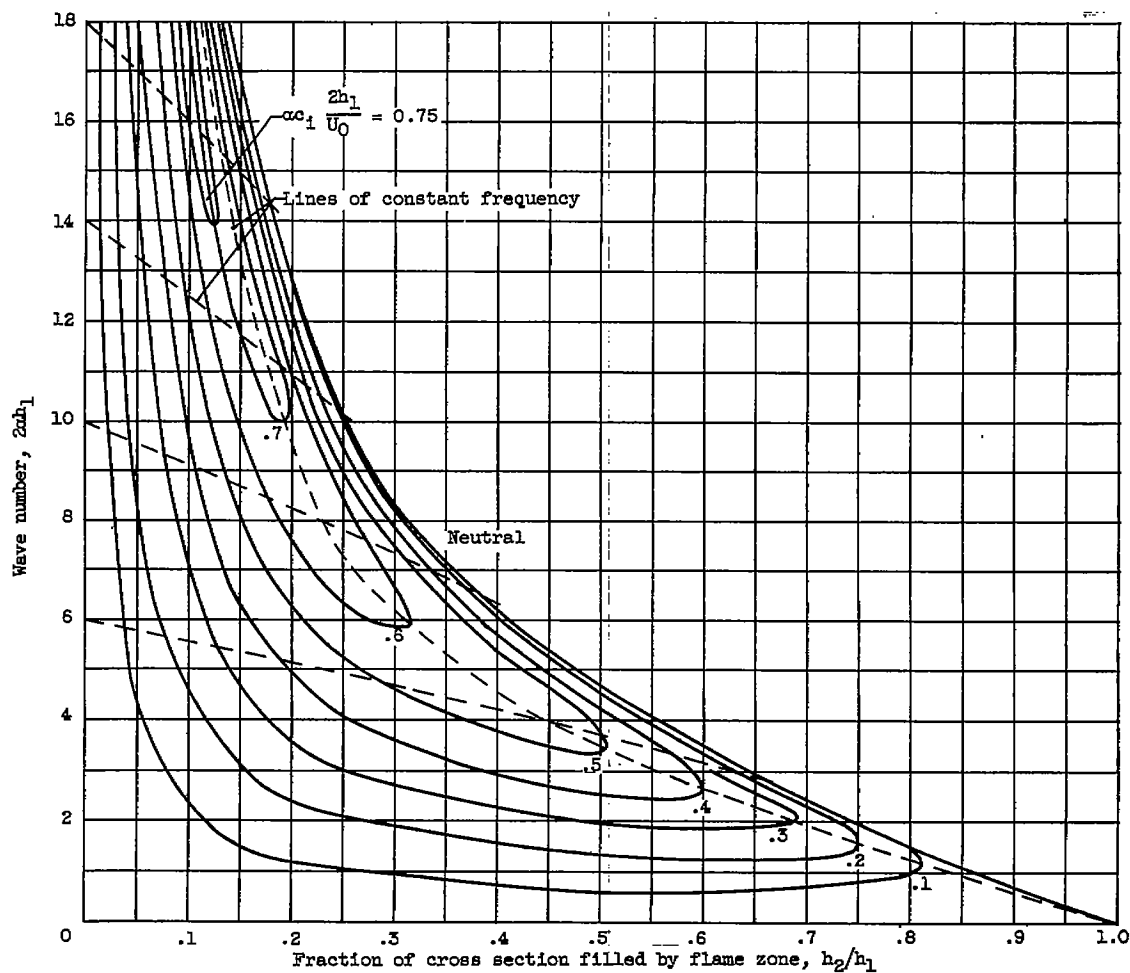
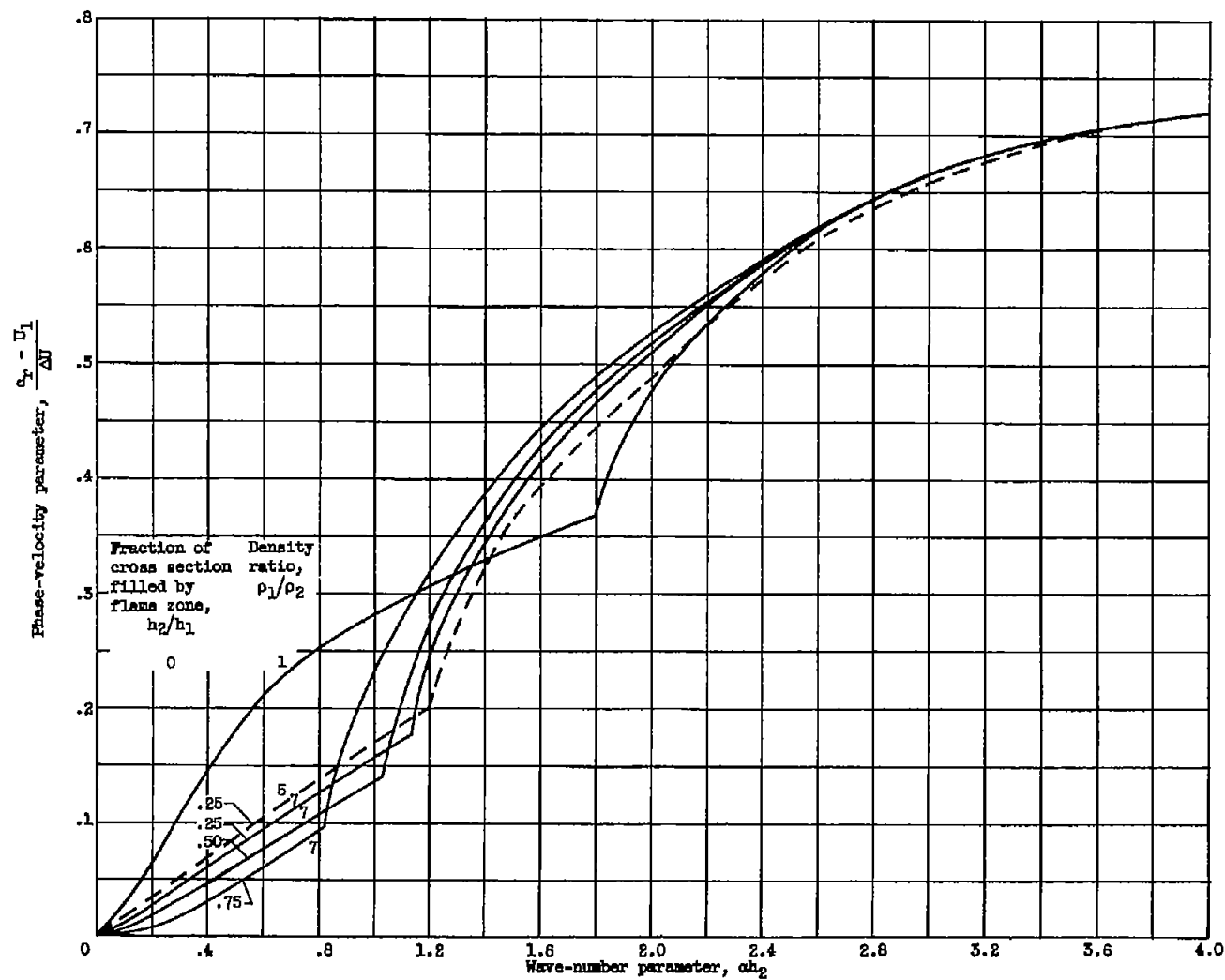
(a) Density ratio ρ_1/ρ_2 , 7.

Figure 4. - Stability map for flame in a duct. Contours of constant amplification rate α_{c1} are given by lines of constant $\alpha_{c1} \frac{2h_1}{U_0}$. Lines of constant frequency show path given disturbance originating at flameholder takes as it propagates along flame zone at phase velocity c_r .



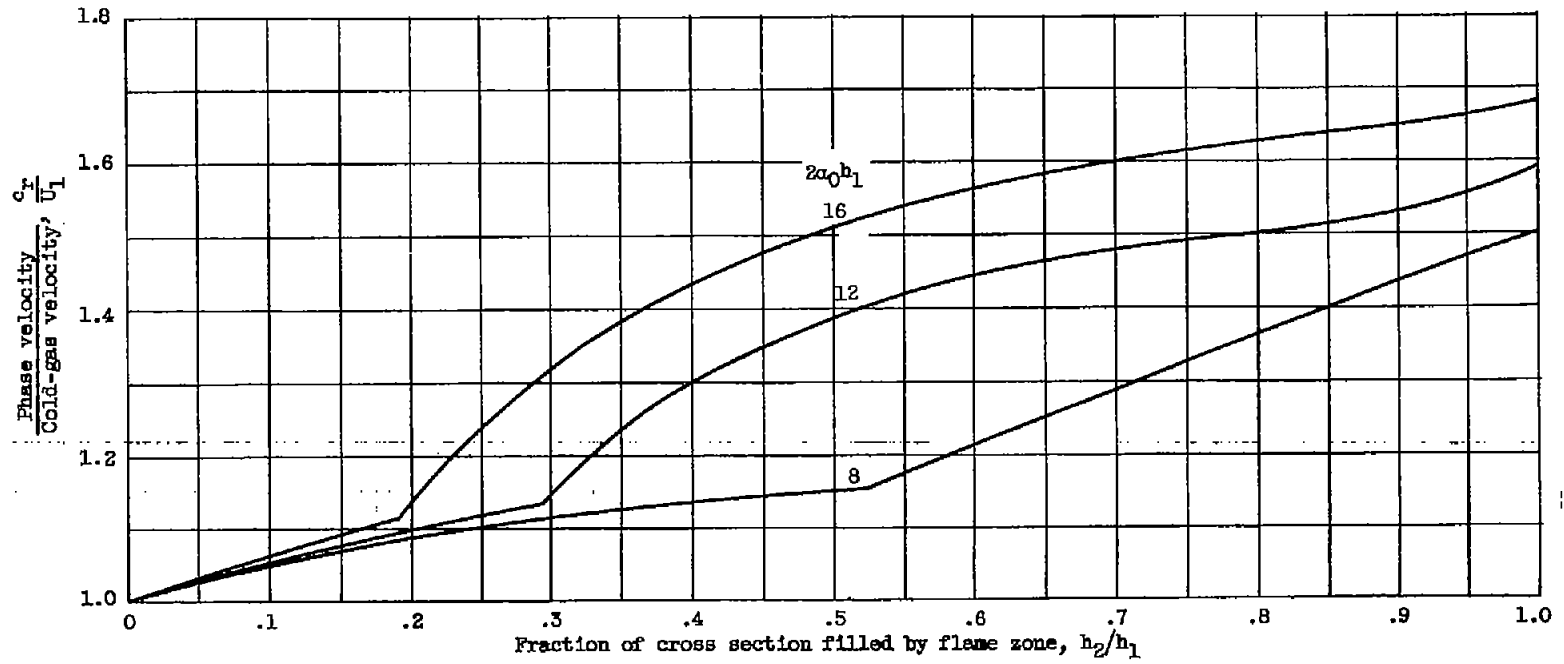
(b) Density ratio ρ_1/ρ_2 , 5.

Figure 4. - Concluded. Stability map for flame in a duct. Contours of constant amplification rate αc_1 are given by lines of constant $\alpha c_1 \frac{2h_1}{U_0}$. Lines of constant frequency show path given disturbance originating at flameholder takes as it propagates along flame zone at phase velocity c_r .



(a) $\frac{c_r - U_1}{\Delta U}$ For amplified and neutral disturbances as function of ch_2 .

Figure 5. - Phase-velocity parameters.



(b) c_x/U_1 At three frequencies as function of h_2/h_1 for density ratio ρ_1/ρ_2 of 7.

Figure 5. - Concluded. Phase-velocity parameters.

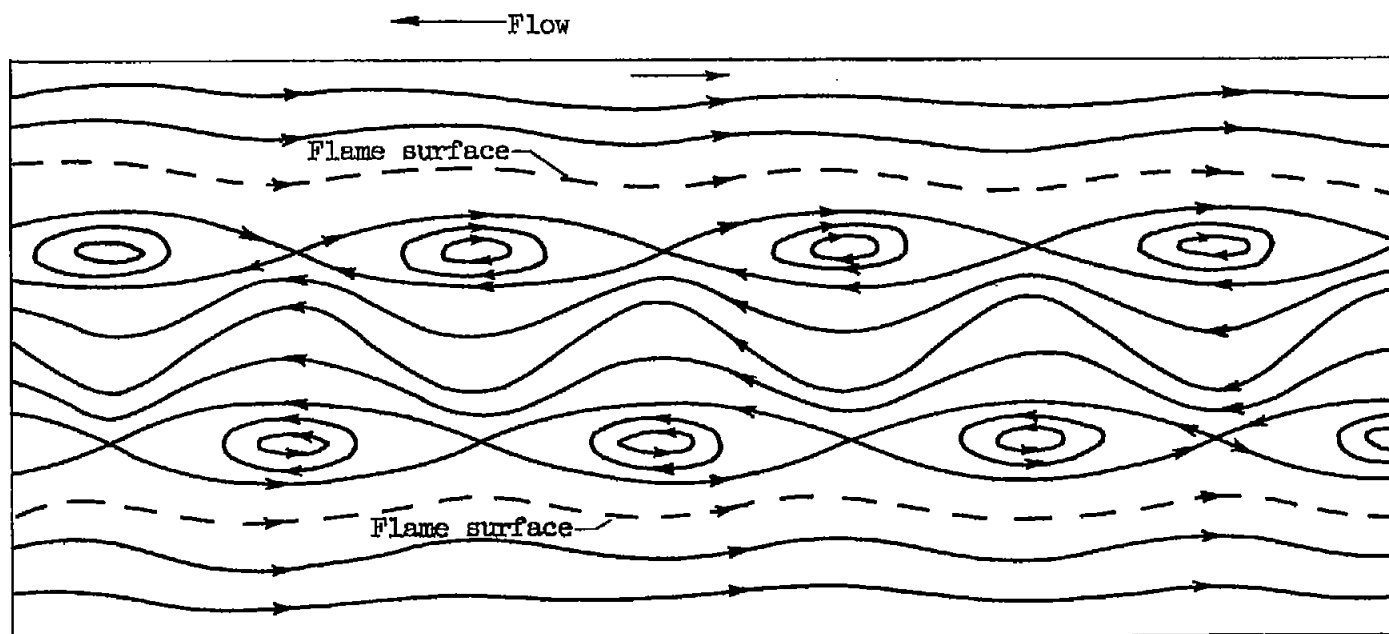
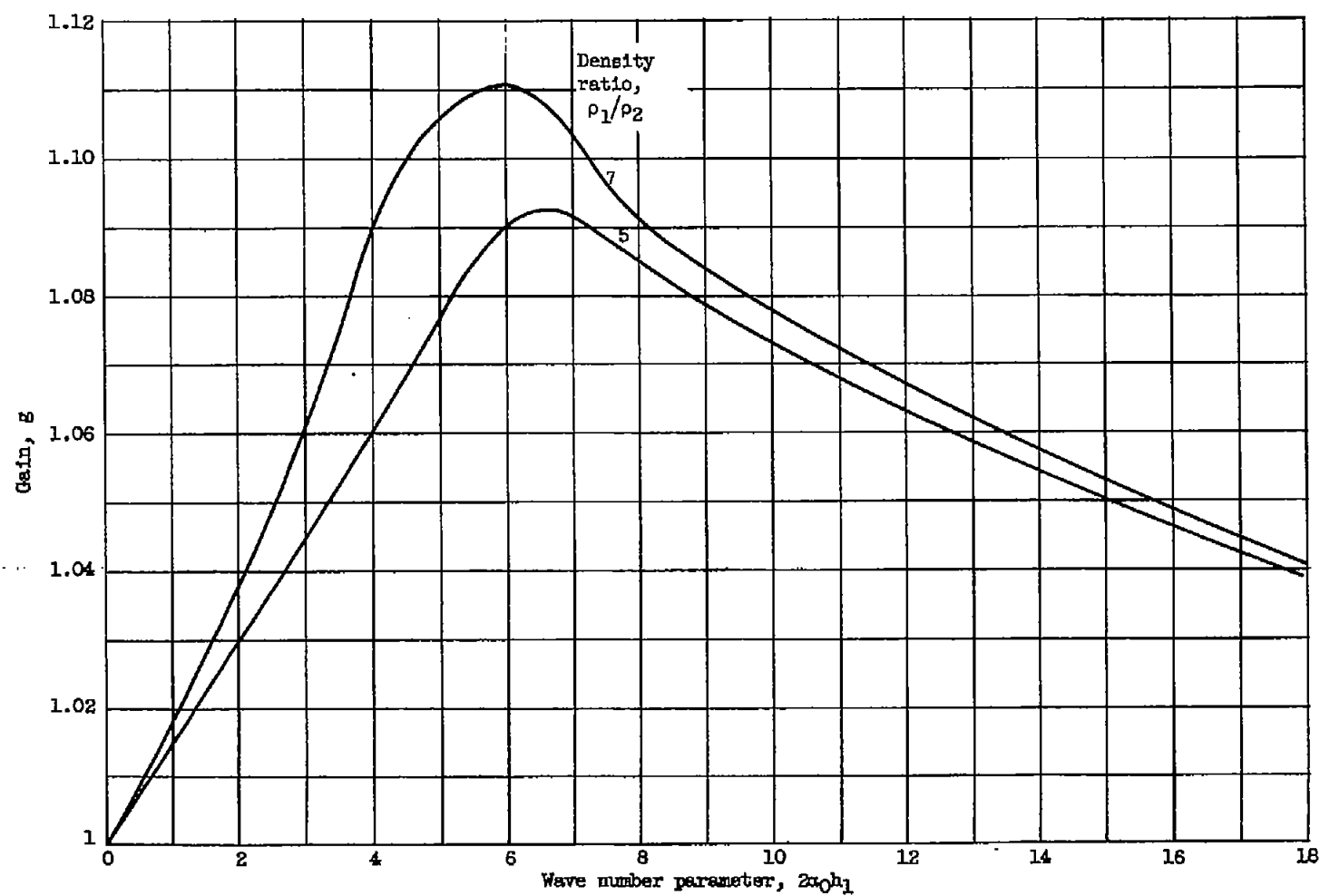
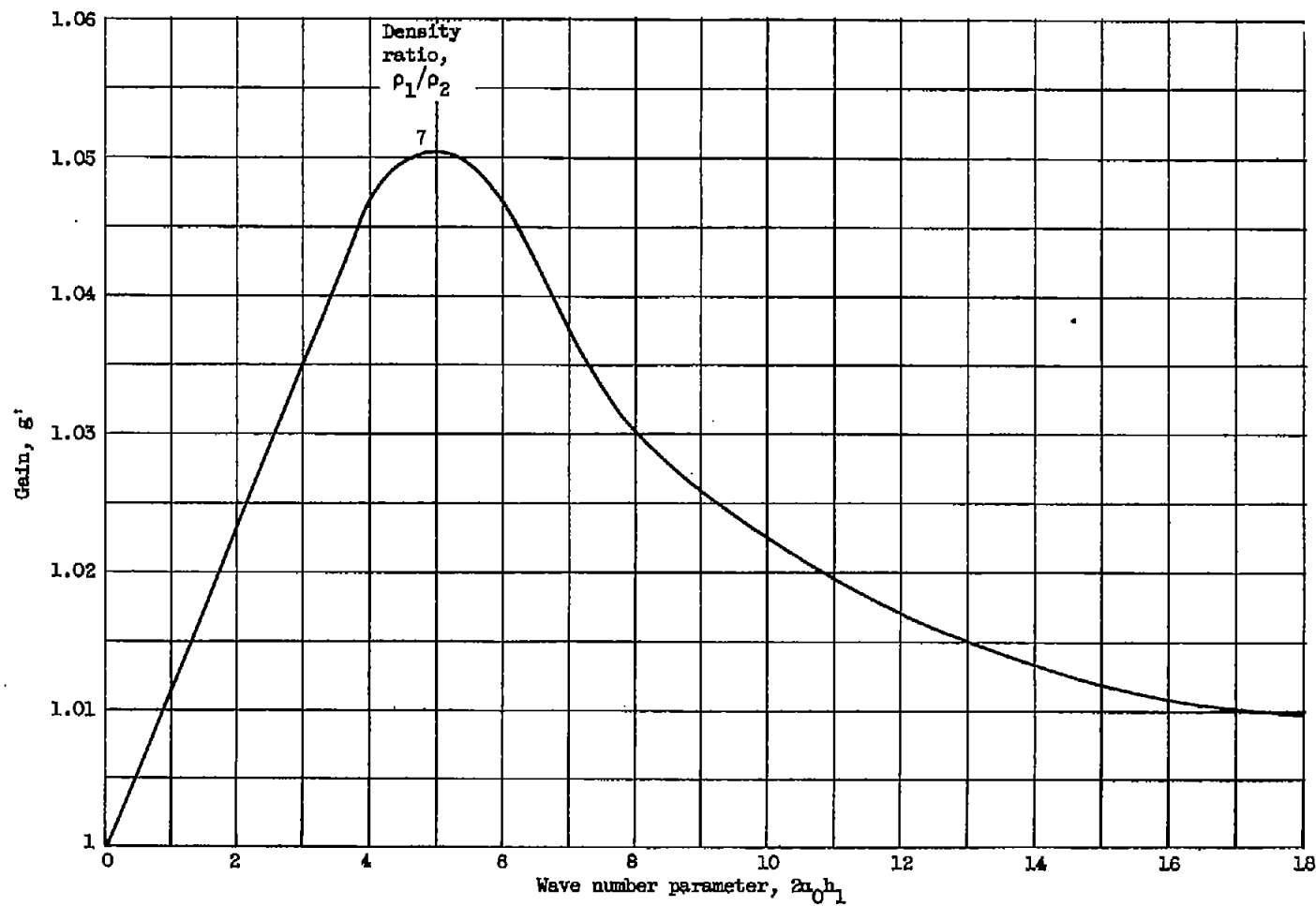


Figure 6. - Streamlines of neutral disturbance as seen by observer moving at phase velocity c_r .



(a) Gain g ; $v' = v_0' g^{\frac{1}{K_1}}$, where $K_1 = dh_2/dx$.

Figure 7. - Gains for flame filling the duct.



(b) Gain g' ; $v' = v_0'(g')^{\frac{1}{K_2}}$, where $K_2 = \frac{dF}{d\frac{x}{h_1}}$.

Figure 7. - Concluded. Gains for flame filling the duct.

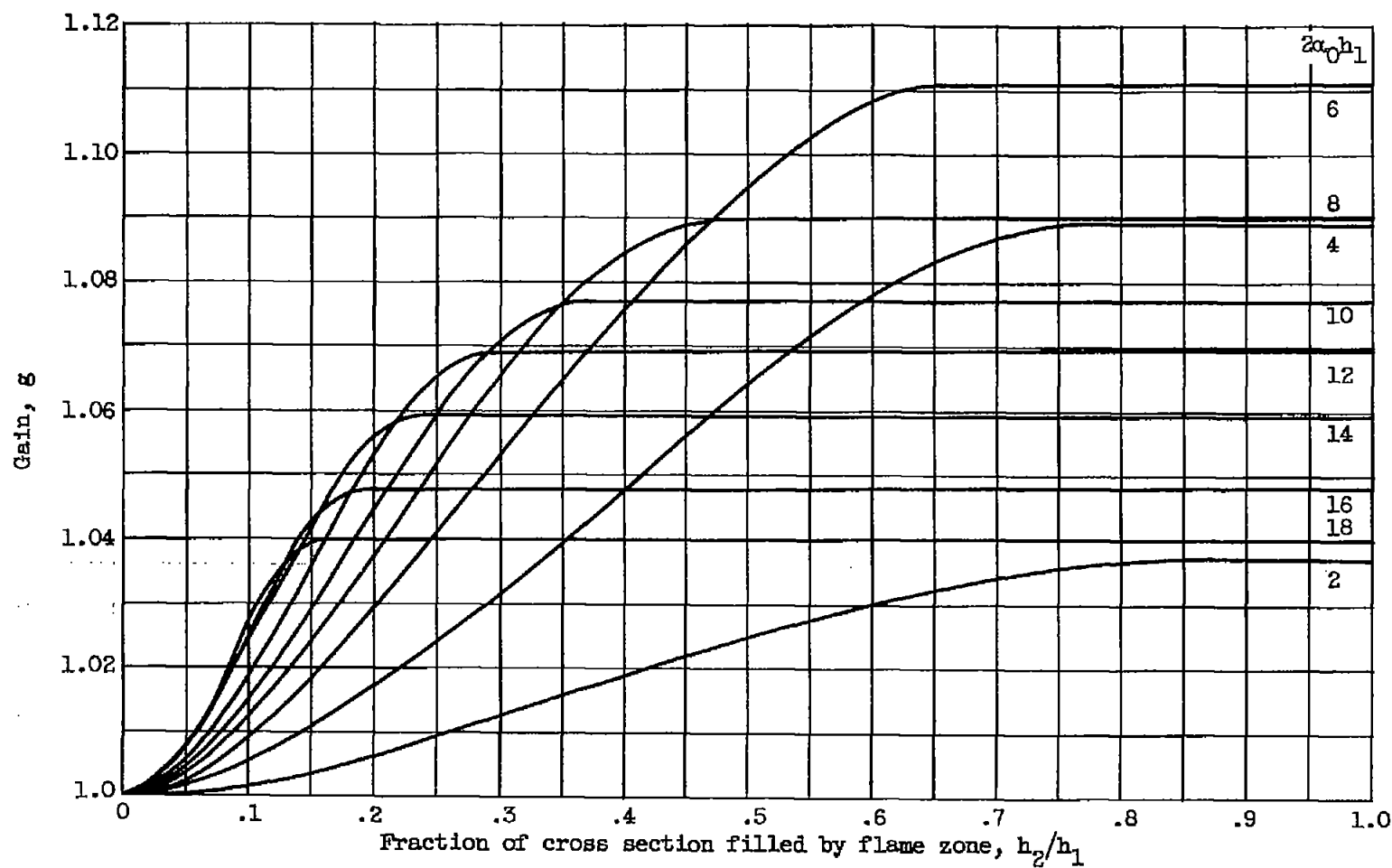
(a) Gain g .

Figure 8. - Gains as function of h_2/h_1 for family of initial wave numbers $2\alpha_0 h_1$. Density ratio ρ_1/ρ_2 , 7.

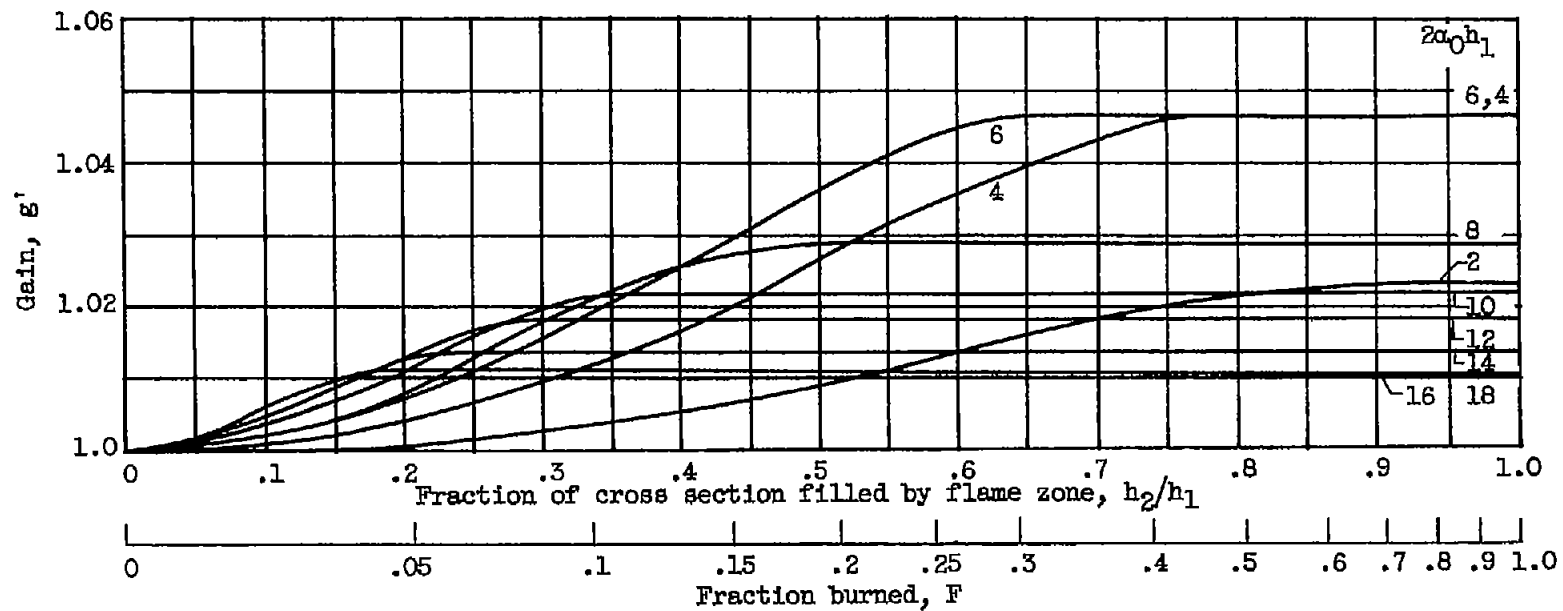
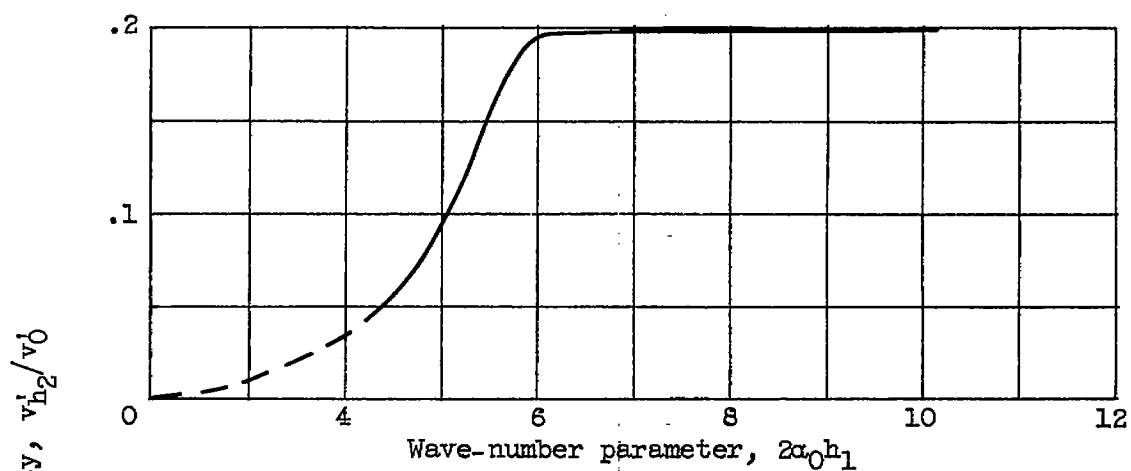
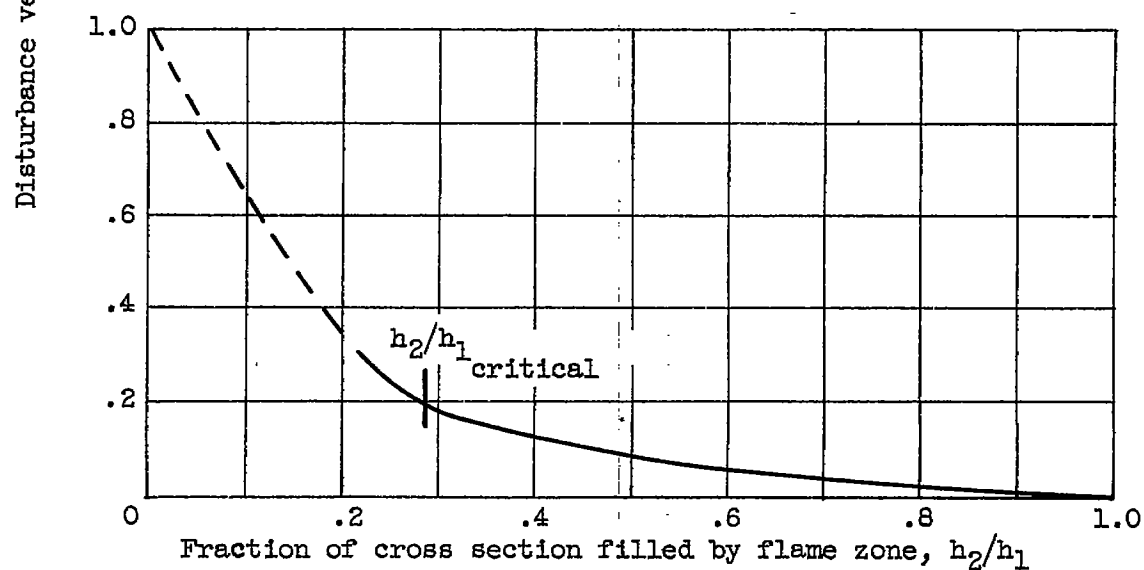
(b) Gain g' .

Figure 8. - Concluded. Gains as function of h_2/h_1 for family of initial wave numbers $2\alpha_0 h_1$. Density ratio ρ_1/ρ_2 , 7.



(a) v'_{h2}/v'_0 At critical h_2/h_1 .



(b) v'_{h2}/v'_0 For $2\alpha_0 h_1 = 12$.

Figure 9. - Disturbance-velocity distributions.

3877

CI-13 back

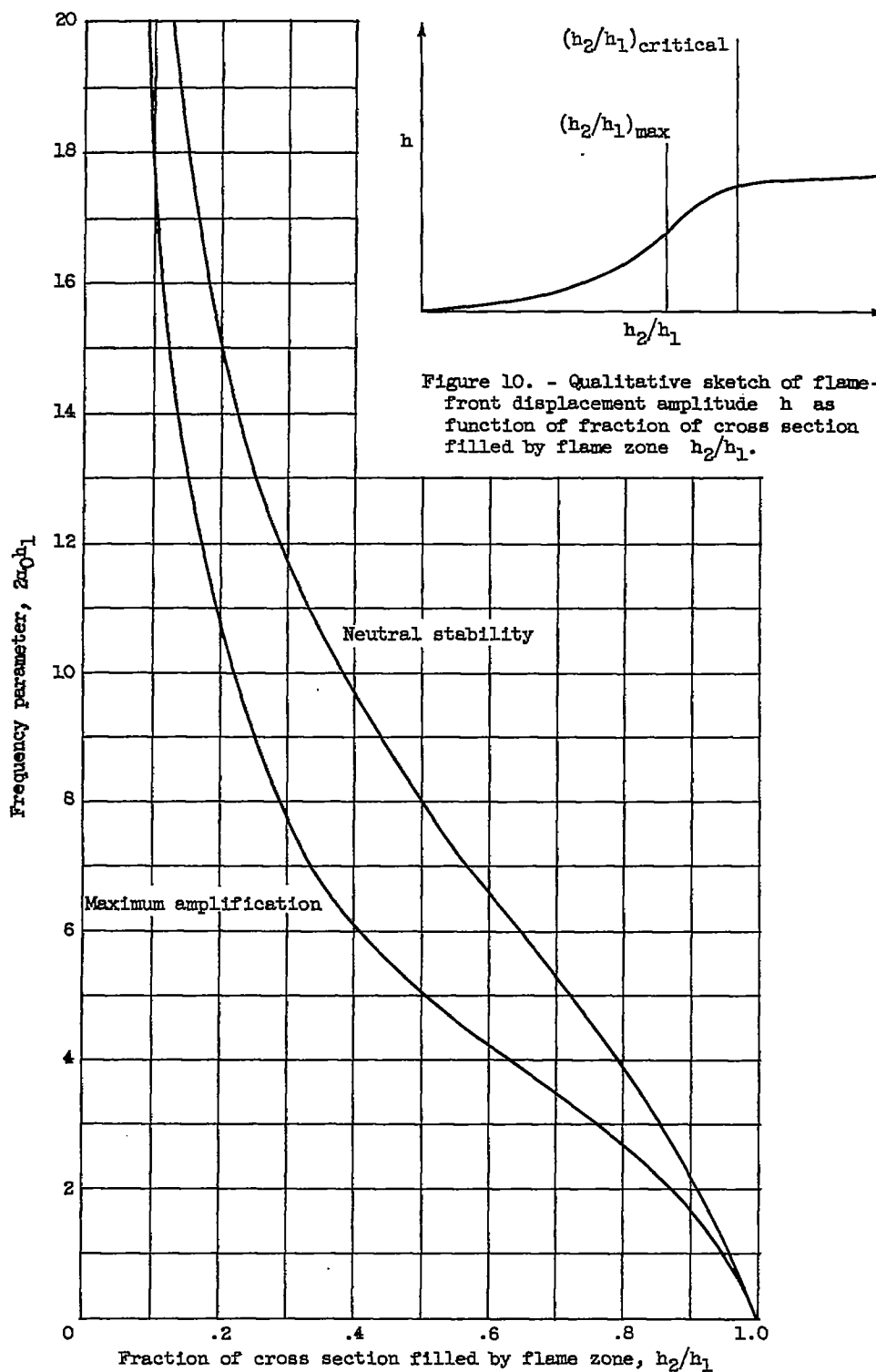


Figure 11. - Frequencies that give maximum increase in local flame speed. Density ratio ρ_1/ρ_2 , 7.

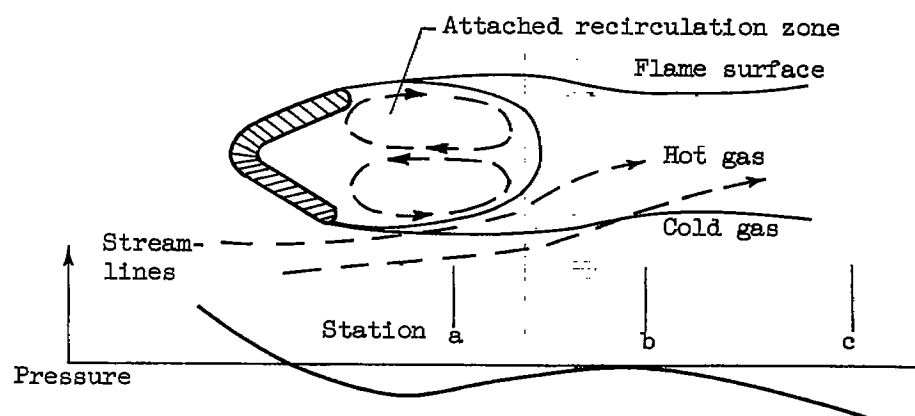


Figure 12. - Qualitative sketch of flameholder wake.

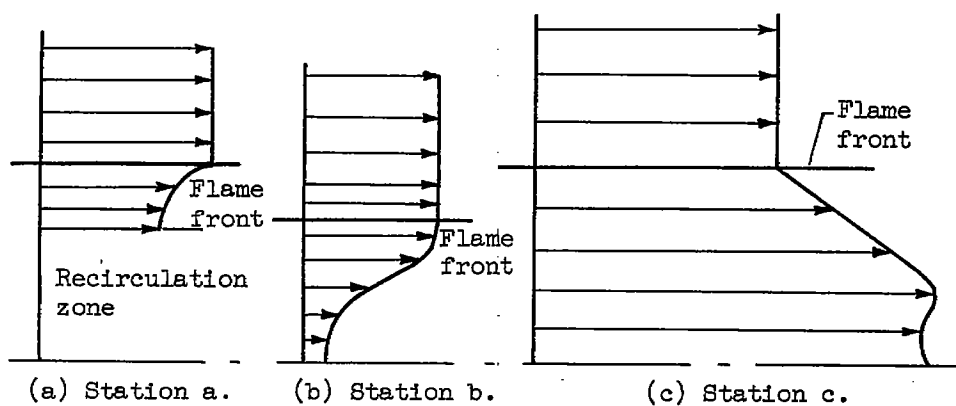
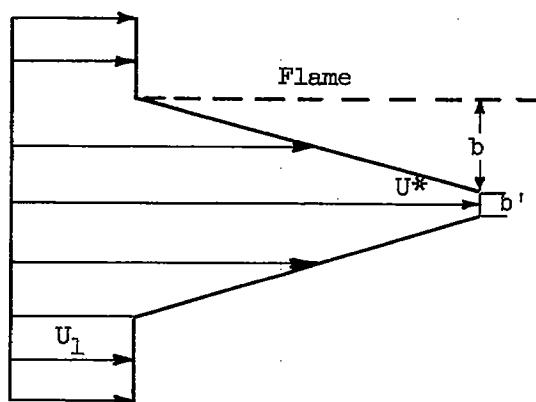


Figure 13. - Qualitative velocity profiles in flameholder wake.

Figure 14. - Idealized velocity profile in flameholder wake. U_1 , flow velocity in cold gas; U^* , flow velocity at apex of hot gas.

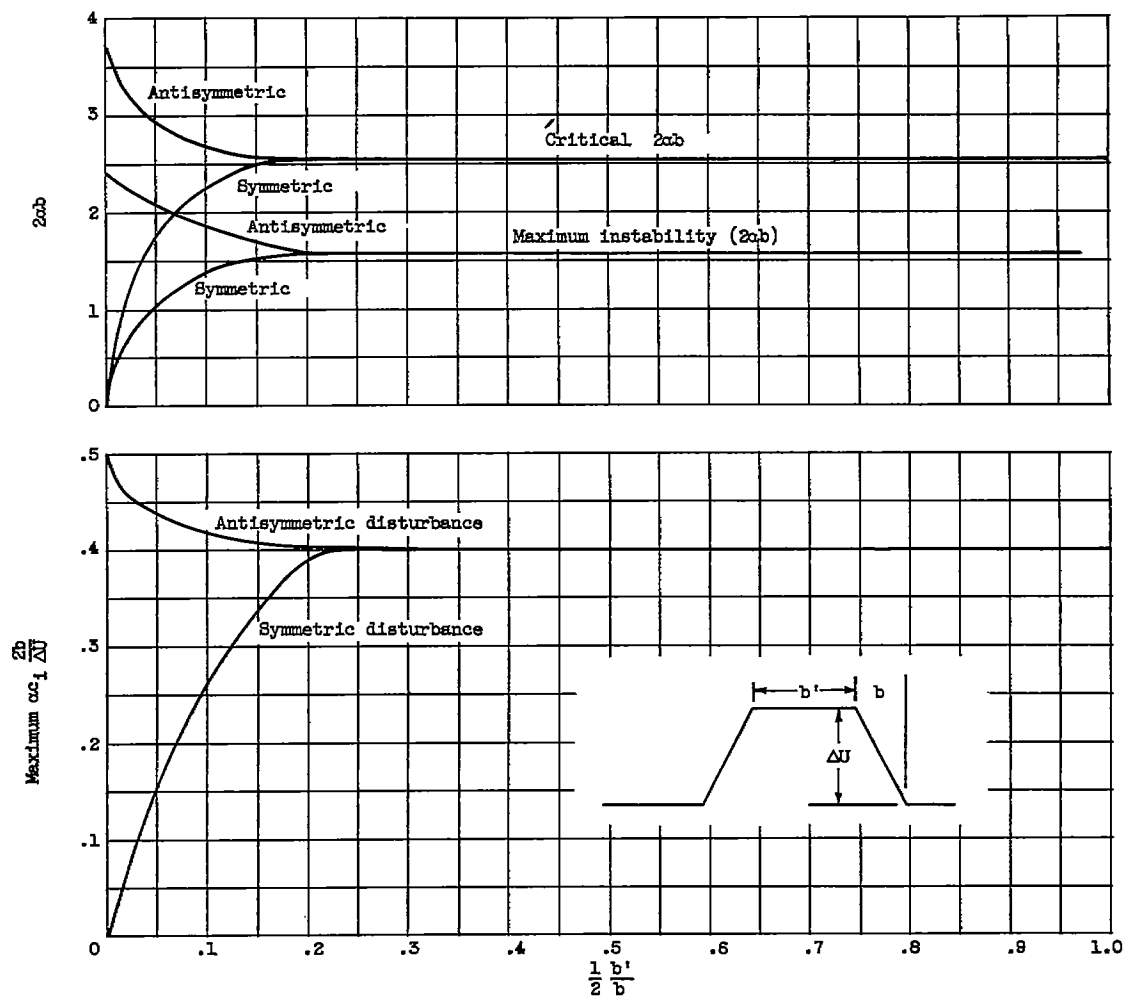


Figure 15. - Effect of velocity profile on amplification-rate parameter $\alpha c_1 \frac{2b}{\Delta U}$ and on wave numbers for neutral stability and maximum instability.

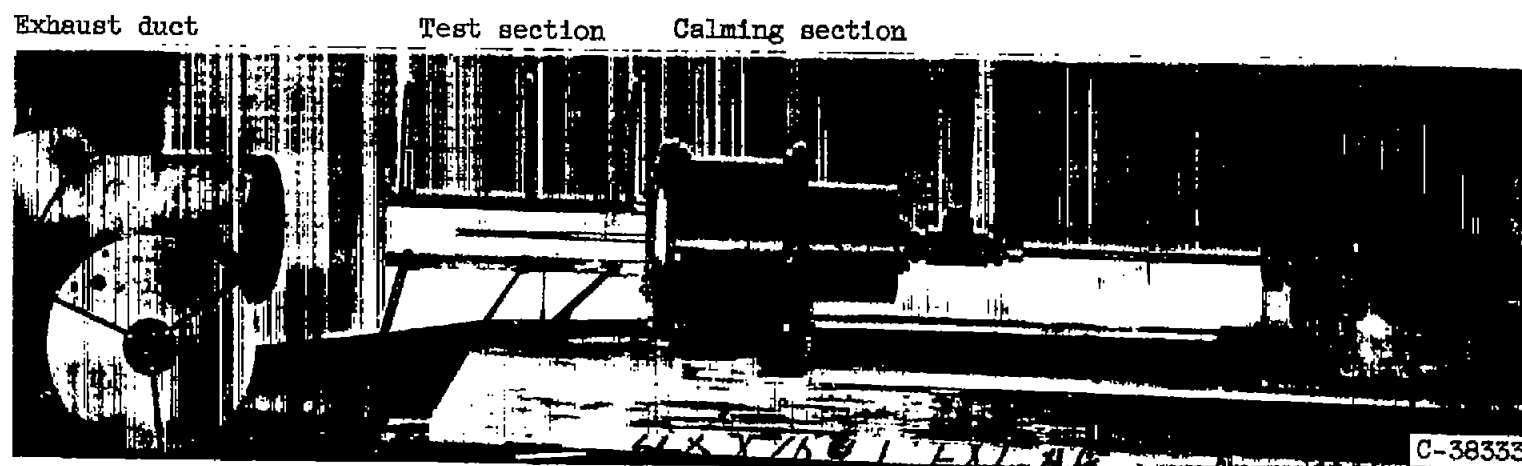


Figure 16. - Combustor.

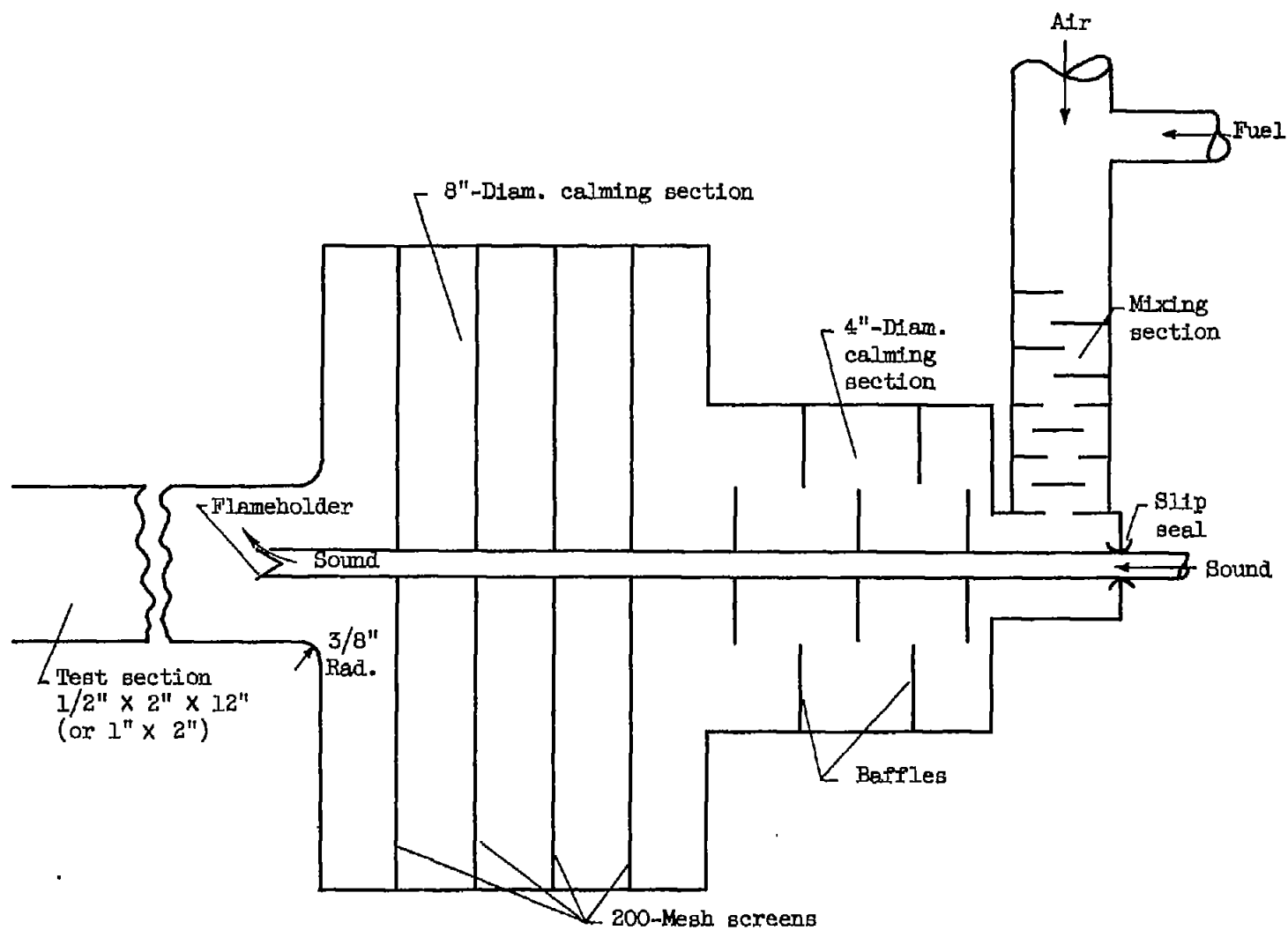


Figure 17. - Schematic drawing of test section.

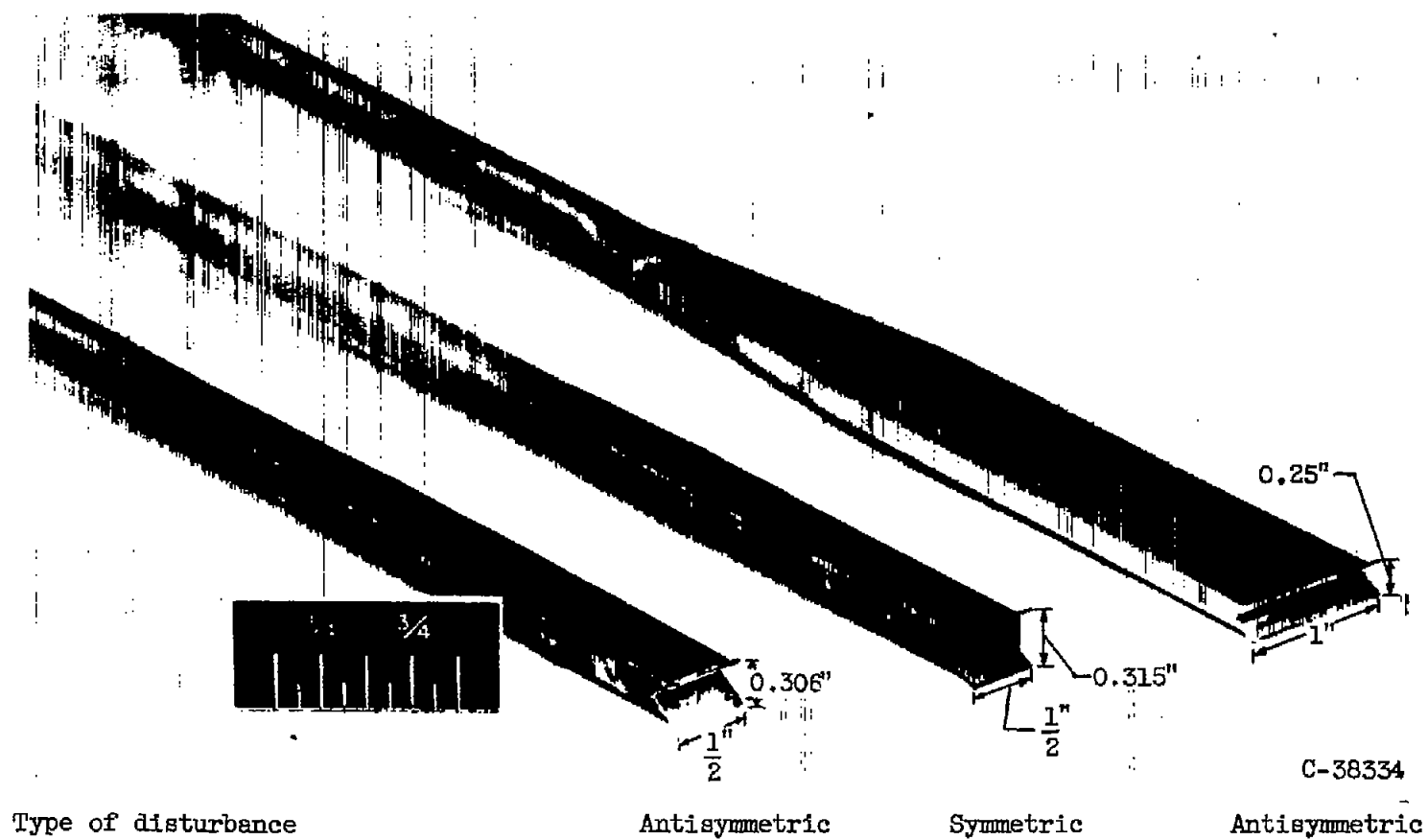


Figure 18. - Flameholders.

KACA TM 3830

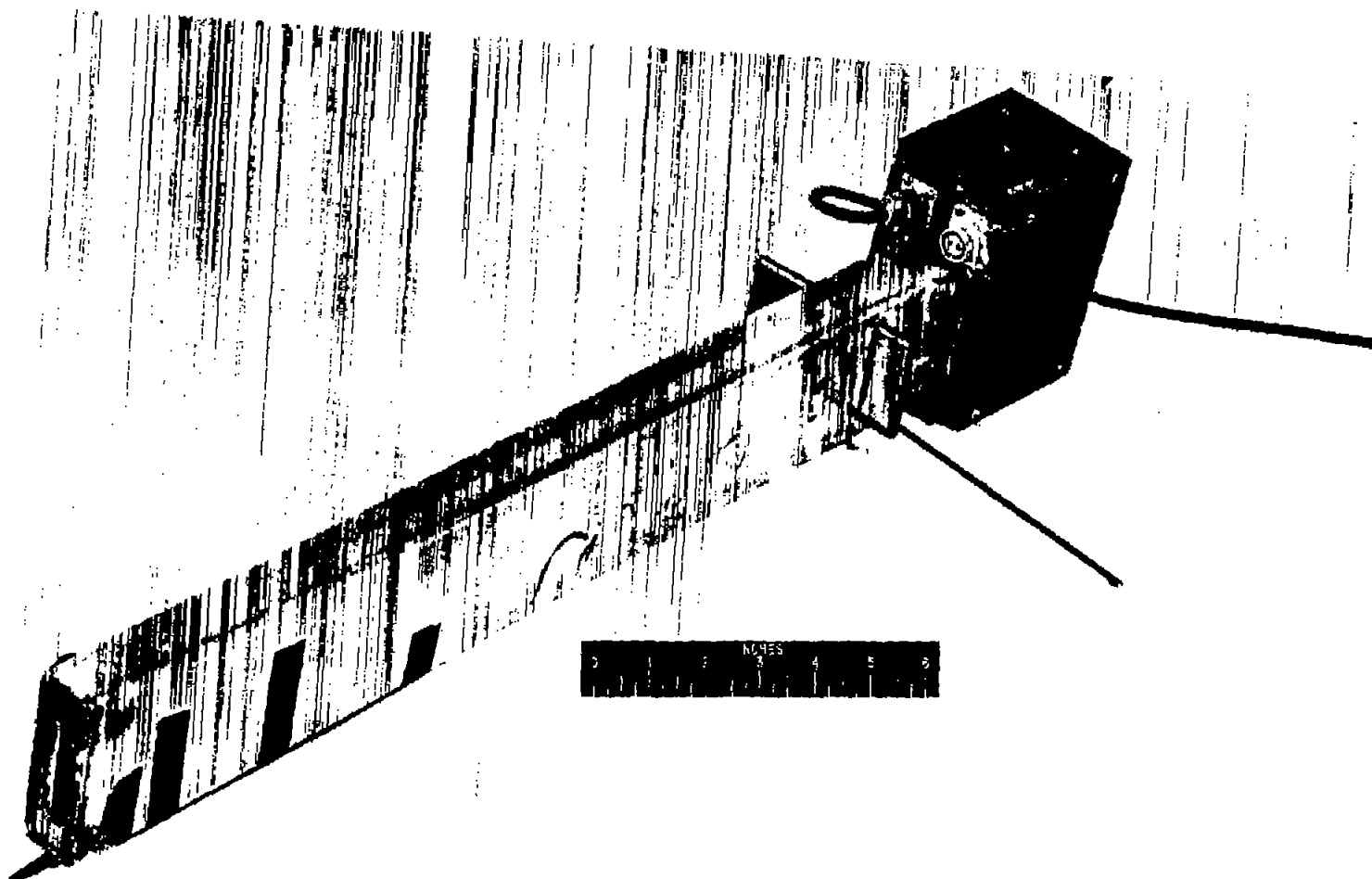


Figure 19. - Photomultiplier probe.

C-38335

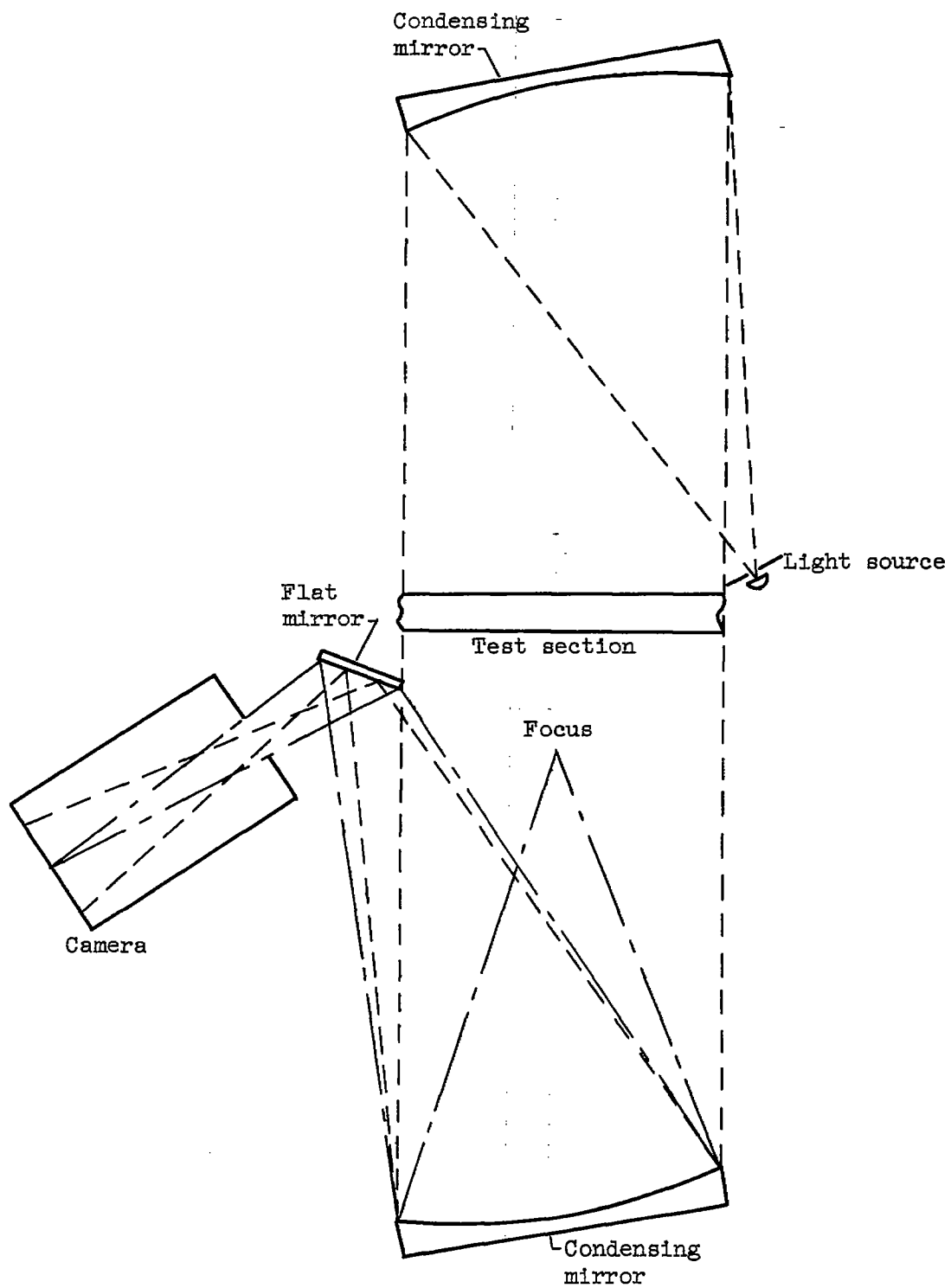


Figure 20. - Schematic drawing of shadowgraph apparatus.

3877

CY-14 back

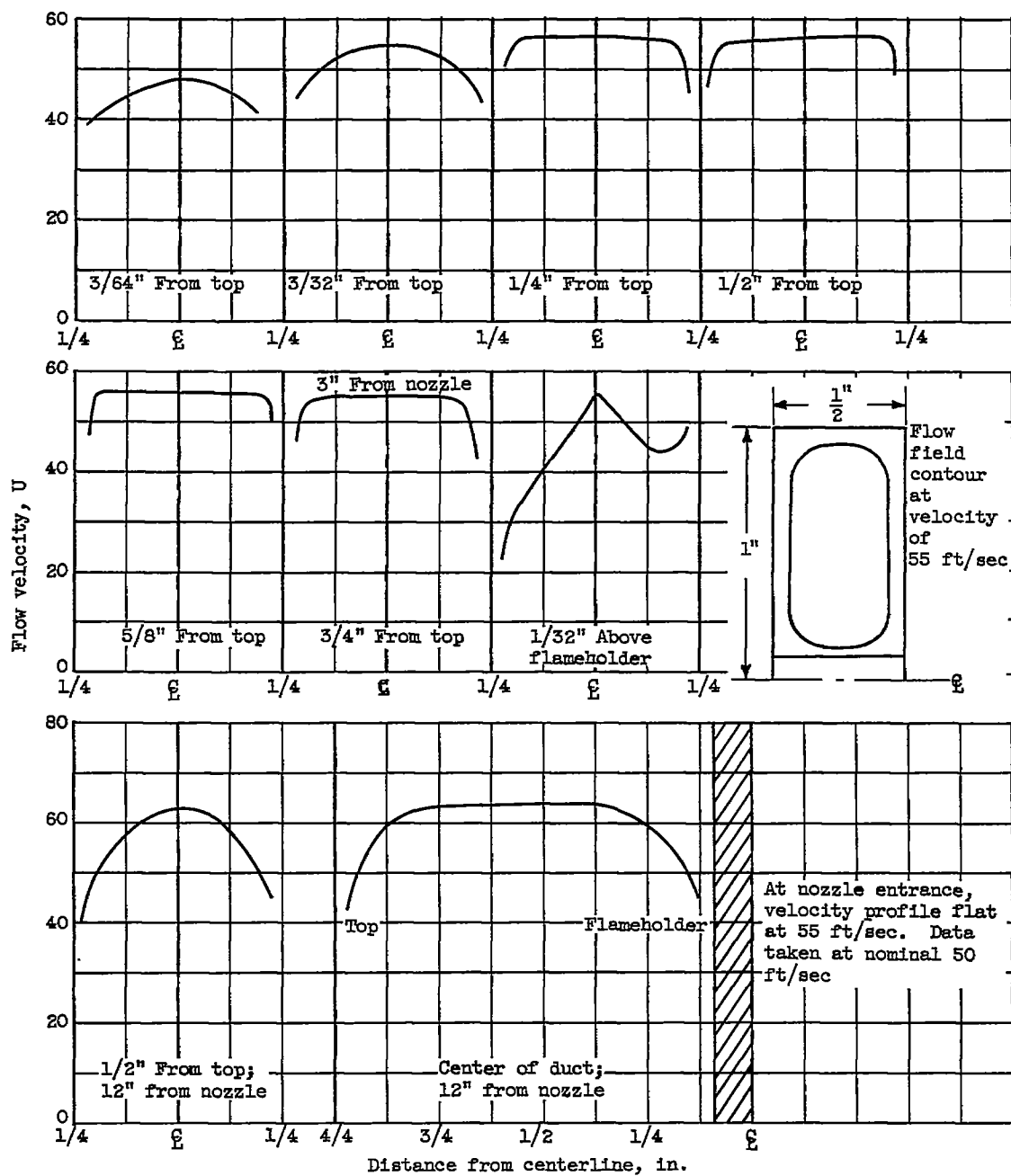


Figure 21. - Time-average velocity profiles with cold flow.

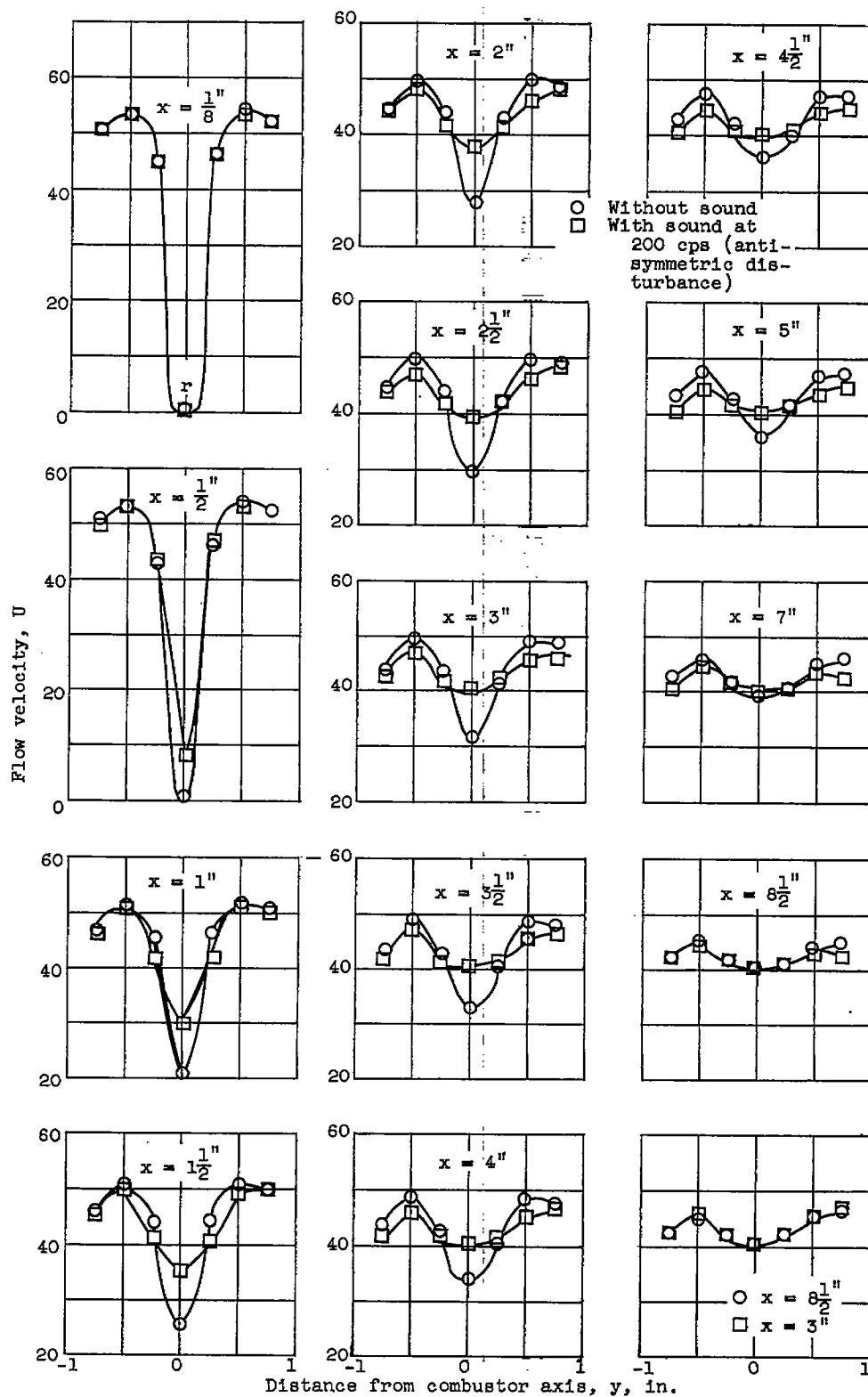


Figure 22. - Velocity profiles in wake of 0.306-inch flameholder.

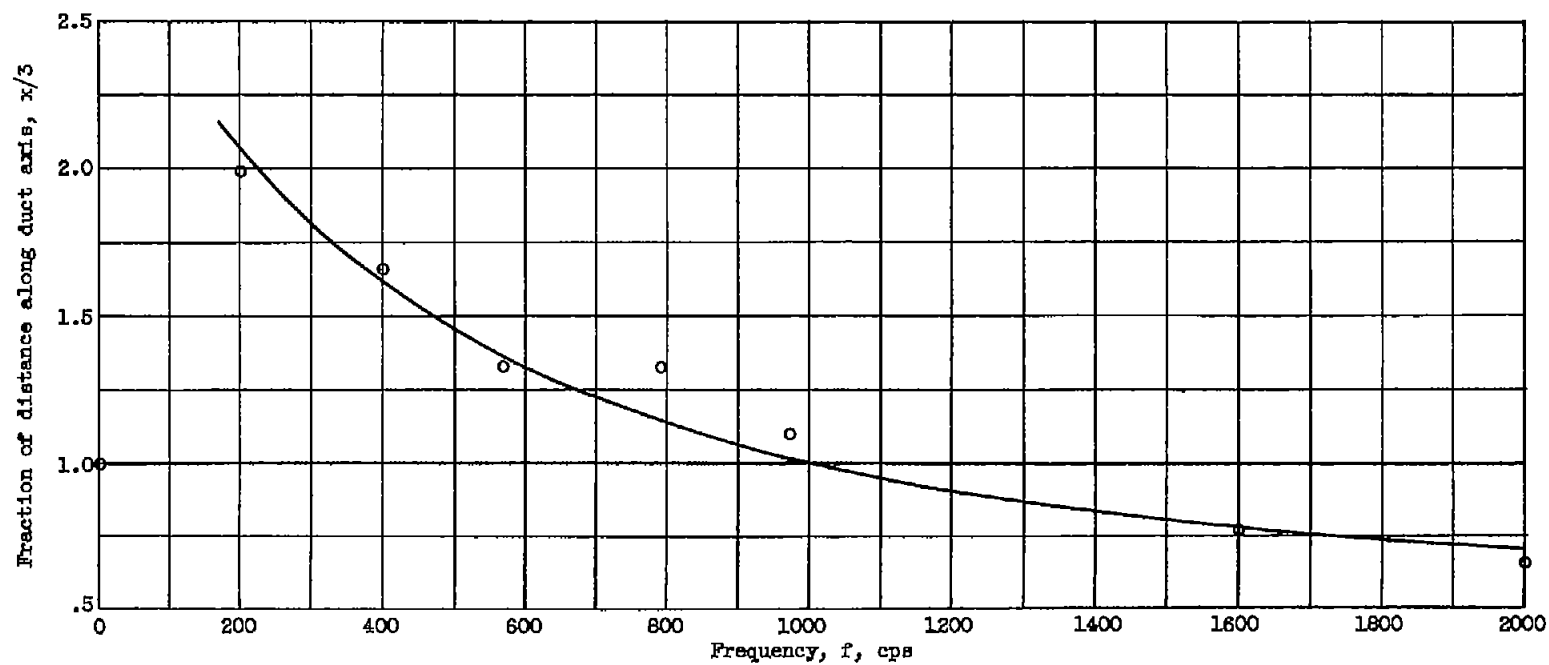


Figure 23. - Axial length required to achieve mixing to arbitrary extent.

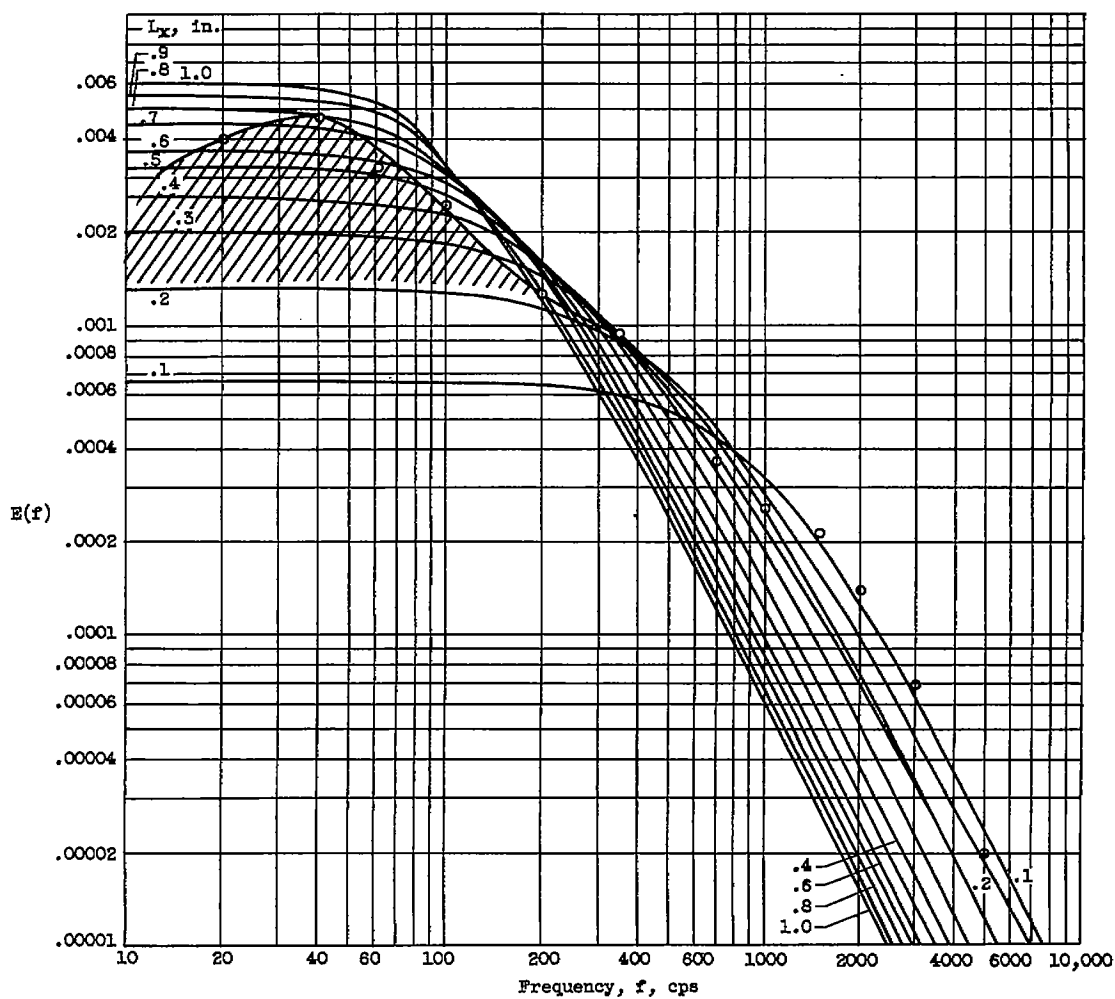


Figure 24. - Turbulence u' spectra for flow velocity U of 50 feet per second.

$$E(f) = \frac{\frac{4L_x}{U}}{1 + \left(\frac{2\pi}{U} L_x\right)^2 f^2}, \text{ measured } 1/8 \text{ inch above flameholder lip.}$$

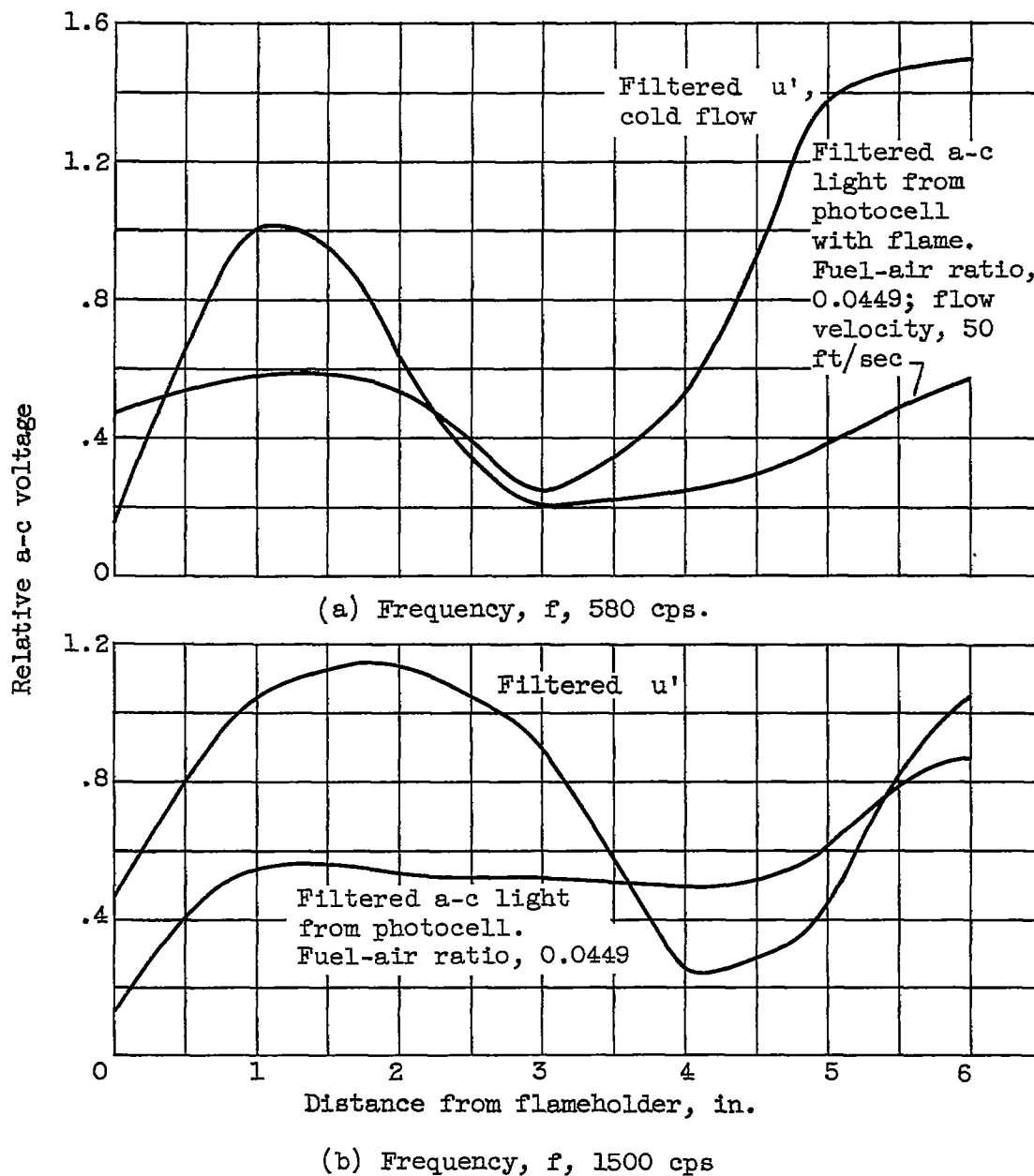


Figure 25. - Comparison of hot-wire and photomultiplier measurements showing effect of plane waves near exhaust of duct. Flow velocity U , 50 feet per second.

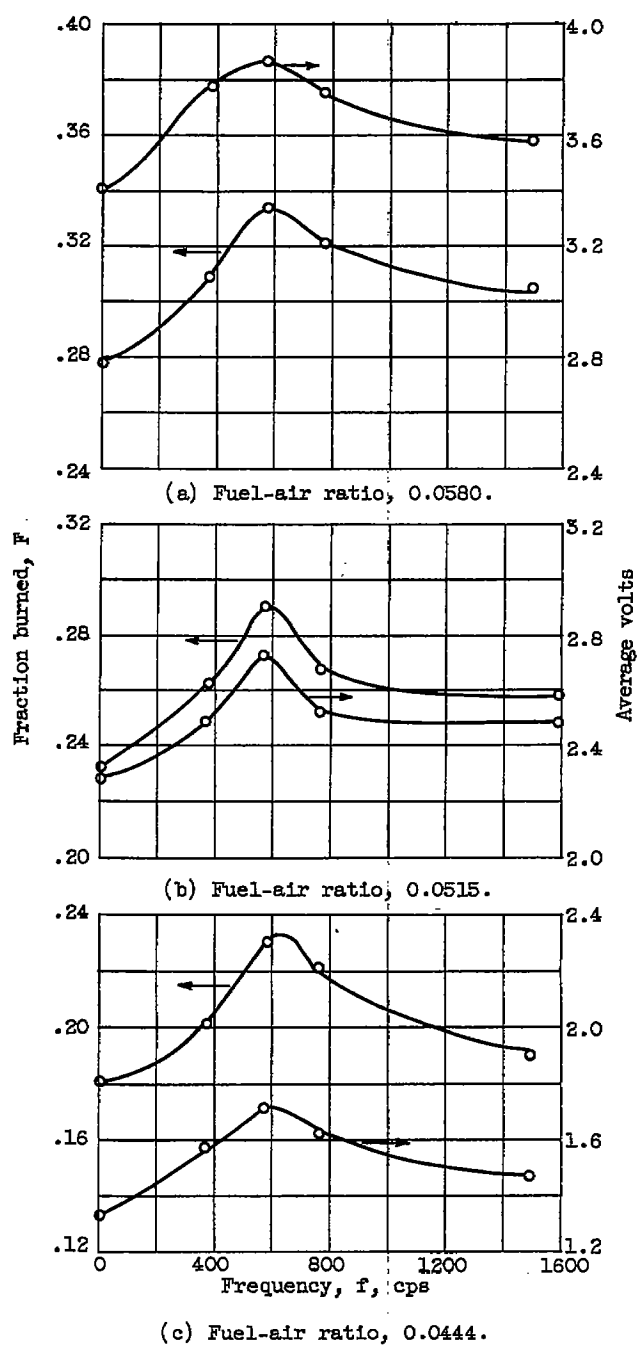
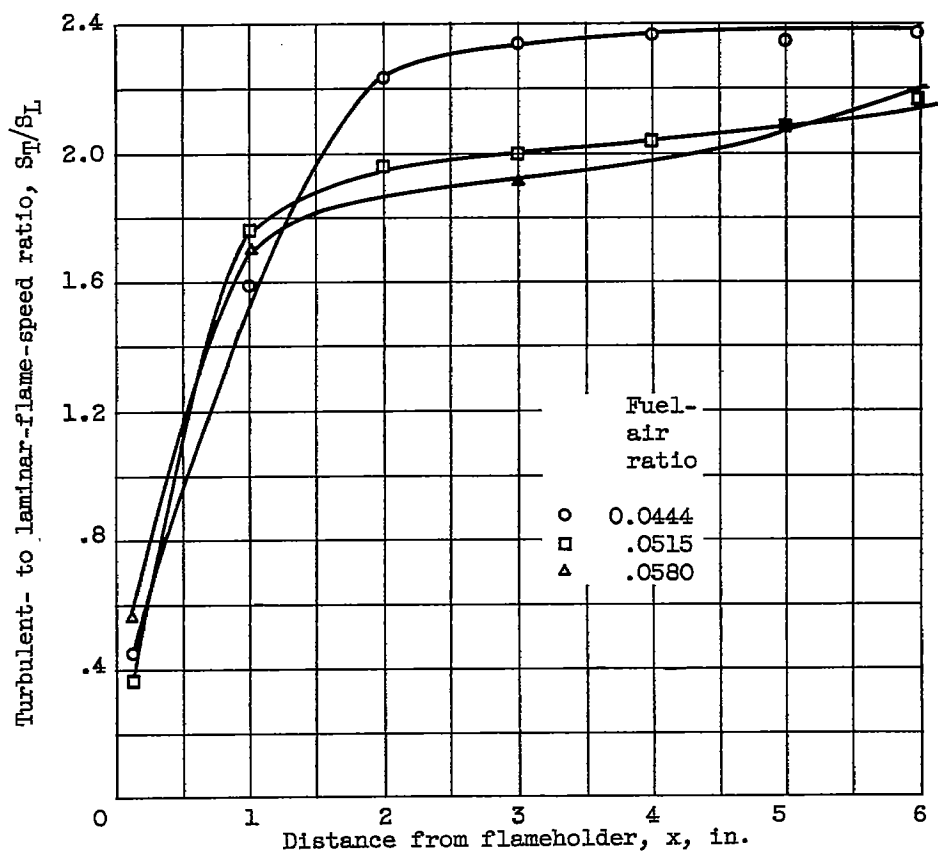
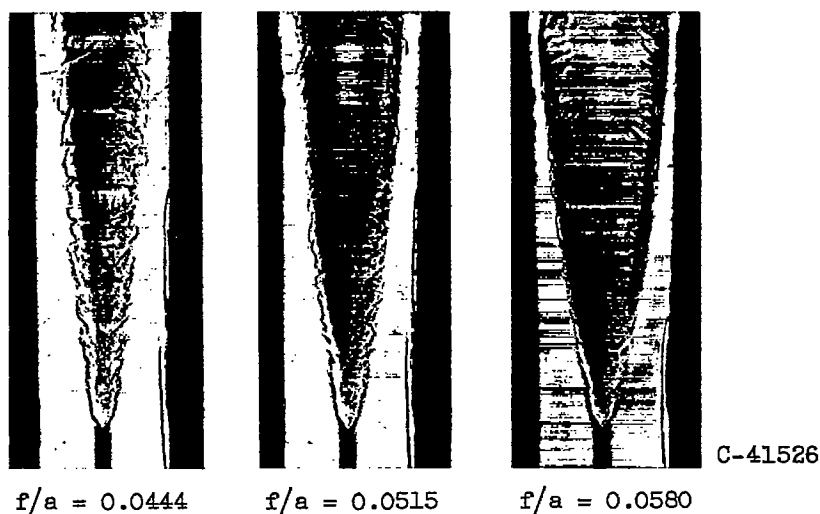
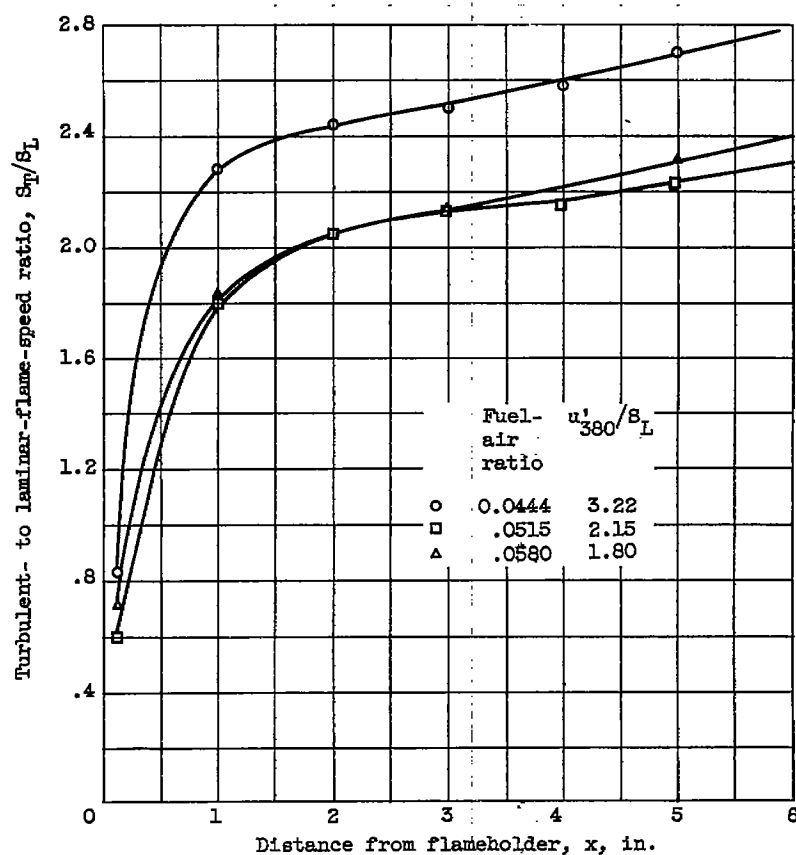
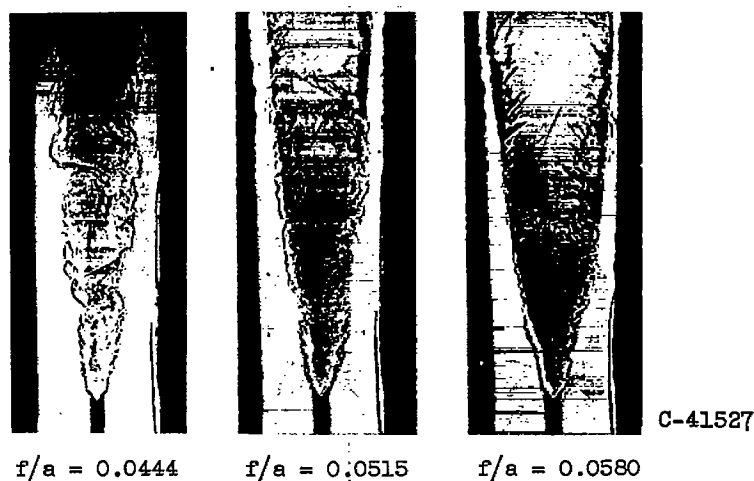


Figure 26. - Comparison of fraction burned obtained by momentum-pressure-drop measurement with average voltage obtained by photomultiplier survey. Flow velocity U , 50 feet per second; length, 6 inches; disturbance velocity u' , 2.38 feet per second; antisymmetric disturbance.



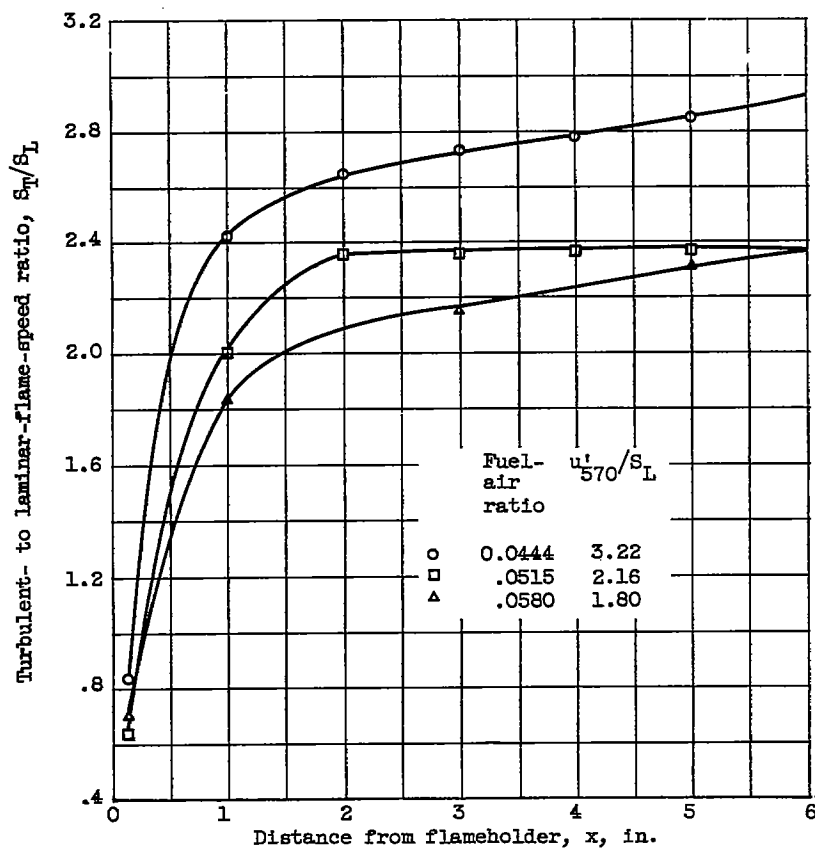
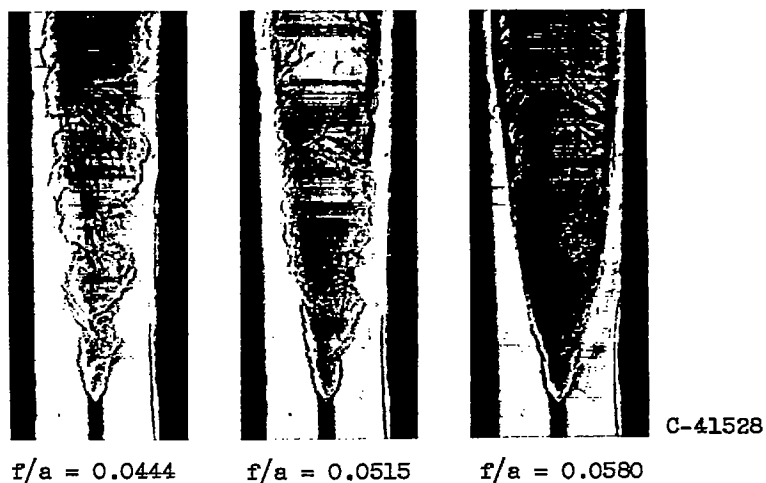
(a) No disturbance.

Figure 27. - Comparison of S_T/S_L and flame appearance for three fuel-air ratios. Flow velocity at plane of flameholder U_0 , 50 feet per second; 0.306-inch flameholder.



(b) With antisymmetric disturbance at 380 cps.

Figure 27. - Continued. Comparison of S_T/S_L and flame appearance for three fuel-air ratios. Flow velocity at plane of flameholder U_0 , 50 feet per second; 0.306-inch flameholder.

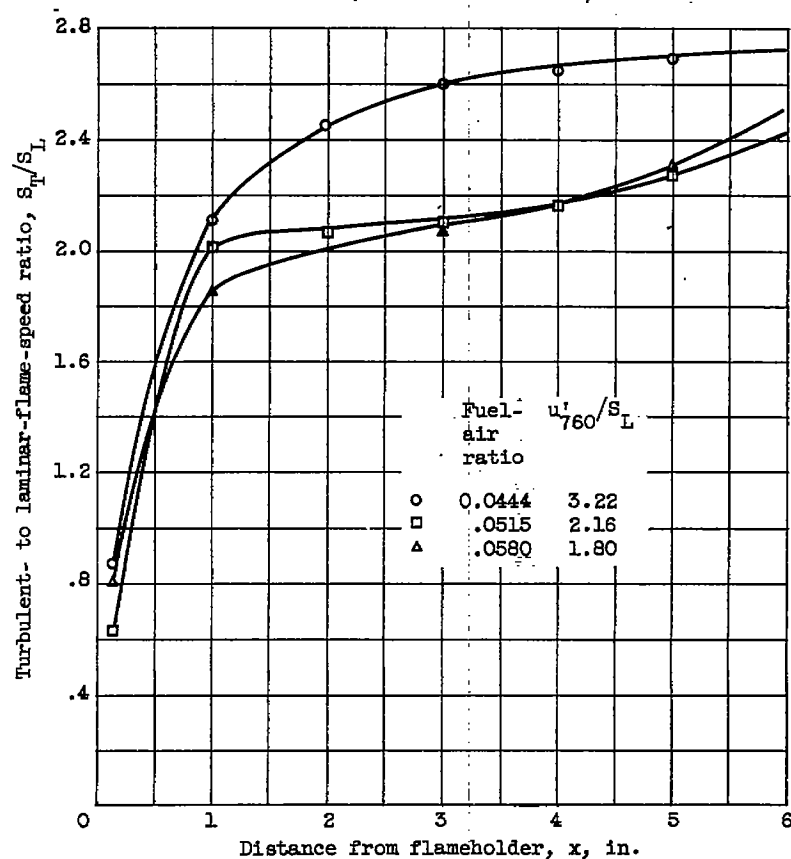


(c) With antisymmetric disturbance at 570 cps.

Figure 27. - Continued. Comparison of S_T/S_L and flame appearance for three fuel-air ratios. Flow velocity at plane of flameholder U_0 , 50 feet per second; 0.306-inch flameholder.

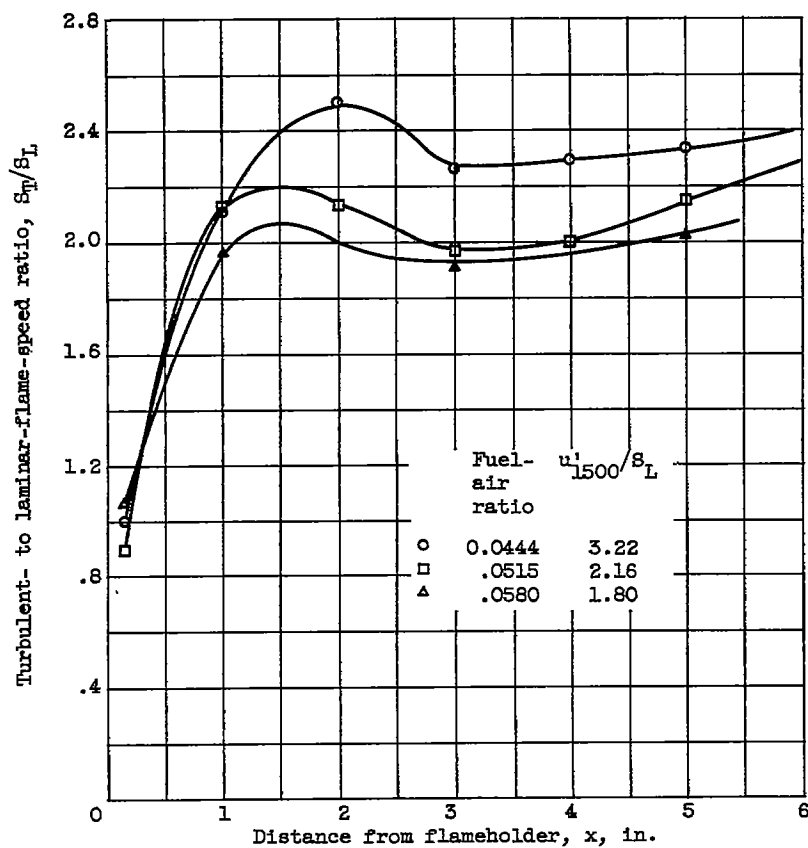
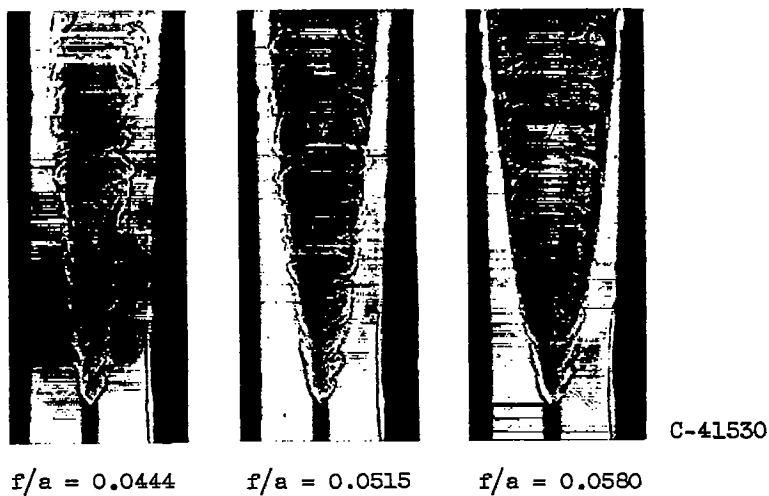


C-41529

 $f/a = 0.0444$ $f/a = 0.0515$ $f/a = 0.0580$ 

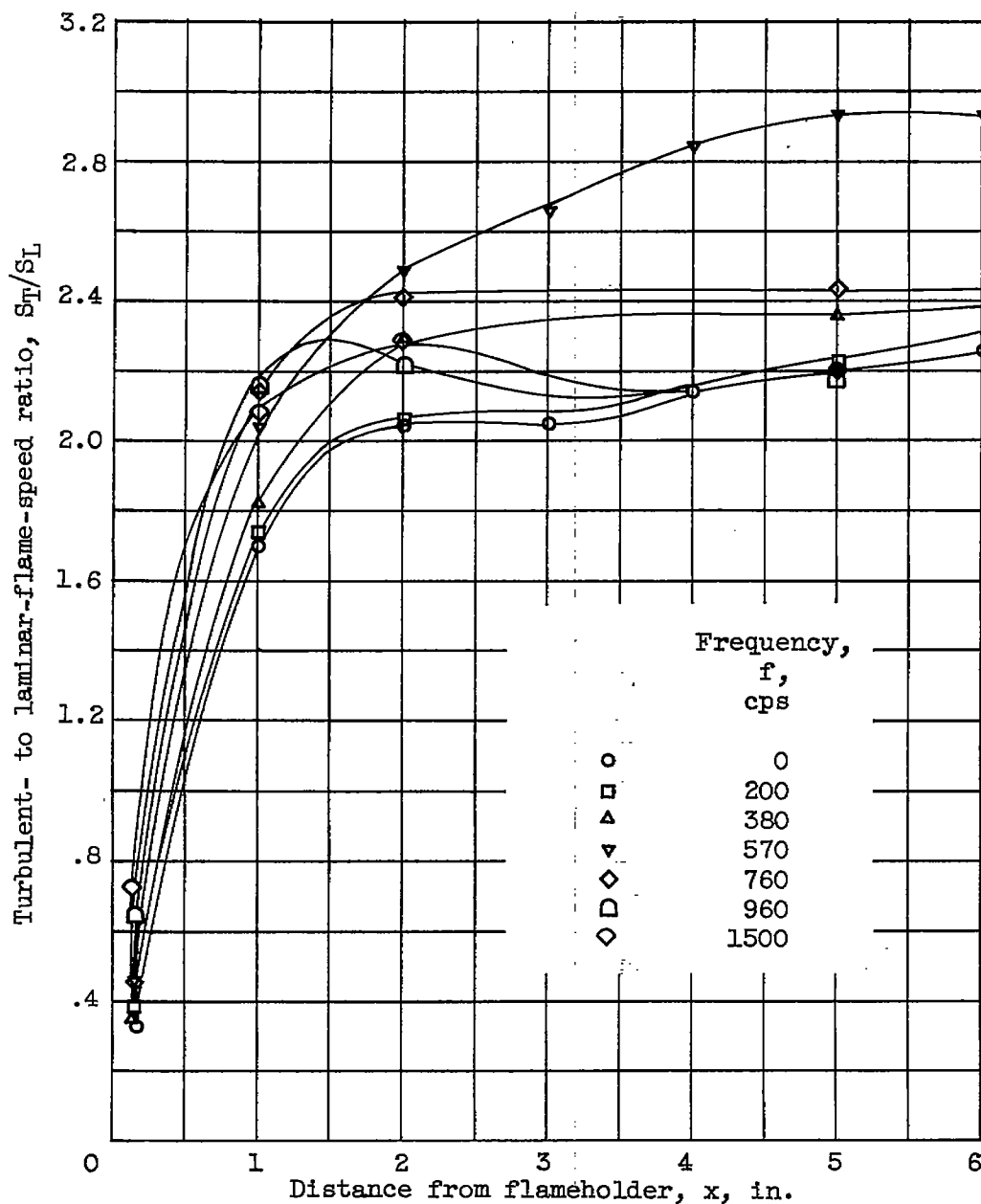
(d) With antisymmetric disturbance at 760 cps.

Figure 27. - Continued. Comparison of S_T/S_L and flame appearance for three fuel-air ratios. Flow velocity at plane of flameholder U_0 , 50 feet per second; 0.306-inch flameholder.



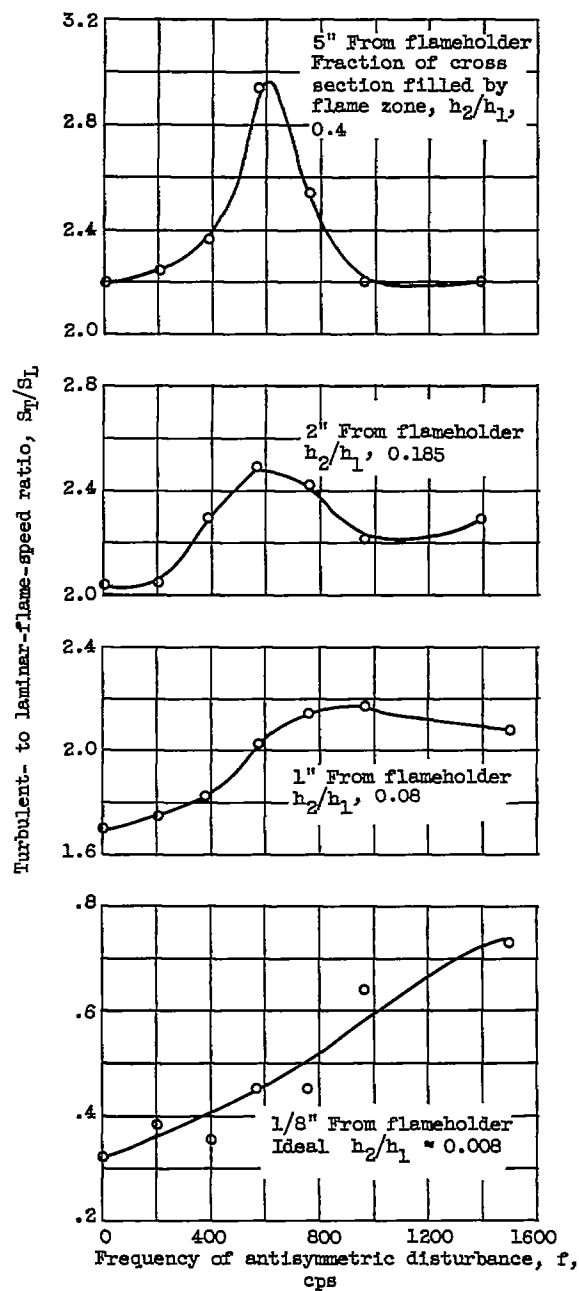
(e) With antisymmetric disturbance at 1500 cps.

Figure 27. - Concluded. Comparison of S_T/S_L and flame appearance for three fuel-air ratios. Flow velocity at plane of flameholder U_0 , 50 feet per second; 0.306-inch flameholder.



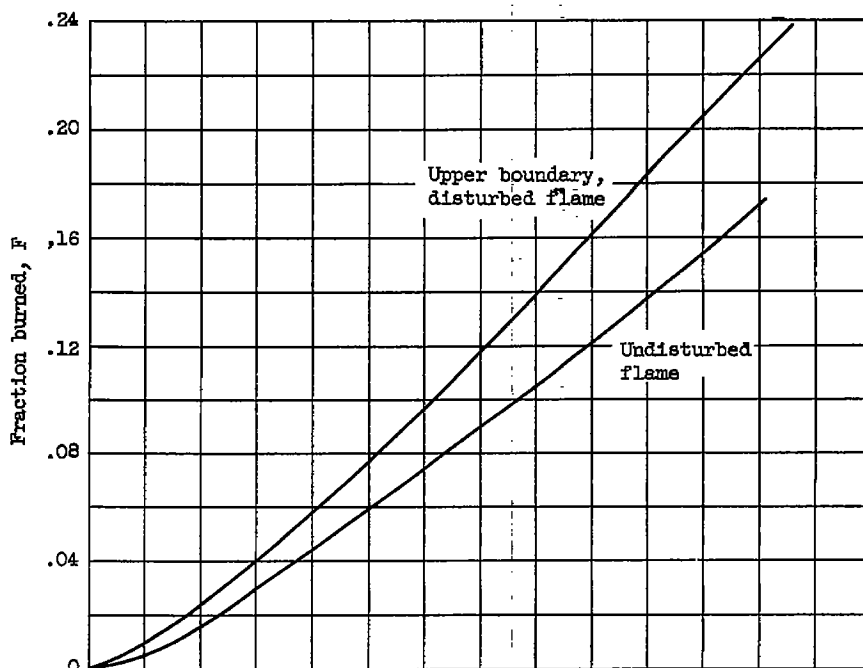
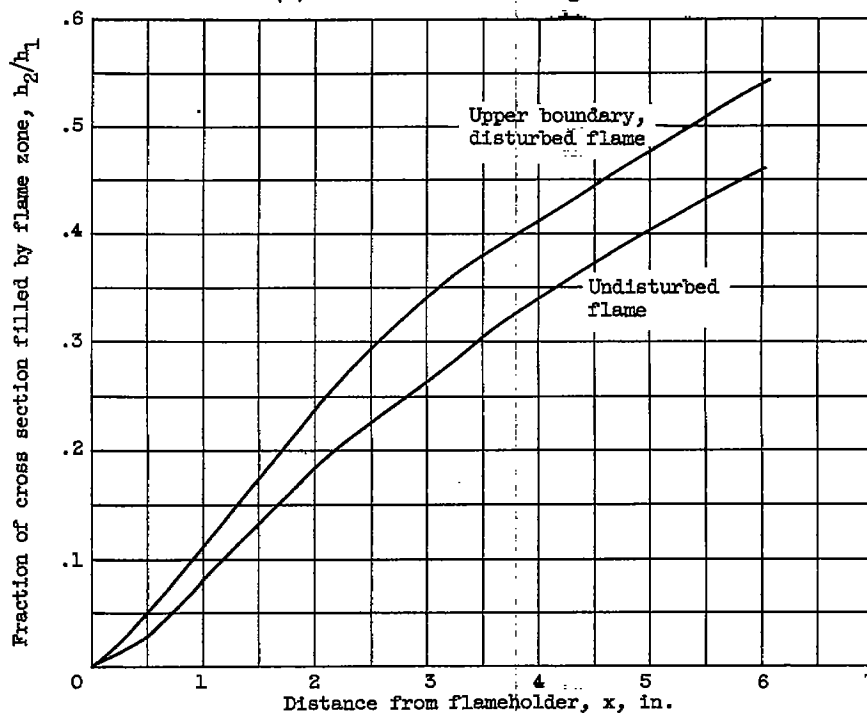
(a) Variation of S_T/S_L with distance from flameholder.

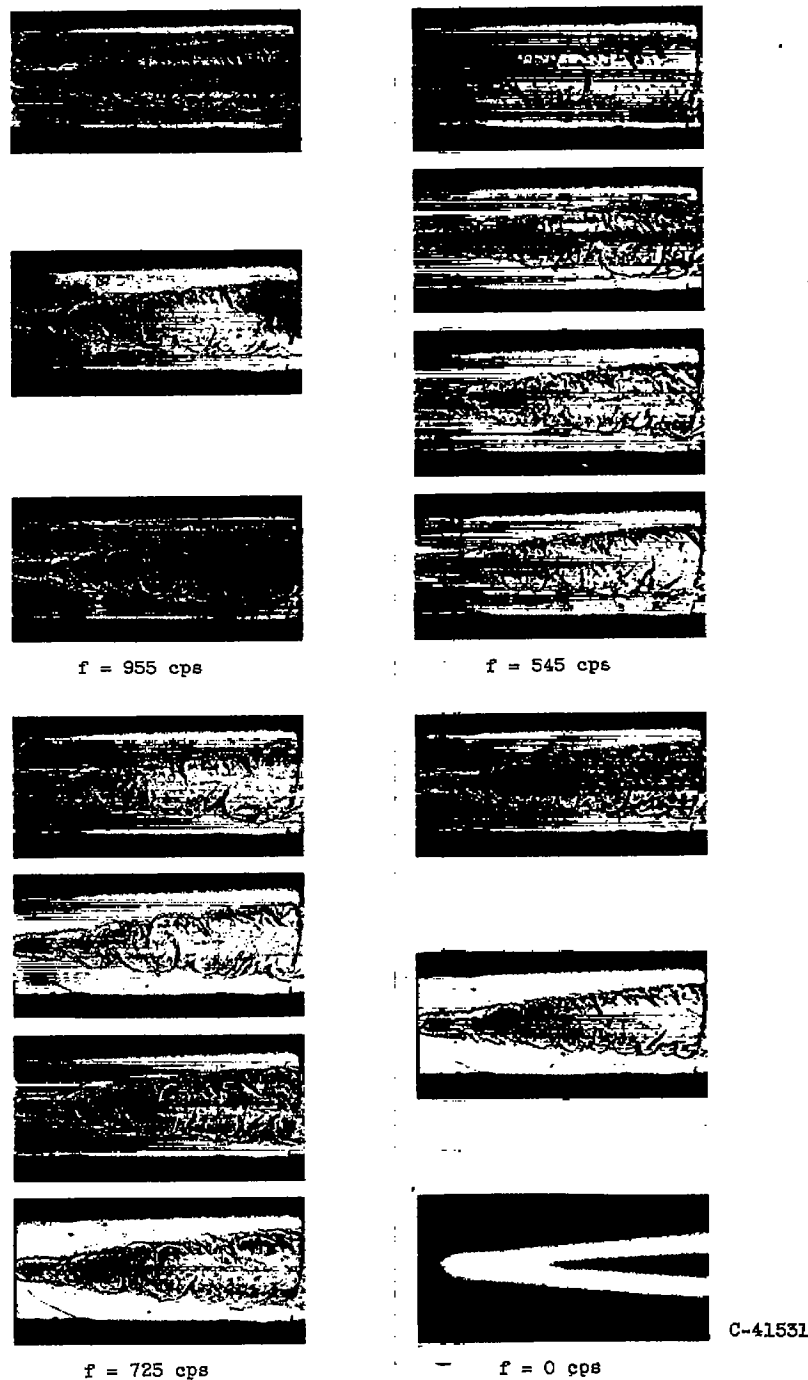
Figure 28. - Effect of frequency on flame-speed distribution. Flow velocity U , 50 feet per second; fuel-air ratio, 0.0444; disturbance velocity, 2.16 feet per second; test section depth, 1/2 inch; 0.306-inch flameholder; antisymmetric disturbance.



(b) Variation of S_T/S_L with frequency for various distances from flameholder.

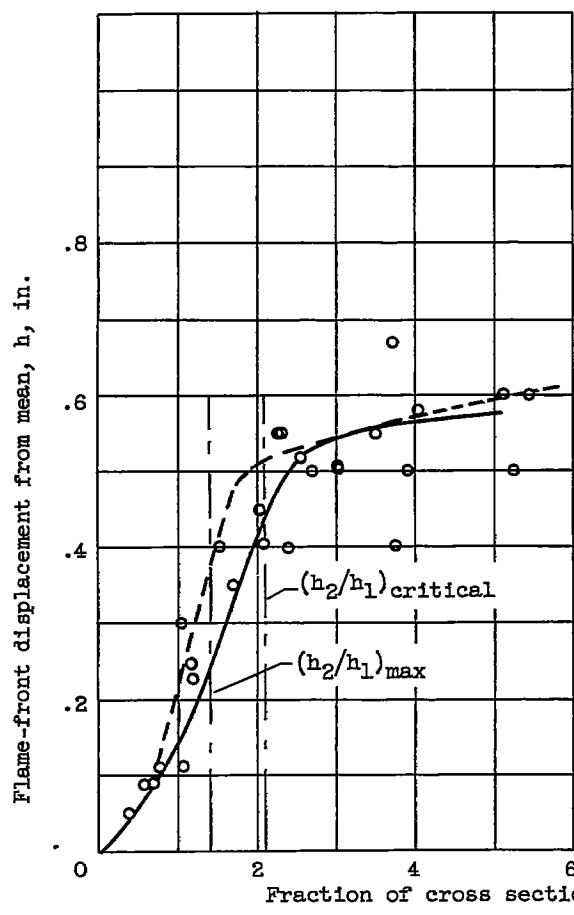
Figure 28. - Concluded. Effect of frequency on flame-speed distribution. Flow velocity U , 50 feet per second; fuel-air ratio, 0.0444; disturbance velocity, 2.16 feet per second; test section depth $1\frac{1}{2}$ inches; 0.306-inch flameholder; antisymmetric disturbance.

(a) Fraction burned F against x .(b) h_2/h_1 against x .Figure 29. - Distribution of fraction burned F and idealized h_2/h_1 for data of figure 28(a).

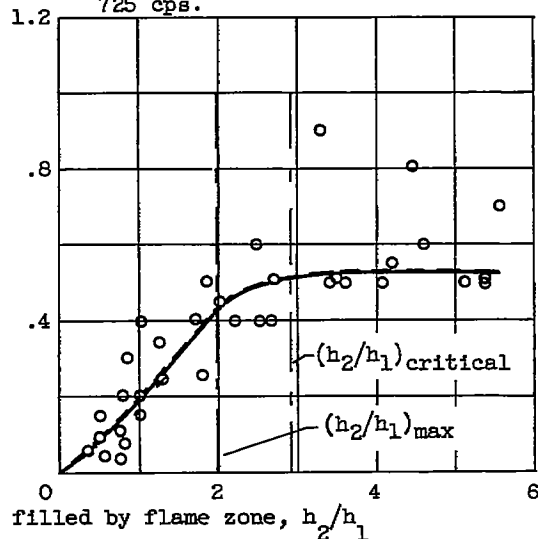
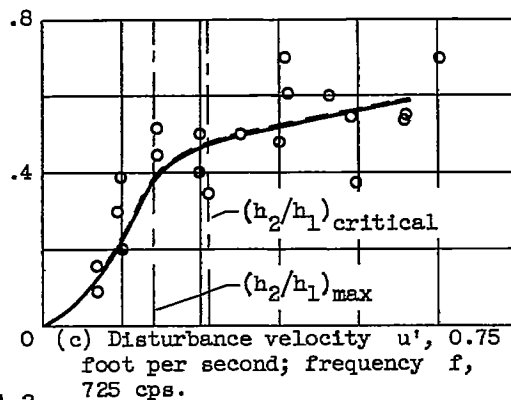


(a) Flame shadowgraphs for disturbance velocity u' of 0.75 foot per second at various frequencies f .

Figure 31. - Displacement measured on flame front for small-amplitude disturbances. Flow velocity U , 50 feet per second; fuel-air ratio, 0.0484; turbulent disturbance velocity u' , 0.303 foot per second.



(b) Disturbance velocity u' ,
0.6 foot per second; fre-
quency f , 725 cps.



(d) Disturbance velocity u' ,
0.75 foot per second; fre-
quency f , 545 cps.

Figure 31. - Concluded. Displacement measured on flame front for small-amplitude disturbances. Flow velocity U , 50 feet per second; fuel-air ratio 0.0484; turbulent disturbance velocity u' , 0.303 foot per second.

3877

CY-16 back

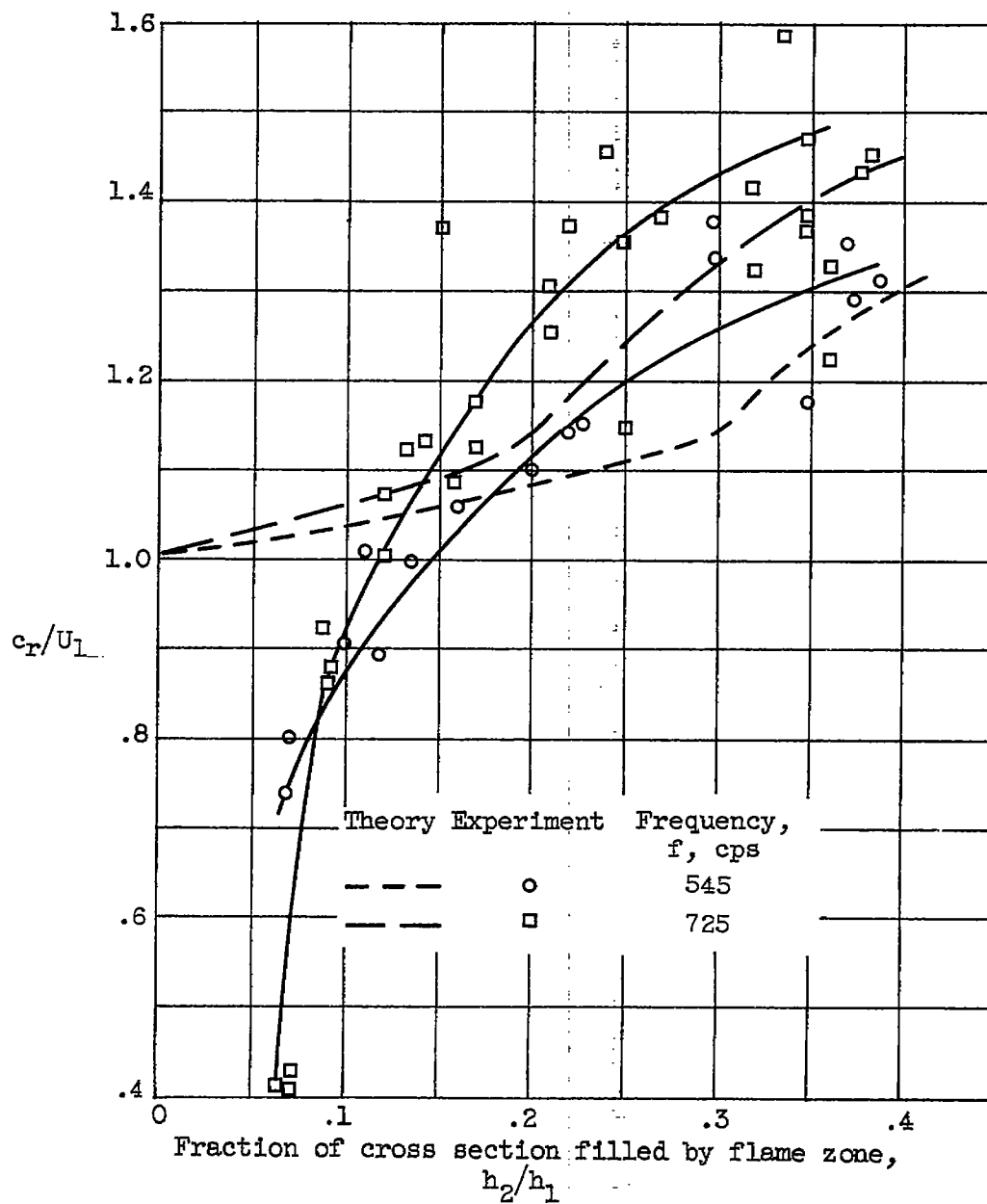


Figure 32. - Propagation velocities for small-amplitude disturbances.

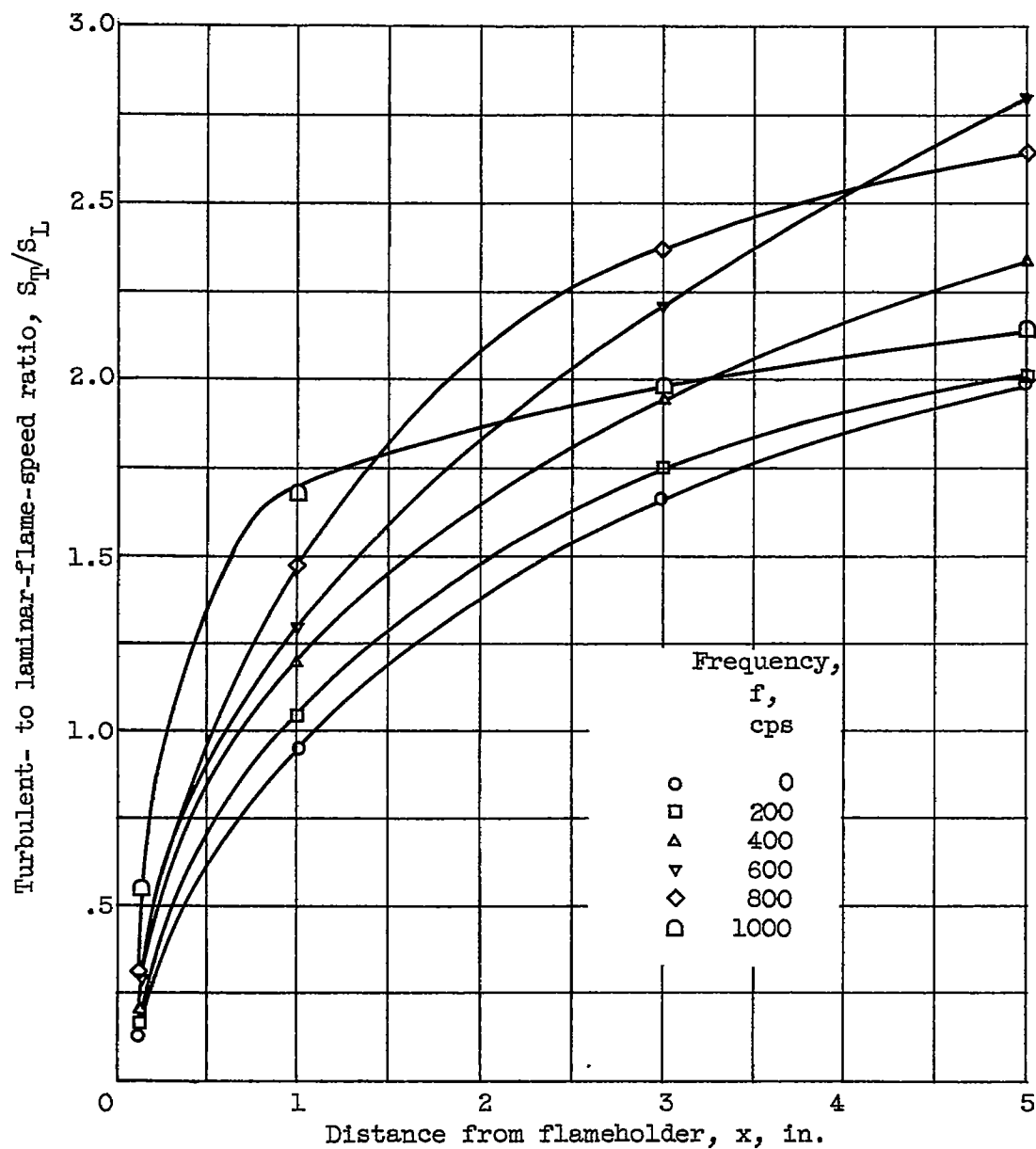


Figure 33. - Flame-speed distribution in 1-inch-deep test section. Flow velocity at plane of flameholder U_0 , 50 feet per second; fuel-air ratio, 0.0493; 1/4-inch flameholder.

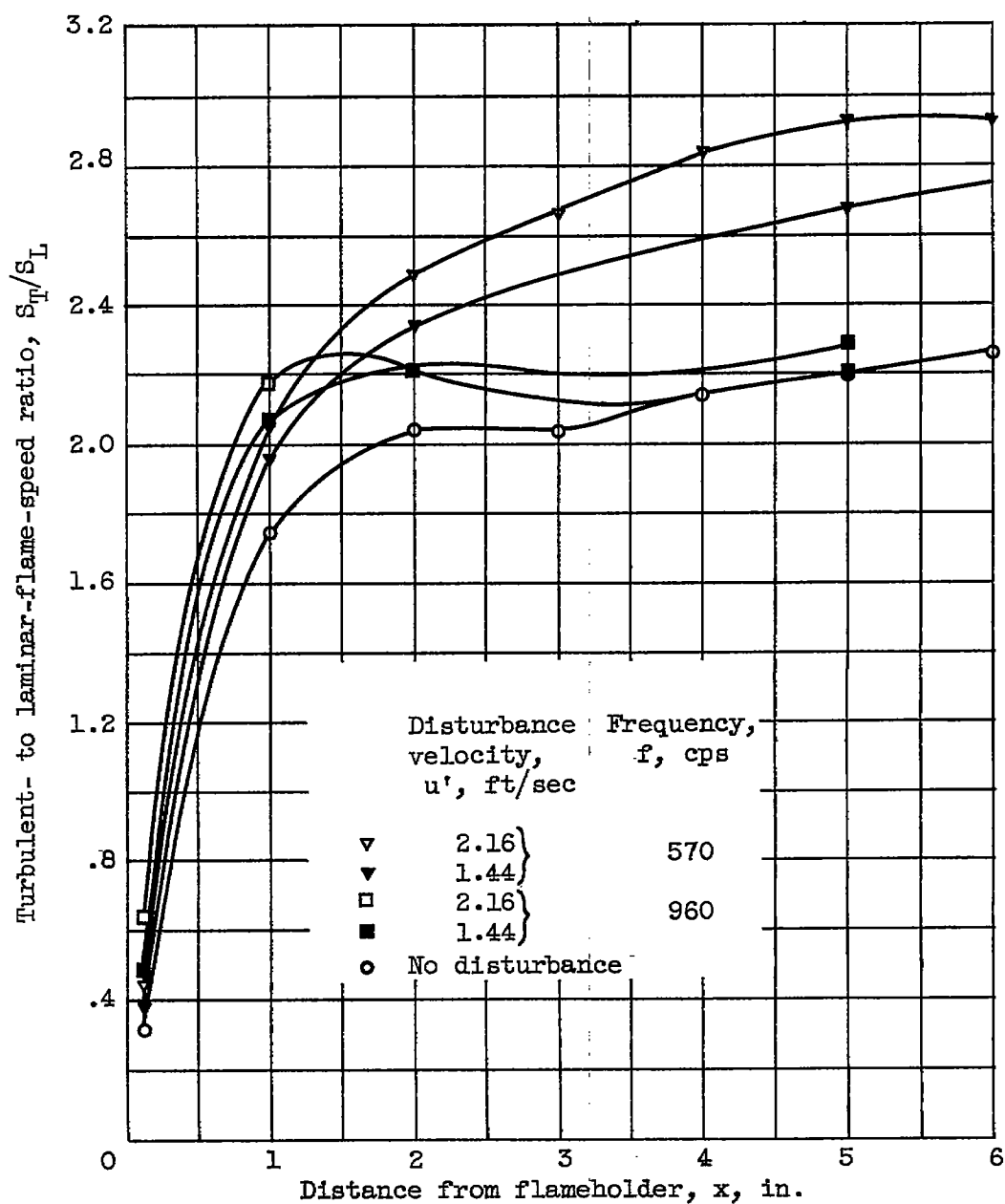
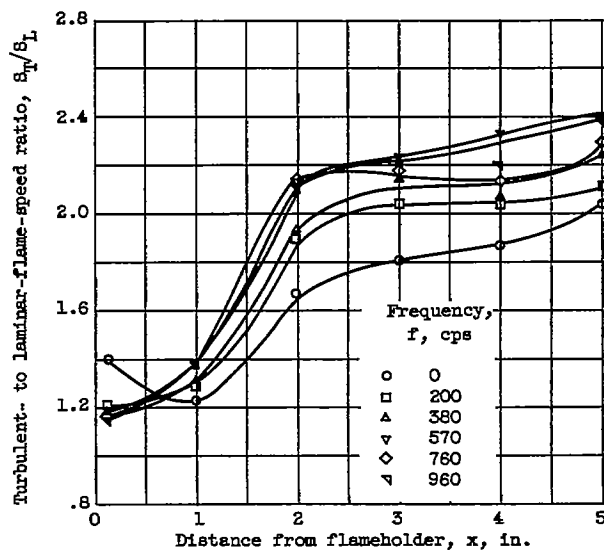
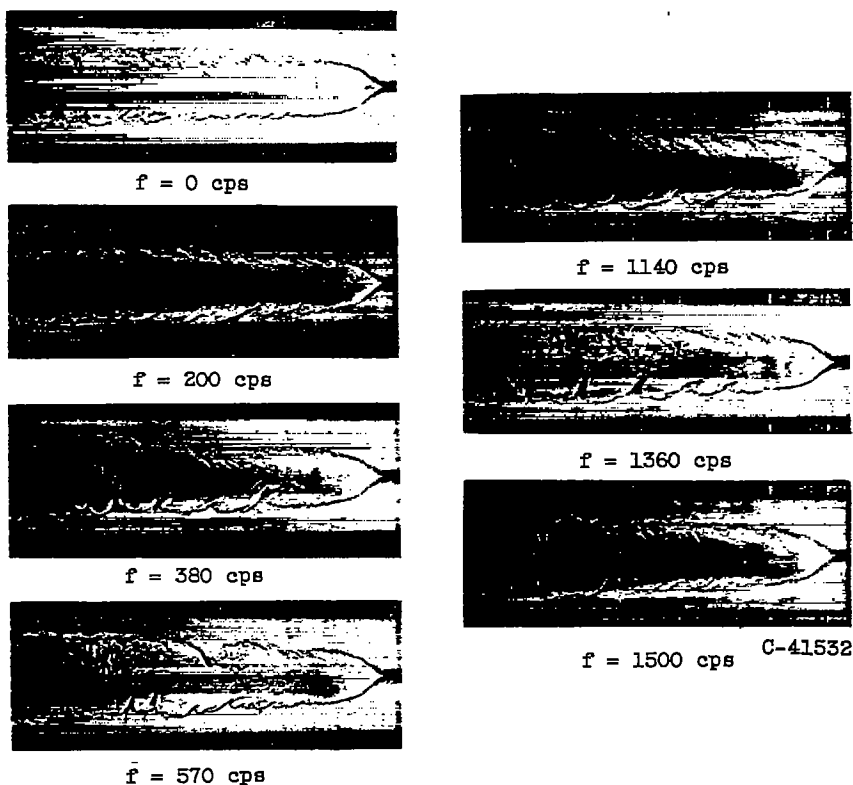


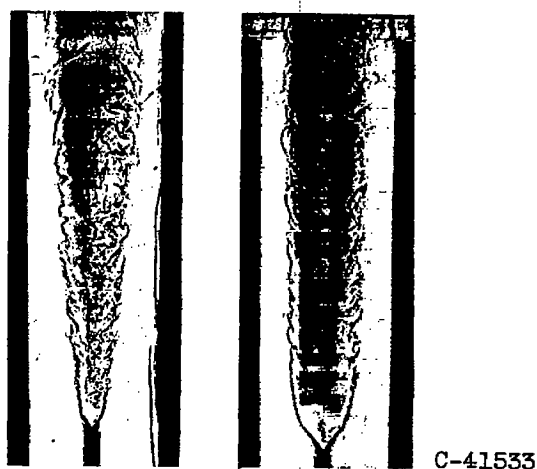
Figure 34. - Effect of amplitude on flame-speed distribution. Flow velocity U , 50 feet per second; fuel-air ratio, 0.0444.

3877



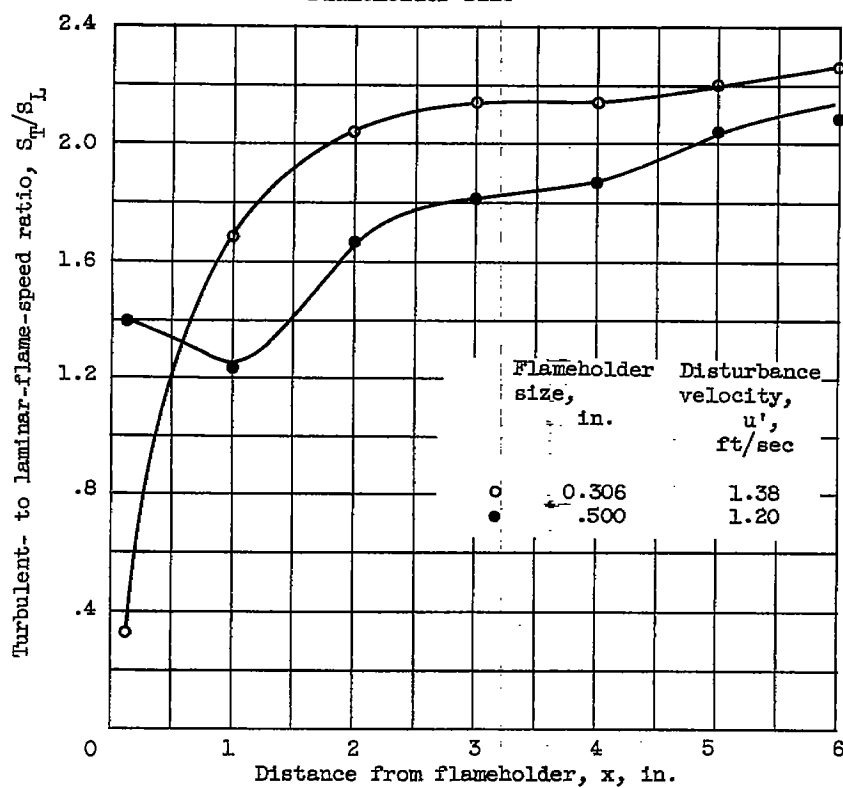
(a) 0.500-Inch flameholder with antisymmetric disturbances. Disturbance velocities: u'_{total} , 2.22 feet per second; $u'_{turbulent}$, 1.2 feet per second; $u'_{frequency}$, 1.87 feet per second.

Figure 35. - Comparison of S_T/S_L and flame appearance for 0.500- and 0.306-inch flameholders. Flow velocity U , 50 feet per second; fuel-air ratio, 0.0444.



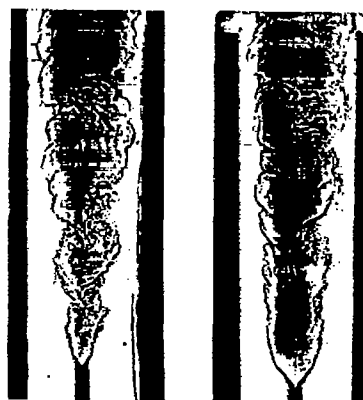
0.306" 0.500"

Flameholder size



(b) Both flameholders without disturbance.

Figure 35. - Continued. Comparison of S_T/S_L and flame appearance for 0.500- and 0.306-inch flameholders. Flow velocity U , 50 feet per second; fuel-air ratio, 0.0444.

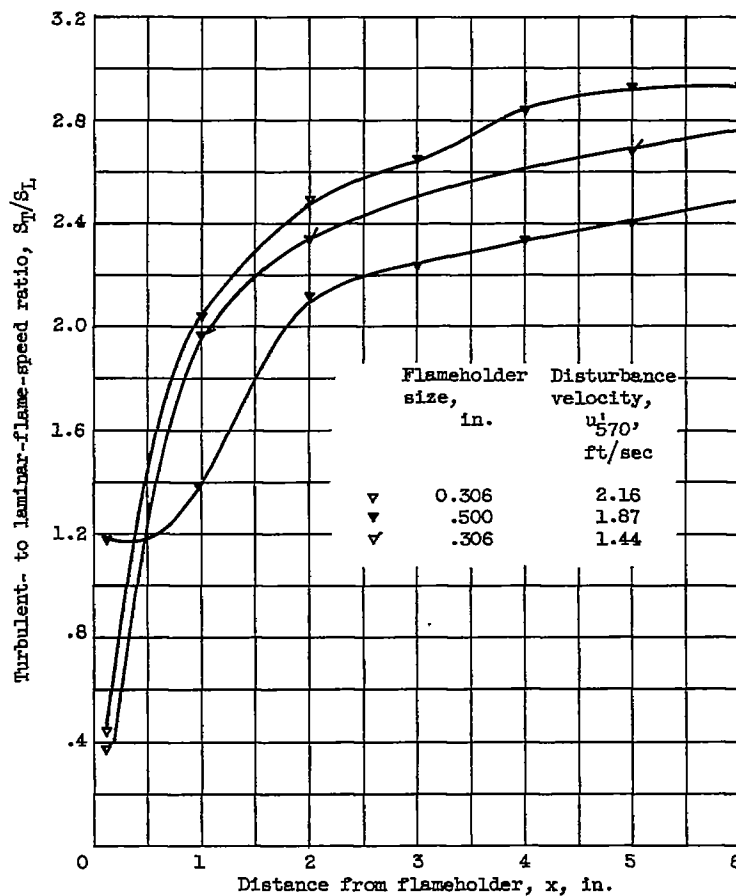


0.306"

0.500"

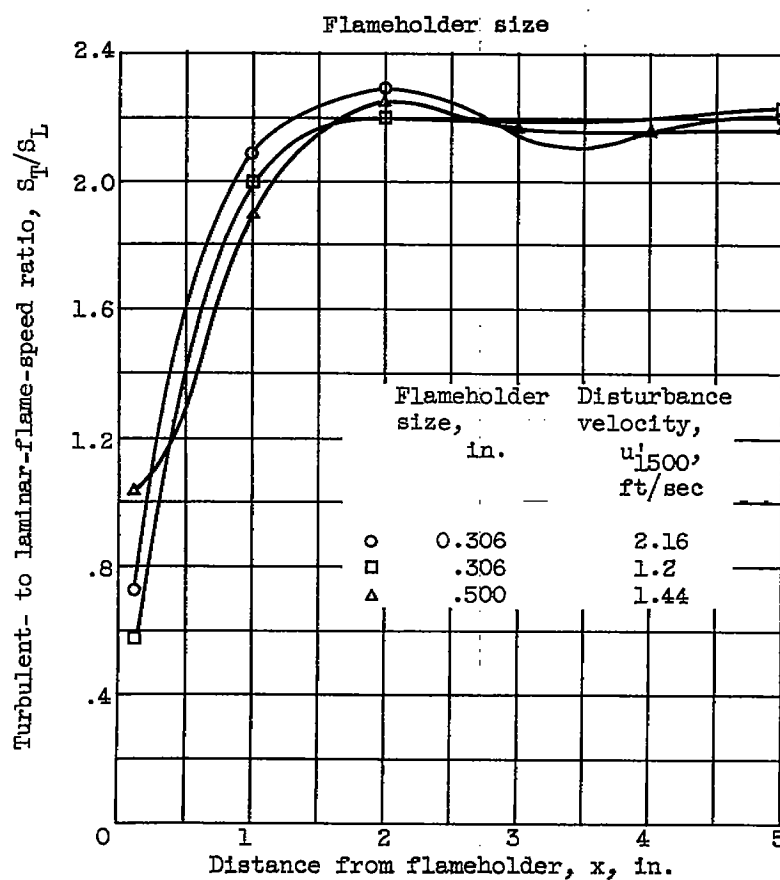
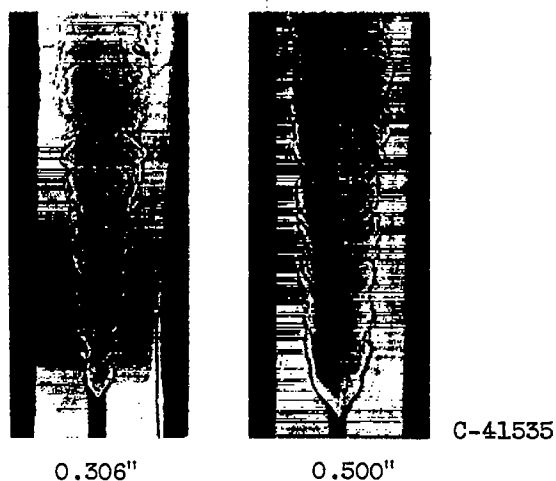
C-41534

Flameholder size



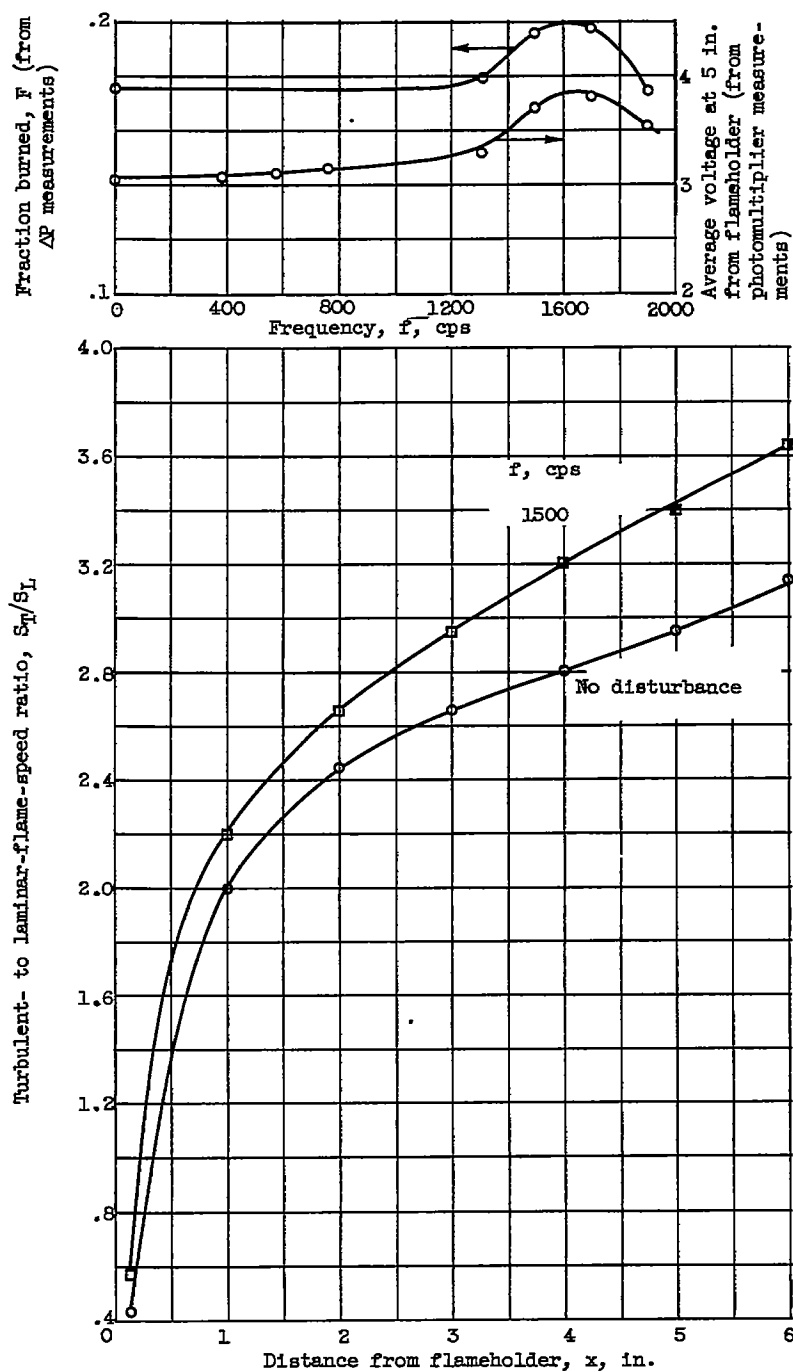
(c) Both flameholders with disturbance at 570 cps.

Figure 35. - Continued. Comparison of S_T/S_L and flame appearance for 0.500- and 0.306-inch flameholders. Flow velocity U , 50 feet per second; fuel-air ratio, 0.0444.



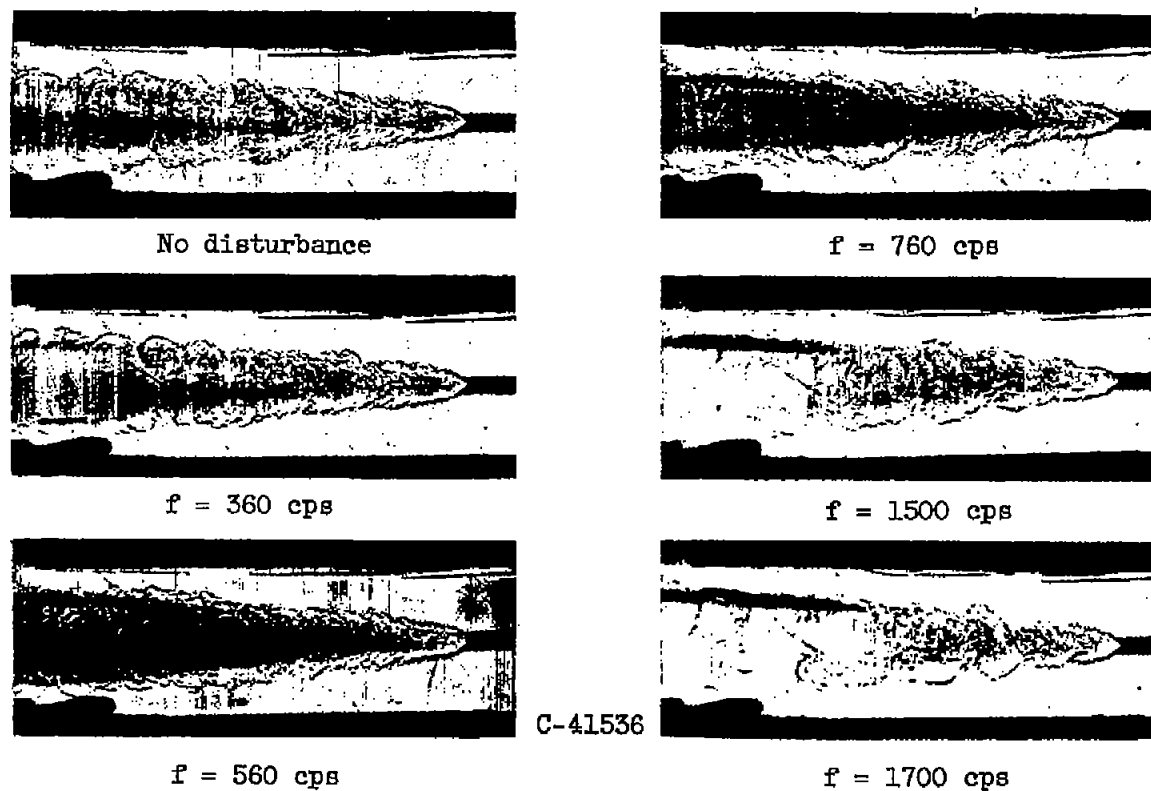
(d) Both flameholders with disturbance at 1500 cps.

Figure 35. - Concluded. Comparison of S_T/S_L and flame appearance for 0.500- and 0.306-inch flameholders. Flow velocity U , 50 feet per second; fuel-air ratio, 0.0444.



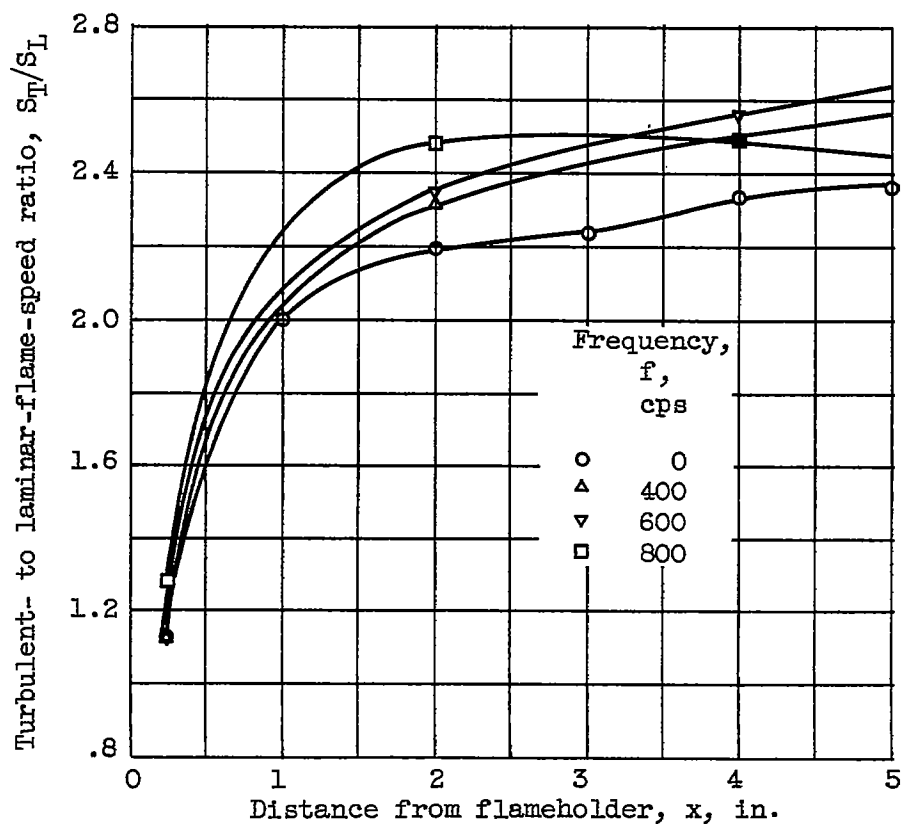
(a) S_T/S_L distribution and comparison of fraction burned with average voltage.

Figure 36. - S_T/S_L distribution, shadowgraphs, and comparison of fraction burned with average voltage. Flow velocity U , 100 feet per second; fuel-air ratio, 0.0493; antisymmetric disturbance.



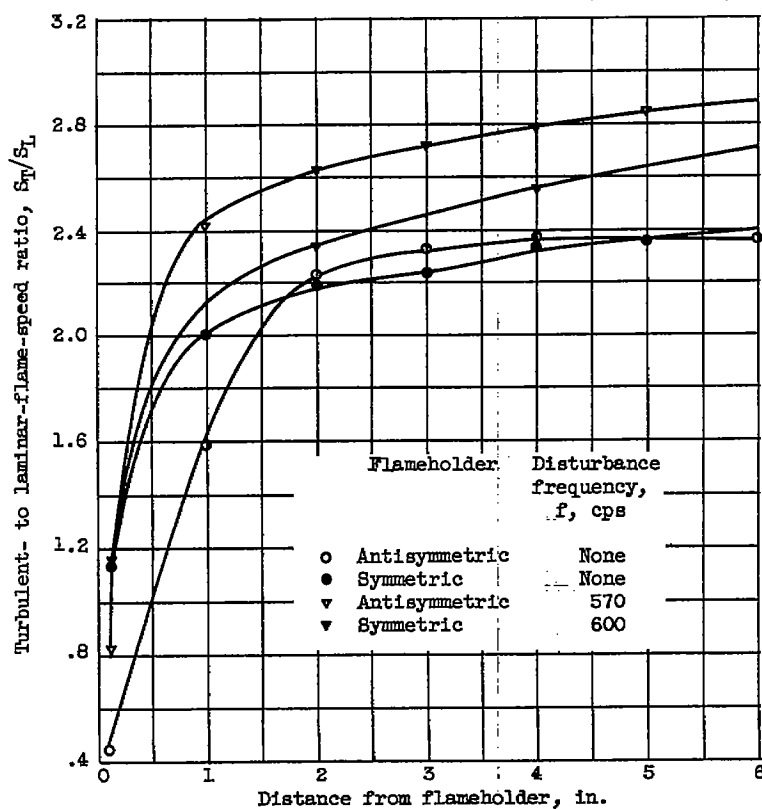
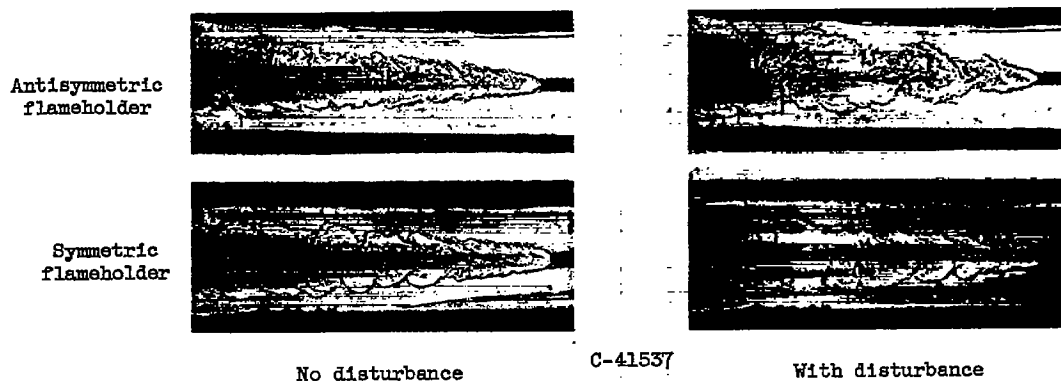
(b) Shadowgraphs for various frequencies f .

Figure 36. - Concluded. S_T/S_L distribution, shadowgraphs and comparison of fraction burned with average voltage. Flow velocity U , 100 feet per second. Fuel-air ratio, 0.0493; antisymmetric disturbance.



(a) S_T/S_L distribution for symmetric disturbances. Disturbance amplitude unknown; input same as for figure 28(a).

Figure 37. - Comparison of S_T/S_L obtained with flameholder for producing symmetric disturbances with S_T/S_L obtained with flameholder for producing antisymmetric disturbances. Flow velocity U , 50 feet per second; fuel-air ratio, 0.0444.



(b) Comparison of symmetric and antisymmetric flameholders with and without disturbance.

Figure 37. - Concluded. Comparison of S_T/S_L obtained with flameholder for producing symmetric disturbances with S_T/S_L obtained with flameholder for producing antisymmetric disturbances. Flow velocity U , 50 feet per second; fuel-air ratio, 0.0444.



Direct photograph of flame through stroboscope; frequency f , 600 cps



Shadowgraph of excited flame; frequency f , 760 cps



C-41538

Eddy trail

Figure 38. - Comparison of photographs of excited flame with eddy trail.

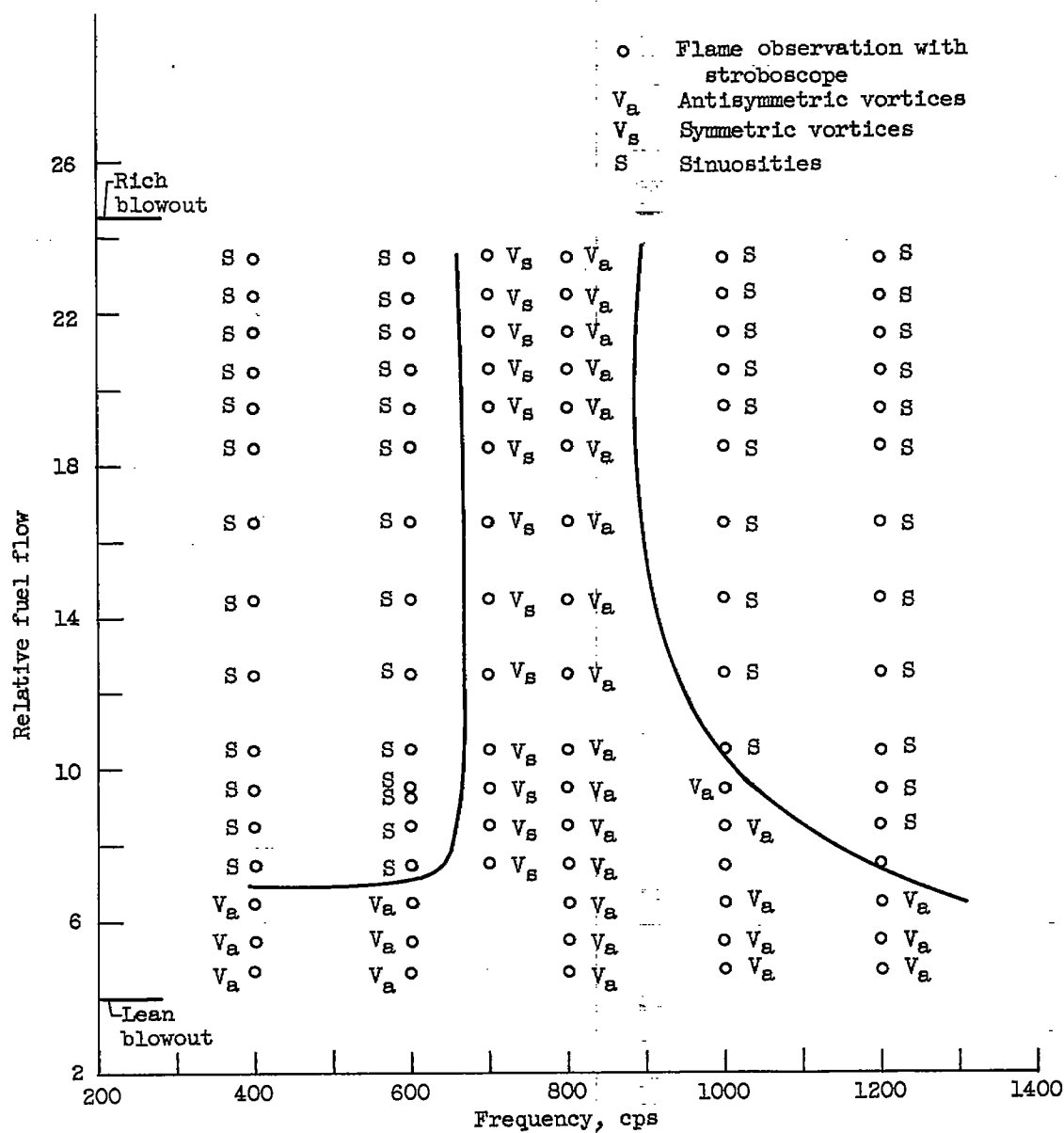
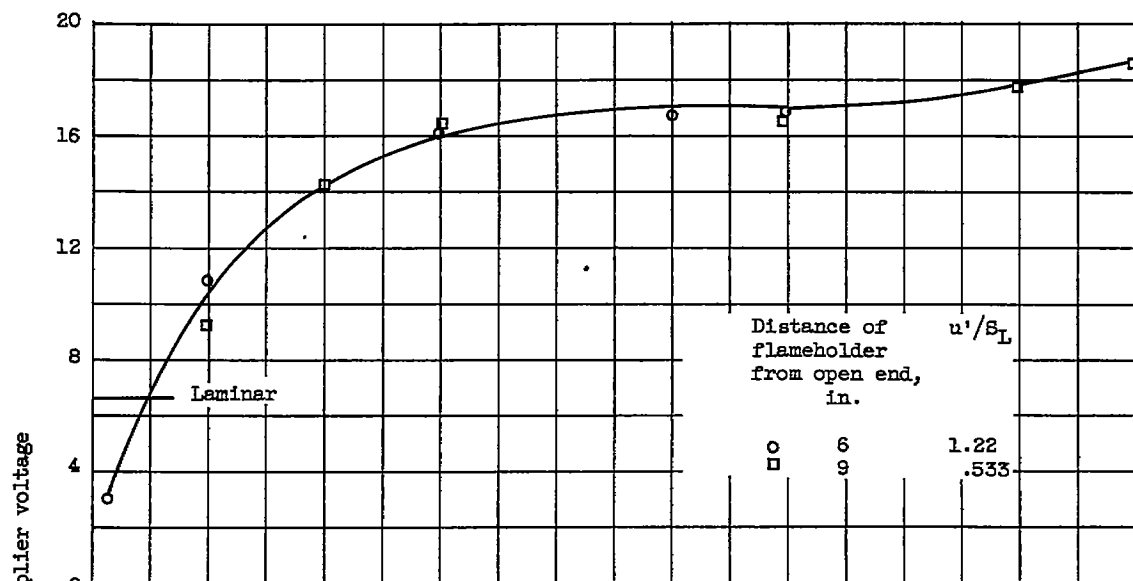
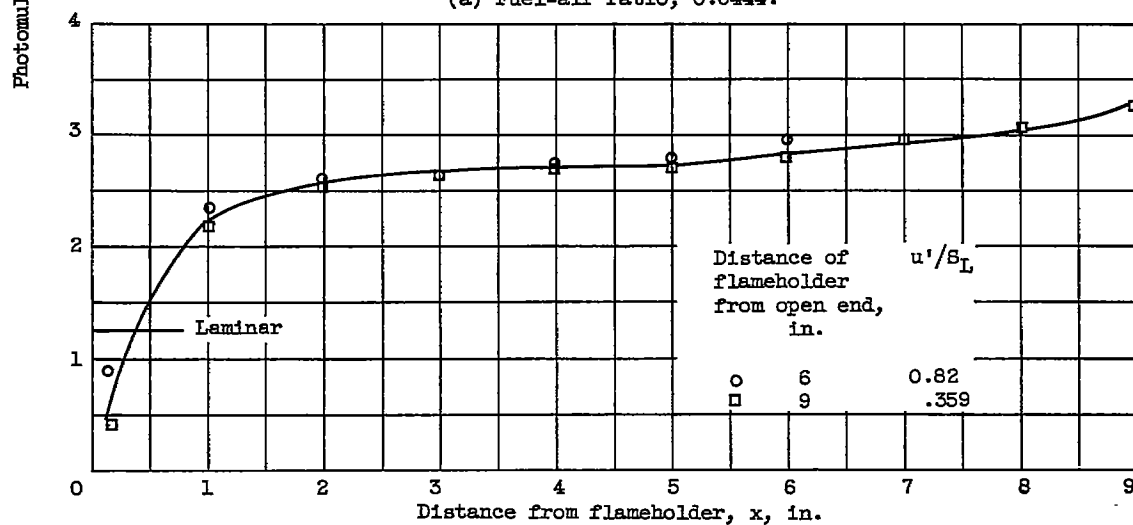


Figure 39. - Observations of vortex shedding excited by antisymmetric disturbances.



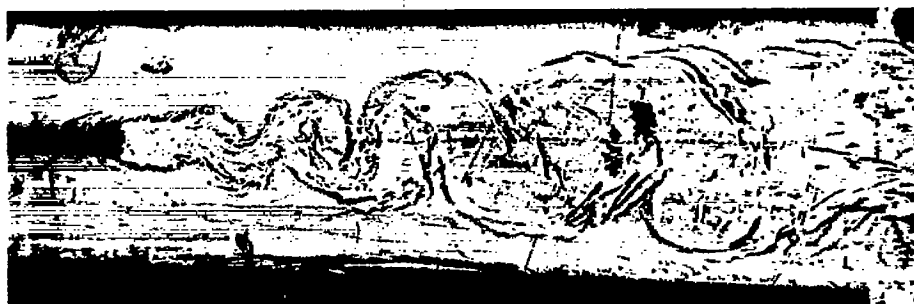
(a) Fuel-air ratio, 0.0444.



(b) Fuel-air ratio, 0.0515.

Figure 40. - Comparison of relative flame speeds at two flameholder positions.
Flow velocity U , 50 feet per second.

With screens
and disturbance



With screens
and no dis-
turbance



C-41540

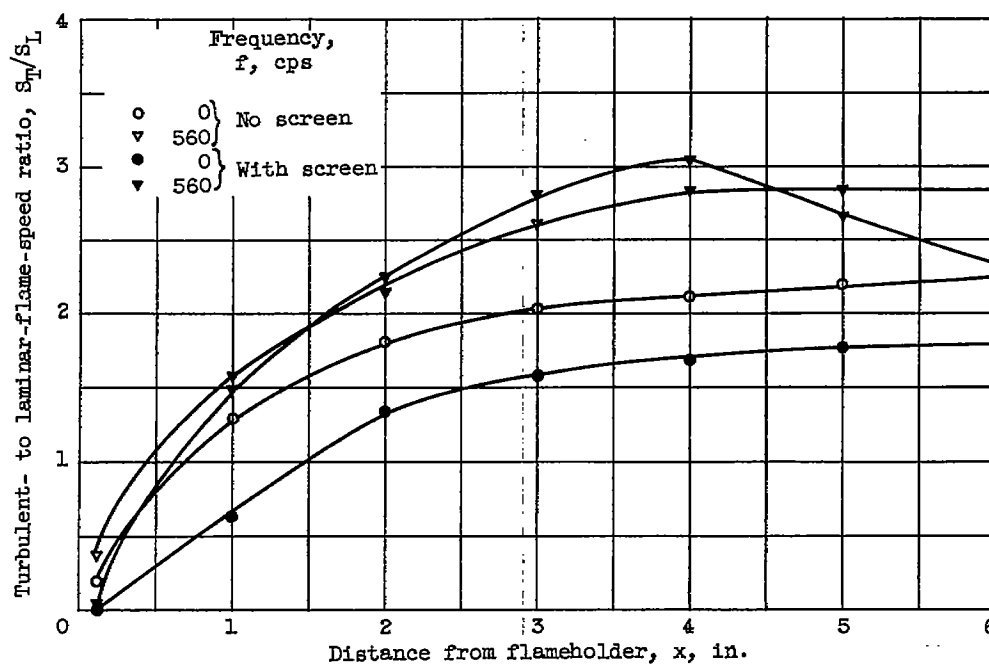


Figure 41. - Comparison of flame speeds with and without banks of 200-mesh screens upstream of flameholder.

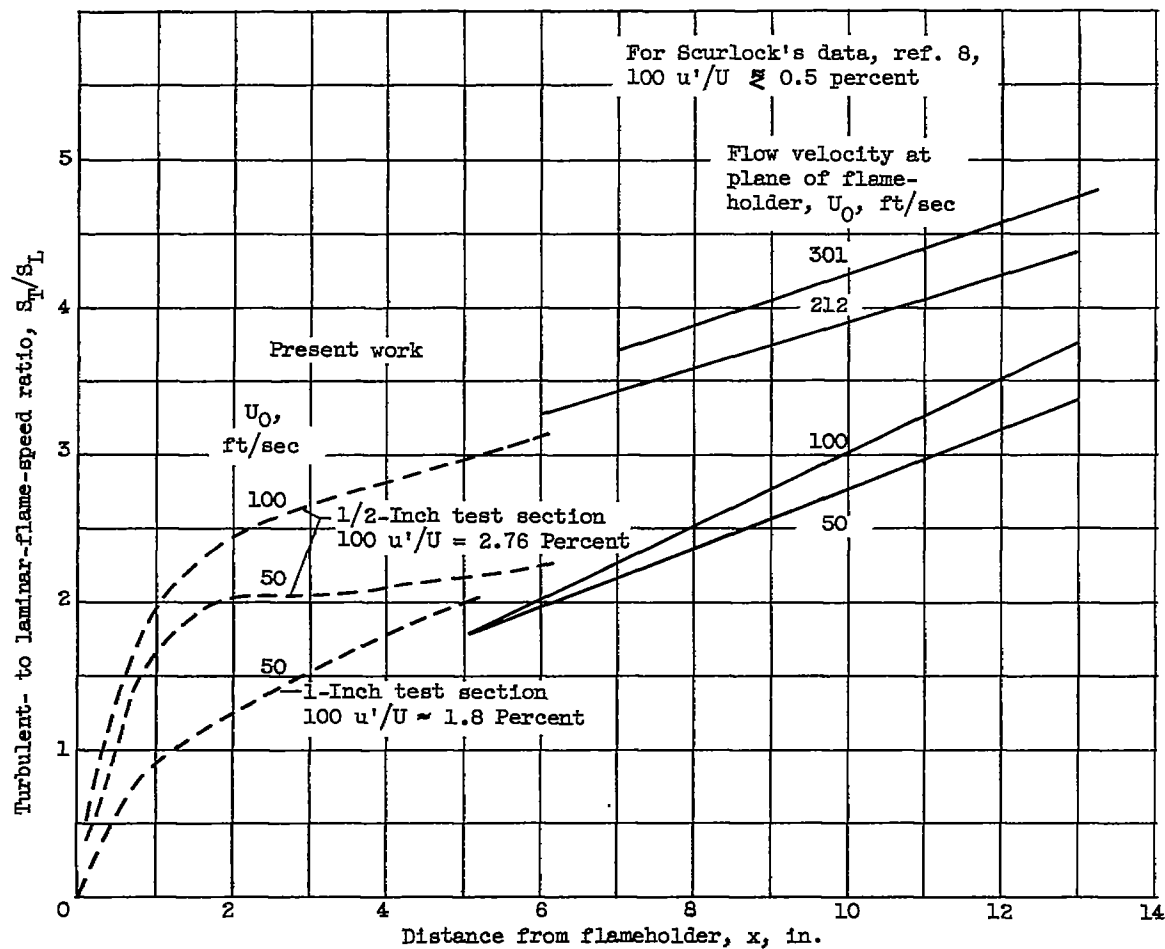


Figure 42. - Comparison of S_T/S_L taken in 1/2-inch- and 1-inch-wide ducts with Scurlock's data.

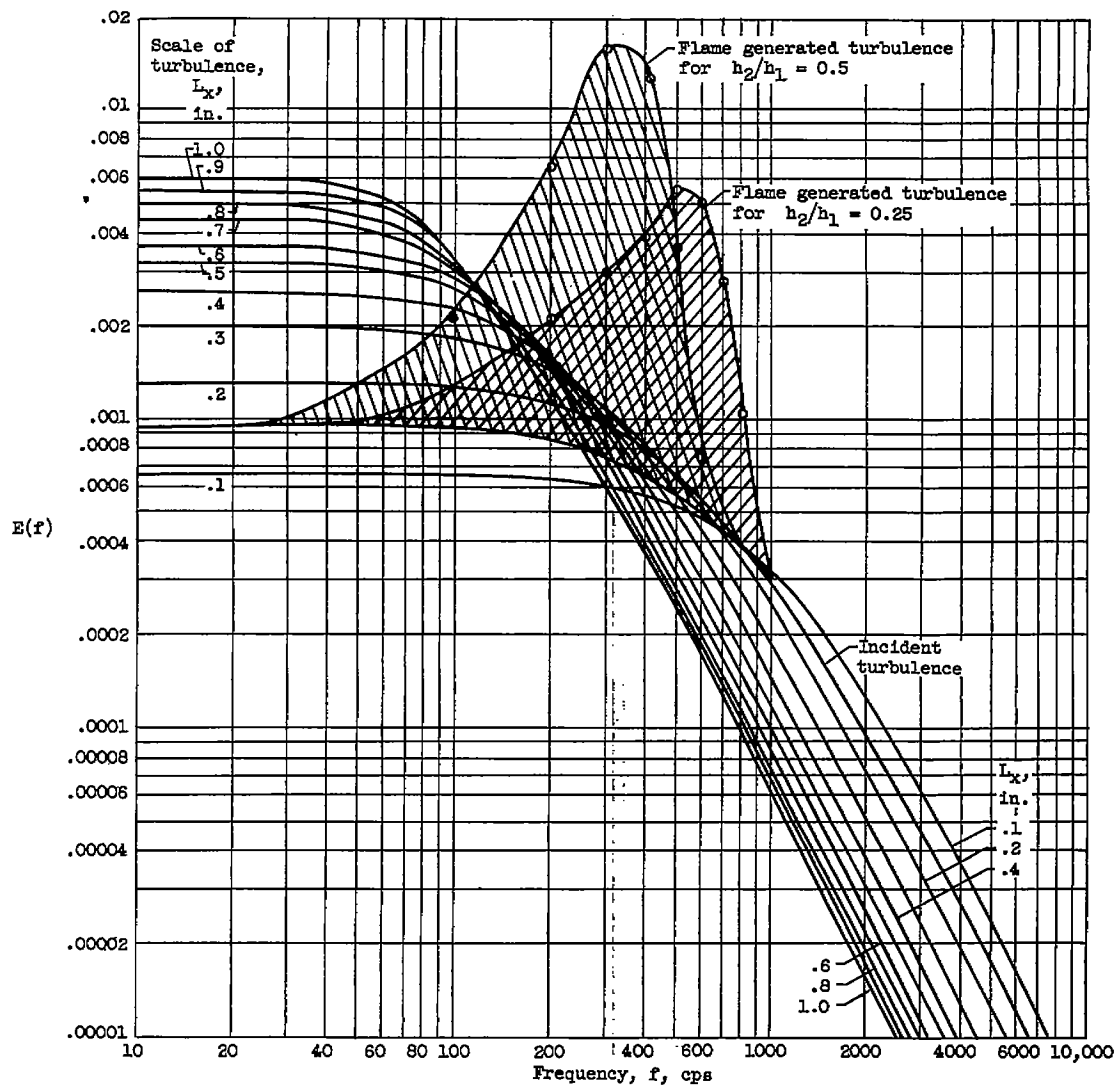


Figure 43. - Spectra of incident and flame amplified turbulence.

$$E(f) = \frac{\frac{4L_x}{U}}{1 + \left(\frac{2\pi}{U} L_x\right)^2 f^2}$$

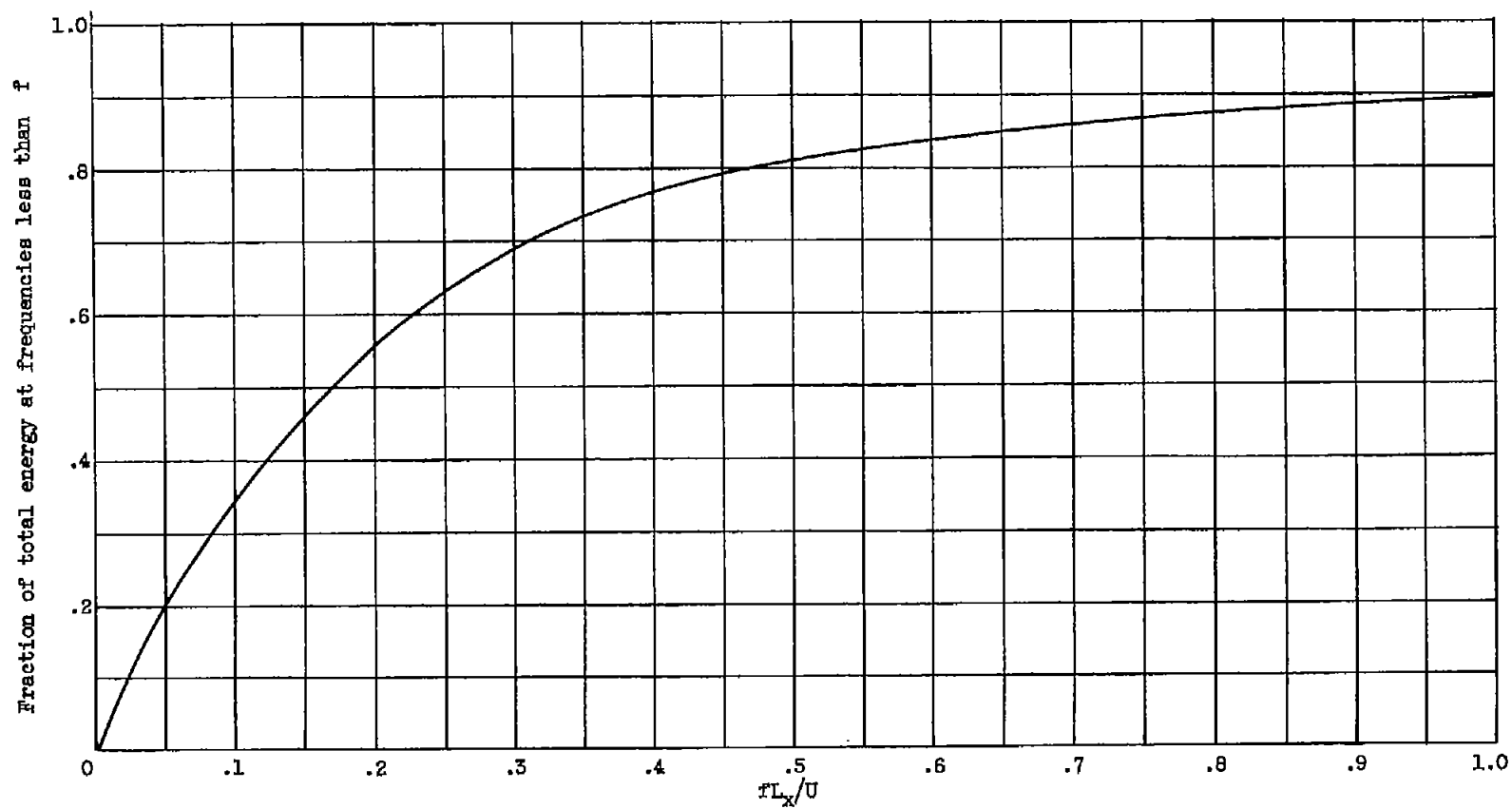


Figure 44. - Turbulence energy distribution for exponential correlation coefficient.

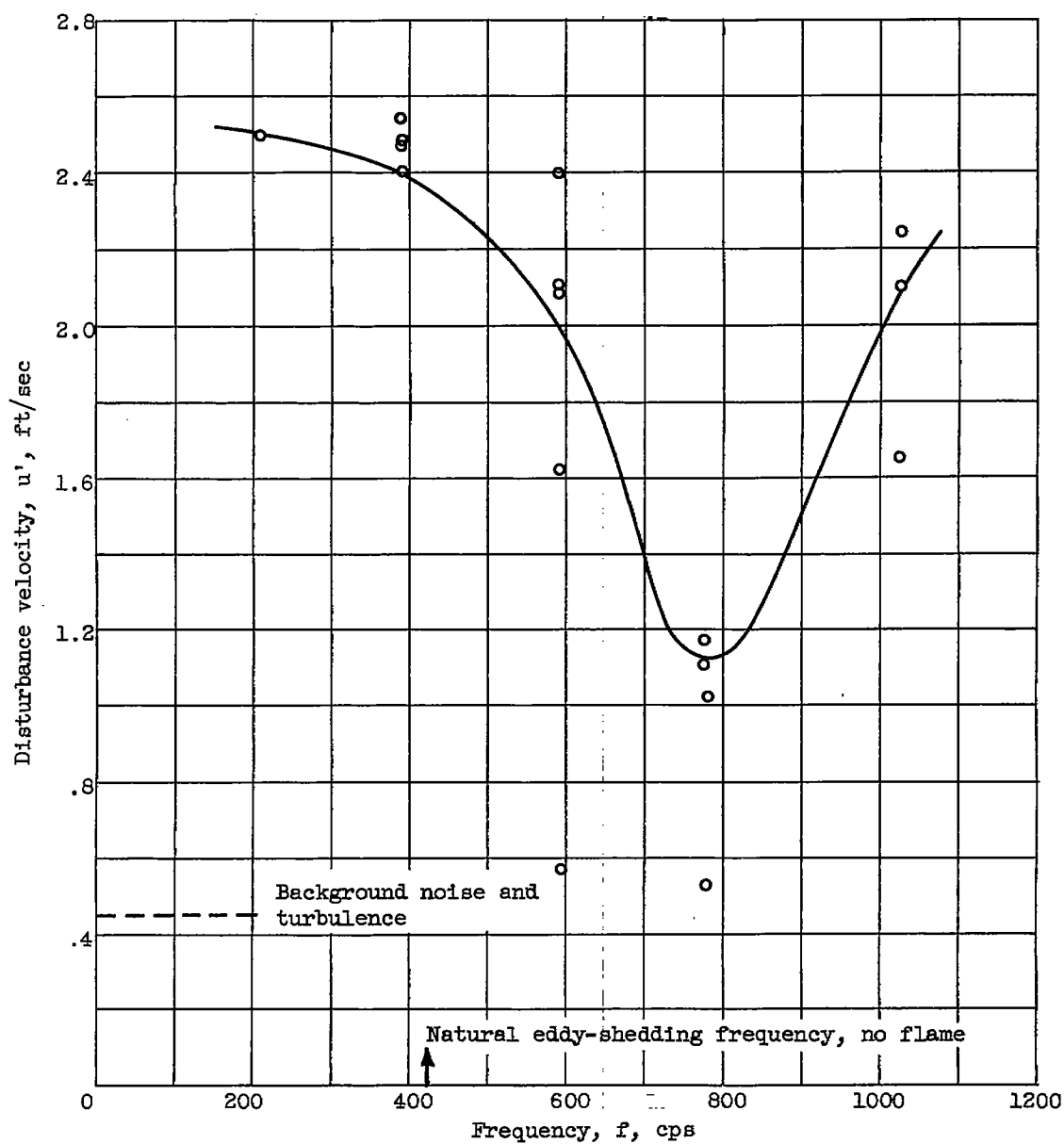
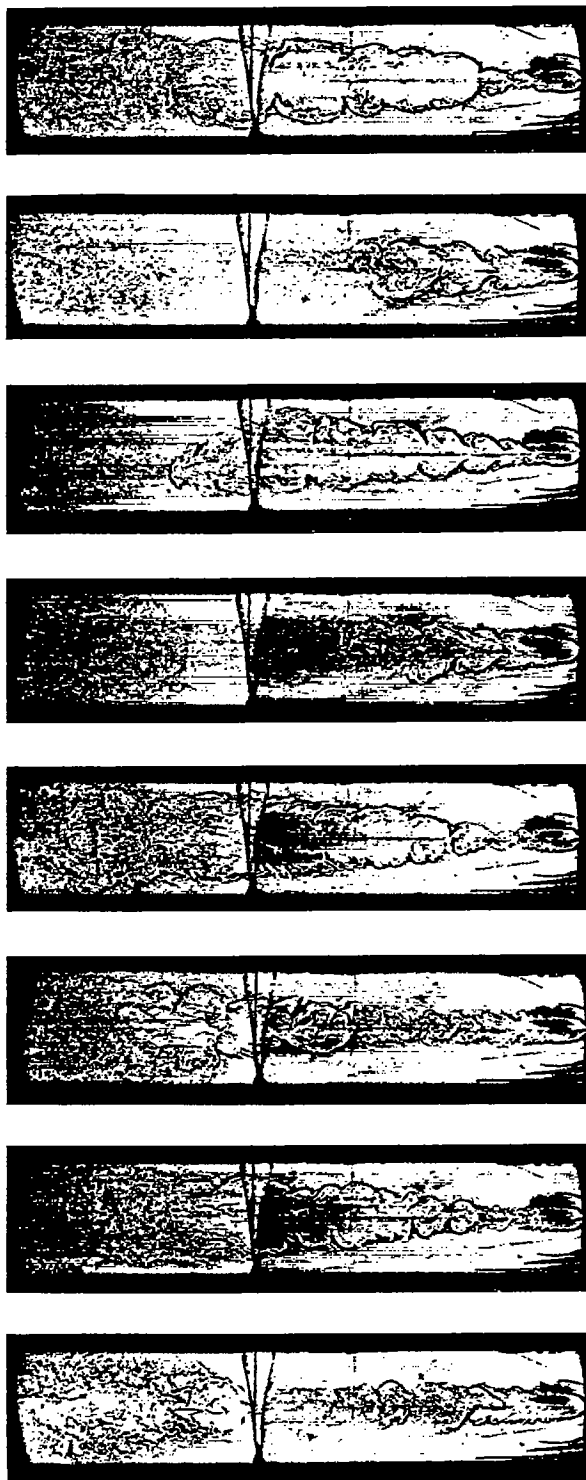


Figure 45. - Distribution with frequency of disturbance velocities required to produce blowout at fixed velocity and fuel-air ratio. Flow velocity at plane of flameholder U_0 , 50 feet per second; 0.306-inch flameholder placed $5/8$ inch from nozzle; duct length, 5.7 inches; antisymmetric disturbances.



C-41541

Figure 46. - Spontaneous oscillations showing intermittent flame interruption. Frequency f , 85 cycles per second; fuel-air ratio, 0.0444; flow velocity U , 50 feet per second.

LIST OF FIGURES



Figure	Mentioned on page -
1. - Geometry of flow field. U , flow velocity in x-direction; ρ , density.	17,20
2. - Amplification-rate parameter $\alpha_1 \frac{2h_2}{\Delta U}$ for  profile .	25,26,41
3. - Wave number $2\alpha h_2$ for neutral stability and maximum in- stability, and amplification-rate parameter $\alpha_1 \frac{2h_2}{\Delta U}$ at maximum instability for  profile.	25,26
4. - Stability map for flame in a duct. Contours of constant amplification rate α_1 are given by lines of constant $\alpha_1 \frac{2h_1}{U_0}$. Lines of constant frequency show the path a given disturbance originating at flameholder takes as it propagates along flame zone at phase velocity c_r	26,31
5. - Phase-velocity parameters.	27,28,34,59
6. - Streamlines of neutral disturbance as seen by observer moving at phase velocity c_r	28
7. - Gains for flame filling the duct.	31,66
8. - Gains as function of h_2/h_1 for family of initial wave numbers $2\alpha_0 h_1$. Density ratio ρ_1/ρ_2 , 7.	31
9. - Disturbance-velocity distributions.	33
10. - Qualitative sketch of flame-front displacement amplitude h as function of fraction of cross section filled by flame zone h_2/h_1	36,58
11. - Frequencies that give maximum increase in local flame speed. Density ratio ρ_1/ρ_2 , 7.	38,57
12. - Qualitative sketch of flameholder wake.	39
13. - Qualitative velocity profiles in flameholder wake.	39

Figure	Mentioned on page -
14. - Idealized velocity profile in flameholder wake. U_1 , flow velocity in cold gas; U^* , flow velocity at apex of hot gas. . . .	39
15. - Effect of velocity profile on amplification-rate parameter $\alpha c_1 \frac{2b}{\Delta U}$ and on wave numbers for neutral stability and maximum instability.	42,61
16. - Combustor.	45,47
17. - Schematic drawing of test section.	45
18. - Flameholders.	45
19. - Photomultiplier probe.	46
20. - Schematic drawing of shadowgraph apparatus.	47
21. - Time-average velocity profiles with cold flow.	47
22. - Velocity profiles in wake of 0.306-inch flameholder.	47
23. - Axial length required to achieve mixing to arbitrary extent. .	47
24. - Turbulence u' spectra for flow velocity U of 50 feet per second. $E(f) = \frac{\frac{4L_x}{U}}{1 + \left(\frac{2\pi}{U} L_x\right)^2 f^2}$, measured 1/8 inch above flameholder lip.	48
25. - Comparison of hot-wire and photomultiplier measurements showing effect of plane waves near exhaust of duct. Flow velocity U , 50 feet per second.	52
26. - Comparison of fraction burned obtained by momentum-pressure-drop measurement with average voltage obtained by photomultiplier survey. Flow velocity U , 50 feet per second; length, 6 inches; disturbance velocity u' , 2.38 feet per second; antisymmetric disturbance.	53,55
27. - Comparison of S_T/S_L and flame appearance for three fuel-air ratios. Flow velocity at plane of flameholder U_0 , 50 feet per second; 0.306-inch flameholder	55,56,57

Figure

Mentioned
on page -

28. - Effect of frequency on flame-speed distribution. Flow velocity U , 50 feet per second; fuel-air ratio, 0.0444; disturbance velocity, 2.16 feet per second; test section depth, 1/2 inch; 0.306-inch flameholder; antisymmetric disturbance 57,59
29. - Distribution of fraction burned F and idealized h_2/h_1 for data of figure 28(a). 58
30. - Frequency giving maximum increase in flame speed as function of h_2/h_1 compared with results of stability analysis. 58,59
31. - Displacement measured on flame front for small-amplitude disturbances. Flow velocity U , 50 feet per second; fuel-air ratio, 0.0484; turbulent disturbance velocity u' , 0.303 foot per second. . . . 58
32. - Propagation velocities for small-amplitude disturbances. . . . 59
33. - Flame-speed distribution in 1-inch-deep test section. Flow velocity at plane of flameholder U_0 , 50 feet per second; fuel-air ratio, 0.0493; 1/4-inch flameholder. 59
34. - Effect of amplitude on flame-speed distribution. Flow velocity U , 50 feet per second; fuel-air ratio, 0.0444. 59
35. - Comparison of S_T/S_L and flame appearance for 0.500- and 0.306-inch flameholders. Flow velocity U , 50 feet per second; fuel-air ratio, 0.0444. 59,60
36. - S_T/S_L distribution, shadowgraphs, and comparison of fraction burned with average voltage. Flow velocity U , 100 feet per second; fuel-air ratio, 0.0493; antisymmetric disturbance. 60,61
37. - Comparison of S_T/S_L obtained with flameholder for producing symmetric disturbances with S_T/S_L obtained with flameholder for producing antisymmetric disturbances. Flow velocity U , 50 feet per second; fuel-air ratio, 0.0444. 61
38. - Comparison of photographs of excited flame with eddy trail. . . . 63
39. - Observations of vortex shedding excited by antisymmetric disturbances. 63

Figure

Mentioned
on page -

40. - Comparison of relative flame speeds at two flameholder positions. Flow velocity U , 50 feet per second. 64
41. - Comparison of flame speeds with and without banks of 200-mesh screens upstream of flameholder. 64
42. - Comparison of S_T/S_L taken in 1/2-inch- and 1-inch-wide ducts with Scurlock's data. 64
43. - Spectra of incident and flame amplified turbulence.
- $$E(f) = \frac{\frac{4I_x}{U}}{1 + \left(\frac{2\pi}{U} I_x\right)^2 f^2} 66$$
44. - Turbulence energy distribution for exponential correlation coefficient. 66
45. - Distribution with frequency of disturbance velocities required to produce blowout at fixed velocity and fuel-air ratio. Flow velocity at plane of flameholder U_0 , 50 feet per second; 0.306-inch flameholder placed 5/8 inch from nozzle; duct length, 5.7 inches; antisymmetric disturbances. 69
46. - Spontaneous oscillations showing intermittent flame interruption. Frequency f , 85 cycles per second; fuel-air ratio, 0.0444; flow velocity U , 50 feet per second. 70

AUTHOR INDEX

Berl, 3
Bittker, 45, 50, 52
Blackshear, 4, 50, 68
Bolz, 3, 63
Burlage, 3, 63

Clark, 45, 50, 52

Damkohler, 3
Dryden, 66
Dugger, 54

Ernstein, 3, 63

Fabri, 8
Fenn, 4
Foure, 8
Forney, 4

Garmon, 4
Goldstein, 15, 25, 63
Grover, 3, 48, 63, 64

Haddock, 3
Heisenberg, 11

Karlovitz, 3
Kaskan, 4, 50
Kebely, 3

Laurence, 46, 48
Leason, 3
Lessen, 11
Lin, 9, 11, 12, 15, 24, 67

Marble, 3, 49
Markstein, 3, 65
Mascolo, 3
Mestre, 39
Mickelsen, 3, 46, 48, 63

Newton, 4
Noreen, 4

Pillow, 9, 15, 75
Pretsch, 11

Rayle, 4, 68
Rayleigh, 4, 12, 15, 41
Reiter, 3
Rice, 3
Rosen, 3
Roshko, 48, 69

Savic, 12
Schubauer, 9
Scurlock, 2, 3, 8, 25, 39, 40, 48, 51, 53, 57, 63, 64
Shelkin, 3
Siestrunck, 8
Skramstad, 9
Summerfield, 3

Tower, 4, 68
Truman, 4
Tsien, 8, 13
Tucker, 3

Wohl, 3

Zukowski, 3, 49